Hydrodynamic permeability of staggered and non-staggered regular arrays of squares

Cindy Lloyd

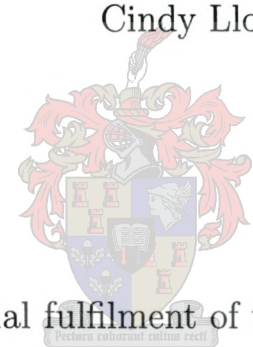

Thesis presented in partial fulfilment of the requirements for the degree of Master of Engineering Science at the University of Stellenbosch.

Promoter: Prof. J.P. Du Plessis

May 2003

Declaration

I, the undersigned, hereby declare that the work contained in this thesis is my own original work and that I have not previously in its entirety or in part submitted it at any university for a degree.

Signature: Date:

Abstract

This work entails an analysis of two-dimensional Newtonian flow through a prismatic array of squares. Both in-line and staggered configurations are investigated, as well as the very low velocity Darcy regime, where Stokes' flow predominates, and the Forchheimer regime, where interstitial inertial effects such as recirculation are present. As point of departure two recently developed pore-scale models are discussed and their results compared to Stokes' flow computational analysis for flow through regular arrays of rectangles. The commercial CFX code is also used to analyse the problem and to determine the accuracy of the assumptions used for the development of the pore-scale models. Finally an improvement is suggested to the RRUC model towards more accurate prediction of permeabilities, especially for porosities below 75%, and whereby its quantitative predictive capability is thus enhanced considerably.

Opsomming

Hierdie werk behels 'n analise van twee-dimensionele vloei deur 'n prismatiese matriks van reghoeke. Beide inlyn en verspringde konfigurasies word ondersoek sowel as Darcy-gebied van baie lae vloeisnelheid, waar Stokes se Wet oorheersend is, en die Forchheimer-gebied waar inersiële effekte soos interne hersirkulasie teenwoordig is. As uitgangspunt word twee modelle bespreek wat onlangs ontwikkel is en hulle resultate word vergelyk met numeriese voorspellings vir Stokes vloei deur 'n geordende matriks van reghoeke. Die kommersiële numeriese pakket CFX is ook gebruik om die probleem te analiseer en om die toepaslikheid van aannames van die onderskeie modelle te bepaal. 'n Verbetering tot die RRUC model word voorgestel wat lei tot meer akkurate voorspelling van permeabiliteite, veral vir porositeite laer as 75%, en waardeur die kwantitatiewe voorspellings-vermoë van die modelle aansienlik verbeter word.

Contents

List of Tables

List of Figures

Nomenclature

Standard characters

c_d	[ ]	Drag coefficient
d	$[m]$	Linear RRUC dimension
d_p	$[m]$	RRUC pore width
g	$[m/s^2]$	Gravitational acceleration
G	[ ]	Frictional factor
G_o	[ ]	Low Reynolds' number asymtotic microscopic frictional factor
G_∞	[ ]	High Reynolds' number asymtotic microscopic frictional factor
k	$[m^2]$	Hydrodynamic permeability
K	[ ]	Dimensionless hydrodynamic permeability
L	$[m]$	Predefined straight line length
L_e	$[m]$	Length of tortuous flow path over L
$\underline{\hat{n}}$	$[m]$	Unit vector in streamwise direction
p	$[Pa]$	Pressure
p_f	$[Pa]$	$\langle p \rangle_f$
q	$[m/s]$	Streamwise superficial speed
Re_p	[ ]	Interstitial Reynolds number

Standard characters ...continued

s	[ ]	Shifting factor
S	$[m^2]$	Surface
S_{face}	$[m^2]$	Surface exposed upstream relative to the streamwise direction
t	$[s]$	Time
u	$[m/s]$	Drift speed, streamwise direction
U	$[m^3]$	Volume
v	$[m/s]$	Speed
w	$[m/s]$	Average speed in streamwise pores

Miscellaneous

$\langle\ \rangle$	Phase average operator
$\langle\ \rangle_f$	Intrinsic phase average operator
$\{\ \}$	Deviation operator
∇	Del operator
$\nabla_{\|\|}$	$\frac{1}{q}\underline{q}\cdot\nabla$
$\nabla_{\perp}$	$\nabla - \frac{1}{q}\underline{q}\cdot\nabla$
$\underline{\ }$	Vector (underlined)
$\underline{\underline{\ }}$	Diadic (double underlined)

Greek symbols

α	[ ]	Constant
β	[ ]	Velocity ratio
γ	[ ]	Coefficient (0 or 1)
Δ	[ ]	Finite difference operator, change in streamwise volume
δ	[ ]	Change in transverse volume
ϵ	[ ]	Porosity, U_f/U_o
λ	[ ]	Streamwise particle shape factor $d_{s\perp}/d_{s\|\|}$
μ	$[N \cdot s/m^2]$	Fluid dynamic viscosity
ρ	$[kg/m^3]$	Fluid density
τ	$[N/m^2]$	Local shear stress
χ	[ ]	Tortuosity
ψ	[ ]	Scalar quantities in U_f

Acronyms

RRUC	Rectangular representative unit cell
FD	Firdaouss and Du Plessis
FD_{num}	FD numerical results obtained using finite element method
FD_{an}	FD analytical
CFX	Commercial CFD code
CFD	Computational fluid dynamics

Subscripts

$\|\|$	Parallel to streamwise direction
$\perp$	Perpendicular to streamwise direction
f	Fluid matter
ff	Fluid-fluid interface
fs	Fluid-solid interface
g	Stagnant
o	Total solid and fluid volume
s	Solid matter
t	Transfer

Chapter 1

Introduction

Although significant theoretical advances have been made over the past few decades towards the understanding and modelling of flow phenomena in porous media, surprisingly few fundamental pore-scale studies have been reported recently on simple geometries, although much can still be learnt from such endeavours.

The study of fluid transport through two-dimensional porous structures has a wide variety of practical applications. In nature a dendrite type of environment is frequently encountered and to study and analyse the complex chemical and physical processes that take place a good understanding of the underlying flow conditions in the porous environment is absolutely necessary [12]. For heat and mass transfer the flow field needs to first be solved. For the RTM (resin transfer moulding) process, where resin is injected into a closed mould filled with dry fibre reinforcement [13], a two-dimensional fluid model which can realistically describe the mould filling process, is necessary.

The study of air flow through cities and through wind breaks are other important applications of two-dimensional fluid models.

1.1 Published Literature

In the published literature there exist several analytical and empirical models for the modelling of a two-dimensional prismatic porous medium.

Hasimoto [14], used a Fourier series method to obtain solutions of the Stokes equations of motion for a viscous fluid past a periodic array of cylinders, as well as developing an equation for the drag coefficient of a rod.

Sangani and Acrivos [18], determined solutions for slow flow past a square and a hexagonal array of cylinders by using a somewhat non-conventional numerical method. The calculated values of the drag on a cylinder as a function of c, the volume fraction of the solids, were shown to be in excellent agreement with the corresponding asymtotic expressions for very dilute arrays ($c \ll 1$) and for very concentrated arrays ($c \rightarrow c_{max}$), where c_{max} is the maximum volume fraction. These solutions were then used to calculate the average temperature difference between the bulk and the cylinders which are heated uniformly under conditions of small Reynolds and Péclet numbers.

Kolodziez [17], provides a survey of theoretical and experimental results given by various authors concerning the resistance of a system of cylindrical bars under perpendicular creeping flow. This system has the form of a bundle of parallel bars and is treated as an anisotropic porous medium, with the flow through being described by the Darcy equation of filtration.

Jackson and James [16], provide a literature survey of experiments and theories related to low Reynolds-number flow through highly porous fibrous porous media. Experimental data was reported for a wide range of materials, from polymer chains to fibreglass.

Sangani and Yao [19], developed a numerical method that takes into account the many particle interactions in a rigorous manner to determine the effective thermal conductivity of a composite medium consisting of parallel circular cylinders of certain conductivity suspended in a matrix. Sangani and Yao [20], then extended this method to treat the problem of determining the permeability of random arrays of infinitely long cylinders. The results for the transverse and longitudinal permeabilities averaged over several configurations of random arrays of cylinders are presented as a function of the area fraction of the cylinders.

Gebart [13], derives the permeability of an idealized unidirectional reinforcement consisting of regularly ordered parallel cylindrical fibres from first principles both for flow along and for flow perpendicular to the fibres.

Howells [15], studies the flow though beds of fixed cylindrical fibres with the aim of finding the shielding radius and drag per unit length as a function of volume fraction occupied by the fibres in the semi-dilute situation.

All the solutions given in the above mentioned literature, are however only applicable to the Darcy flow regime.

An example of a theoretical solution that includes both the Darcy and the Forchheimer regimes is the rectangular representative unit cell (RRUC) model of Du Plessis and Van der Westhuizen [9]. An updated version of this solution was published by Du Plessis [5]. Diedericks [4] extended this updated model to be applicable to two-dimensional anisotropic porous media.

1.2 This work

This study is directed at the close investigation of two pore-scale models for flow through a regular array of square obstacles. The RRUC model was already mentioned and the other is the results from an analytical model by Firdaouss and Du Plessis [12] used to tie together the results of a numerical analysis of Stokes flow through periodic arrays done at CNRS-LIMSI in 2001 [12].

Some discrepancies exist between the hydrodynamic permeability predictions of the two models and one goal of the present work is to analyse the models and their assumptions closely by means of the commercial code CFX. Particular attention will be paid to the manner of subdivision of the void volume into sub-volumes, each with its predominant flow conditions and also the effect of staggering and the tortuosity.

1.3 Layout of thesis

Two proposed analytical models for the prediction of the hydrodynamic permeability, namely the RRUC model of Du Plessis and Van der Westhuizen [9] and the FD (Firdaouss and Du Plessis) model [12], are described in Chapter 2. The RRUC model provides a theoretical model of a two-dimensional prismatic porous medium that includes both the *Darcy regime*, where only viscous drag is present, and *Forchheimer regime*, where inertial drag effects predominate, for an isotropic porous medium. The FD analytical model is used for the prediction of dimensionless hydrodynamic permeabilities in a regular prismatic array, i.e. a particular non-isotropic two-dimensional array of rectangles. Even though the FD analytical model can be used for varying rectangular shaped fibres, only those configurations with square cells have been analysed in this thesis. Numerical results [12], obtained using a numerical code developed at LIMSI, in France, using the finite element method, for the dimensionless permeability for a selection of porosities are also given in Chapter 2. In this thesis these numerical results will be referred to as the FD numerical results.

Results for the dimensionless hydrodynamic permeability for non-staggered (Chapter 3) and staggered (Chapter 4) configurations are presented using a commercial CFD (Computational Fluid Dynamics) code CFX. These results are shown to closely match the FD numerical results previously obtained. The numerical results are then compared to the results predicted by the RRUC and the FD analytical models. The FD analytical model is shown to provide a good prediction for the hydrodynamic permeability for configurations of low porosities, but the RRUC is shown to not provide accurate enough predictions for models of any porosity. Using CFX it is shown that the suggested compartementalization of the fluid section into volumes by the FD analytical model is acceptable only for models of relatively low porosities.

In Chapter 6 the pressure averaging equation is analysed for both the non-staggered and staggered configurations, using the pore-scale volumes that were introduced and discussed in Chapter 5. Using the information obtained by this analysis, an alteration to the RRUC model is suggested. The altered RRUC model is shown to provide a much better correspondence with numerical results for the hydrodynamic permeability than the original RRUC model. The 'RRUC model technique' is also applied to the FD staggered configuration and shown

to give the same equation as the FD analytical model.

In Chapter 7 the analytical models that are discussed in this thesis are compared to results found in other literature. The results obtained by the FD and RRUC non-staggered model are compared to the results given by Sangani and Acrivos [18] for slow flow past a square array of cylinders. It is shown that the calculated drag on the cylinders is higher than the predicted drag on the rectangular fibres for all porosities. The results from both the FD staggered and the RRUC staggered models are then compared to the results given by Sangani and Acrivos [18] for slow flow past a hexagonal array of cylinders. A comparison is also done between the staggered and non-staggered models considered in this work.

Appendix A provides a brief discussion of some aspects of the commercial CFD code CFX which is used in this thesis. In Appendix B the actual calculations done to obtain the numerical results for a non-staggered configuration with porosity $\epsilon = 0.51$, given by CFX, are shown. The calculations that were used to analyze the compartementalization of the fluid volume for the non-staggered configurations, as suggested by RRUC and FD analytical models, are also given. In Appendix C the FD staggered configuration, with porosity $\epsilon = 0.1164$, is analysed and the actual calculations done to obtain the numerical results given by CFX, as well as those used to analyse the assumptions of the FD analytical model, are shown. The pressure averaging equation is analysed for the RRUC model with the FD staggered configuration in Appendix D.

Chapter 2

Existing theory

2.1 RRUC model

The RRUC model is a pore scale modelling procedure to provide closure to general volume averaged transport equations and which is used for the prediction of flow through various types of microstructure. It was first proposed by Du Plessis and Masliyah [8] and uses volume averaged quantities to provide closure for the set of open averaged equations.

2.1.1 Interstitial momentum transport equations

The continuity equation for the interstitial conservation of mass, for incompressible flow, may be expressed as

$$\nabla \cdot \underline{v} = 0, \tag{2.1}$$

where $\underline{v}$ is the actual fluid velocity field within the channels of the porous domain. The Navier-Stokes equation, governing the momentum transport within the interstitial fluid phase, may be written as follows:

$$\rho \frac{\partial \underline{v}}{\partial t} + \nabla \cdot (\rho \underline{v}\,\underline{v}) - \rho \underline{g} + \nabla p - \nabla \cdot \underline{\underline{\tau}} = \underline{0}. \tag{2.2}$$

It is impractical to describe the full interstitial fluid velocity field $\underline{v}$, and thus volume averaged quantities, which may hopefully be measurable in practice, are used to describe the principle dynamics of the flow through porous media.

2.1.2 Volume averaging

By applying volume averaging [22] to the interstitial variables and transport equations, volume averaged quantities can be obtained. According to the phase averaging technique, the interstitial transport variables and equations may be averaged over a Representative Elementary Volume (REV), U_o, which includes both fluid U_f and solid U_s parts. An REV should consist of enough solid and fluid parts so as to make it statistically representative of the properties of the porous medium. It must also be small enough to be used as a differential element in the calculus of volume averaged quantities. The porosity of the porous medium is defined by the following volume ratio for the REV

$$\epsilon \equiv \frac{U_f}{U_o}, \tag{2.3}$$

where U_o is the total volume and U_f is the total fluid volume. An REV is defined for each and every point of the averaging domain and its size, shape and orientation are assumed to remain constant at all times while under consideration.

The *phase average* $\langle \psi \rangle$ of any tensorial quantity ψ of the fluid phase of the REV, is defined as

$$\langle \psi \rangle \equiv \frac{1}{U_o} \iiint_{U_f} \psi \, dU. \tag{2.4}$$

Similarly, the *intrinsic phase average* $\langle \psi \rangle_f$ is defined as

$$\langle \psi \rangle_f \equiv \frac{1}{U_f} \iiint_{U_f} \psi \, dU. \tag{2.5}$$

The *deviation of any fluid phase quantity* $\{\psi\}$ at some point in U_f is defined as

$$\{\psi\} \equiv \psi - \langle\psi\rangle_f . \tag{2.6}$$

Using equation (2.3) we have the following relationship between the phase and intrinsic phase averages:

$$\langle\psi\rangle \equiv \epsilon \langle\psi\rangle_f . \tag{2.7}$$

The *superficial velocity* $\underline{q}$ is defined as the phase average of the interstitial velocity

$$\underline{q} \equiv \frac{1}{U_o} \iiint_{U_f} \underline{v} \, dU, \tag{2.8}$$

and presents the average velocity which would occur in a section where no solids were present within the particular macroscopic boundaries. The direction of $\underline{q}$ is referred to as the *streamwise direction* and any properties referring to this direction will be denoted by a subscript $||$. The direction perpendicular to the streamwise one is denoted by a subscript $\perp$.

The *drift velocity* $\underline{u}$ is defined as the intrinsic phase average velocity

$$\underline{u} \equiv \frac{1}{U_f} \iiint_{U_f} \underline{v} \, dU, \tag{2.9}$$

and represents the average velocity of any fluid particle in the streamwise direction. The relationship between the superficial and drift velocities ($\underline{q} = \epsilon \, \underline{u}$) is known as the Dupuit relationship [3].

For an incompressible fluid the phase averaged continuity equation is as follows

$$\nabla \cdot \underline{q} = 0. \tag{2.10}$$

With no-slip boundary conditions on the fluid-solid interface, volume averaging of the Navier-Stokes equation [5] leads to

$$\rho \frac{\partial \underline{q}}{\partial t} + \rho \nabla \cdot (\underline{q}\,\underline{q}/\epsilon) - \epsilon \rho \underline{g} + \epsilon \nabla p_f - \nabla \cdot \left\langle \underline{\underline{\tau}} \right\rangle + \rho \nabla \cdot \langle \{\underline{v}\}\{\underline{v}\} \rangle + \frac{1}{U_0} \iint_{S_{fs}} \underline{n}\{p\}\, dS - \frac{1}{U_0} \iint_{S_{fs}} \underline{n} \cdot \underline{\underline{\tau}}\, dS = \underline{0}. \tag{2.11}$$

The average flow through a porous medium is time independent and uniform ($\underline{q}$ is constant in magnitude and direction) in many applications since curvature of the streamlines of the average flow field $\underline{q}$ is to a large extent suppressed by the presence of the solid phase. Equation (2.11) simplifies to

$$-\epsilon \nabla p_f = \rho \nabla \cdot \langle \{\underline{v}\}\{\underline{v}\} \rangle + \frac{1}{U_0} \iint_{S_{fs}} \left(\underline{n}\{p\} - \underline{n} \cdot \underline{\underline{\tau}} \right) dS, \tag{2.12}$$

if the average field $\underline{q}$ is uniform. This equation is still 'open' in the sense that further knowledge of the porous medium is needed to quantify the surface integral. A further closure modelling procedure is thus needed to transform equation (2.12) to a closed form for particular applications.

2.1.3 Closure with the RRUC model

A pore-scale closure modelling procedure, the RRUC model, was proposed by Du Plessis and Masliyah [8]. It aimed at approximating the porous material by imbedding the average geometric characteristics of the material as found in an REV within the smallest possible hypothetical rectangular representative unit cell (RRUC). The description of the model below follows closely that of [5].

Assuming uniform discharge through a homogeneous isotropic porous medium, the RRUC simplifies into a cubic representative unit cell of side length d, yielding identical properties

in each of its principle directions and equation (2.12) can be reduced further to

$$-\epsilon \nabla p_f = \frac{1}{U_0} \iint_{S_{fs}} \left(\underline{n} \{p\} - \underline{n} \cdot \underline{\underline{\tau}} \right) dS. \tag{2.13}$$

Due to the isotropy requirement the two surfaces of all parallel pairs will be an equal distance d_p apart. A possible cubic RRUC for a two-dimensional flow through an isotropic medium is shown in Figure 2.1. Piecewise straight streamlines are assumed between and parallel to the plates, as shown in Figure 2.1. It should be noted that, in this work, reference to 'volumes' must be interpreted as volume per unit depth, i.e. volumes may be expressed by two-dimensional areal expressions.

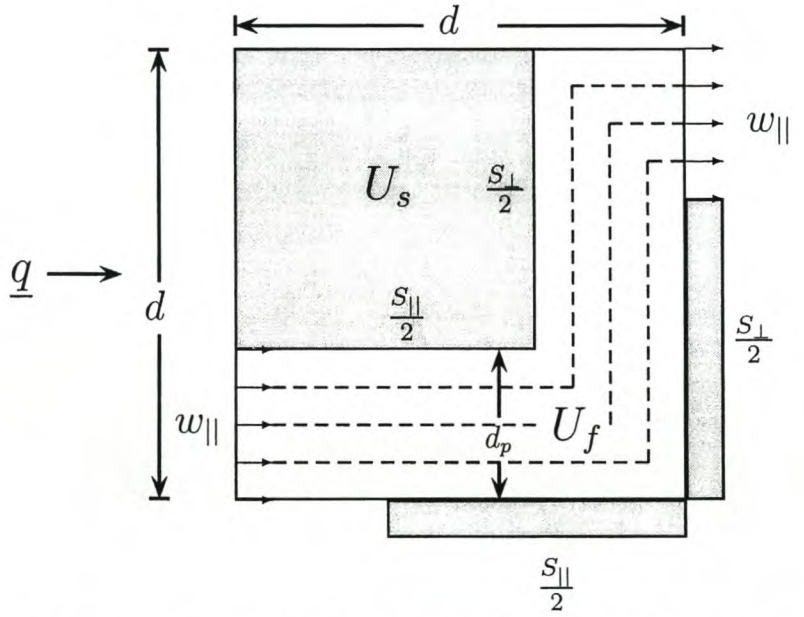

Figure 2.1: Unit cell geometry of a RRUC for 2D porous medium with piece-wise straight streamlines.

The tortuosity [21] of streamlines in a porous medium can be considered as a measure of the non-straightness of streamlines in the pore space. The most basic definition of tortuosity is the path length tortuosity [3], which is defined as the ratio of the average length of the tortuous flow path L_e to the corresponding straight line length L in the streamwise direction

$$\chi \equiv \frac{L_e}{L}. \tag{2.14}$$

In this case, according to the rectangular geometry and associated assumptions all the streamlines in an RRUC are of equal length $L_e = 2d - d_p$ and the predefined displacement is equal to d. Therefore, for the RRUC model the tortuosity χ can be defined as

$$\chi = \frac{(2d - d_p)}{d} = \frac{U_f}{U_{||}}, \tag{2.15}$$

where $U_{||}$ is the effective streamwise volume. A third velocity variable, the *streamwise average pore velocity* $\underline{w}_{||}$ [1] can now be defined as

$$\underline{w}_{||} = \frac{U_o}{U_{||}} \underline{q} = \frac{\chi}{\epsilon} \underline{q}, \tag{2.16}$$

and represents the average velocity of any particle in the streamwise volume $U_{||}$.

Darcy regime

In the Darcy regime of pure viscous drag at low Reynolds number ($Re_p << 1$), the pressure deviation part of the surface integral term, in equation (2.13), is negligible in the streamwise pore section. In the transverse pore sections the shear stresses have no streamwise components. Although, due to the randomness of the medium, the transverse shear stresses of neighbouring RRUCs will cancel vectorially, interstitial transverse pressure drops will still be created. These pressure drops will then contribute to the surface integral term through the pressure deviation part, when evaluated at the streamwisely up- and down- facing surfaces, $S_\perp$. It was assumed, however, that this contribution to the integral of the pressure deviation term may be incorporated by integrating for the wall shear stress over the total solid-fluid interface S_{fs} instead of only over the streamwise part $S_{||}$. In the low Reynolds number limit equation (2.13) is thus given by

$$-\epsilon \nabla p_f = \frac{1}{U_0} \underset{S_{||}}{\iint} (-\underline{n} \cdot \underline{\underline{\tau}})\, dS + \hat{\underline{n}} \frac{1}{U_0} \underset{S_\perp}{\iint} \left| \underline{n} \cdot \underline{\underline{\tau}} \right| dS, \tag{2.17}$$

where $\hat{\underline{n}}$ is the unit vector in the streamwise direction. If the wall shear stress is assumed to be uniform and equal to a constant, τ_w, over S_{fs} in all channel sections, for the low Reynolds

number limit, equation (2.17) reduces to

$$-\epsilon \nabla p_f = \hat{\underline{n}} \frac{1}{U_0} \iint_{S_{fs}} \tau_w \, dS. \tag{2.18}$$

For Newtonian flow between two parallel plates a distance d_p apart and if the average transverse velocity is $\beta w_{||}$ it follows that

$$-\epsilon \nabla p_f = \left(\frac{S_{||} + \beta S_{\perp}}{U_o} \right) . \left(\frac{6 \mu w_{||}}{d_p} \right) \hat{\underline{n}} = \frac{S_{||} + \beta S_{\perp}}{U_o} . \frac{6}{d_p} \left(\frac{\chi}{\epsilon} \right) \mu \underline{q}. \tag{2.19}$$

If we define

$$G_o \equiv \frac{6 \chi}{\epsilon \, d_p} . \frac{S_{||} + \beta S_{\perp}}{U_o}, \tag{2.20}$$

the momentum transport equation for uniform average flow becomes

$$-\epsilon \nabla p_f = G_o \mu \underline{q} \tag{2.21}$$

in the limit of very slow flow. Comparing this equation with the definition of the hydrodynamic permeability

$$k \equiv -\frac{\mu q}{dp/dx}, \tag{2.22}$$

yields the following for the model prediction of permeability

$$k = \frac{\epsilon}{G_o}. \tag{2.23}$$

Forchheimer regime

For the Forchheimer regime (when $Re_p > 100$) inertial drag effects predominate. For purpose of this study the 'high' Reynolds number limit refers to the laminar limit where interstitial recirculation is developed but no turbulence is yet present. The predominance of the pressure

gradient above the shear stresses becomes more enhanced with the increase in Reynolds number, so that the contribution of shear stresses may be discarded, reducing equation (2.13) to

$$-\epsilon \nabla p_f = \frac{1}{U_0} \iint_{S_{fs}} \underline{n}\,\{p\}\, dS. \tag{2.24}$$

It was proposed by Du Plessis [9] that the surface integral term may be modelled by an internal drag condition as follows

$$-\epsilon \nabla p_f = \frac{1}{U_o} . c_d\, S_{face} . \frac{1}{2} \rho\, w_{||}^2\, \hat{\underline{n}} \tag{2.25}$$

$$= \frac{S_\perp}{U_o} . \frac{c_d\, \rho\, q}{4} \left(\frac{\chi}{\epsilon}\right)^2 \underline{q} \tag{2.26}$$

$$= G_\infty\, \mu\, \underline{q}, \tag{2.27}$$

where c_d is the drag coefficient and S_{face} the surface exposed upstream relative to the stream-wise direction. Therefore we have the definition:

$$G_\infty \equiv \frac{\chi\, c_d\, Re_p}{8\, \epsilon\, d_p} \cdot \frac{S_\perp}{U_o}, \tag{2.28}$$

where

$$Re_p \equiv \frac{2\, d_p\, \rho\, q\, \chi}{\epsilon\, \mu}, \tag{2.29}$$

is the interstitial Reynolds number.

Asymptote matching

Combining the above results found for the Darcy and Forchheimner regimes by using the asymptote matching technique (Churchill and Usagi [2]), to produce a result valid for both, we obtain

$$G = [G_o^s + G_\infty^s]^{1/s}, \tag{2.30}$$

where s is the shifting parameter. Equation (2.13) can therefore be written as

$$-\epsilon \nabla p_f = G \mu \underline{q}. \tag{2.31}$$

The shifting parameter may provisionally be taken as unity, since this value produced adequate correlation with experimental results in many cases of Newtonian flow through porous media [9].

Unidirectional fibre bed

An appropriate RRUC for a unidirectional bundle of uniform fibre beds was introduced by Du Plessis [6] and is schematically shown in Figure 2.2.

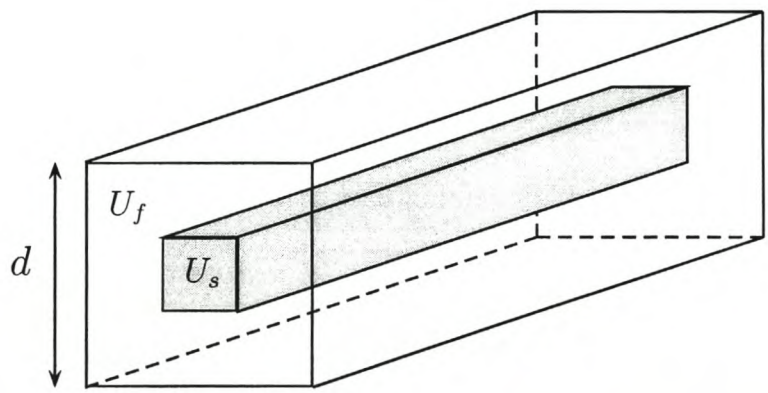

Figure 2.2: Rectangular prismatic RRUC for a unidirectional fibre bed.

Crossflow through this bundle of fibres presents a two-dimensional case of flow through a porous media.

The tortuosity χ, equation (2.15), can be written in terms of the porosity as follows

$$\chi = \frac{\epsilon}{1 - \sqrt{1-\epsilon}}. \tag{2.32}$$

The frictional factor G for a unidirectional fibre bed can therefore be given as

$$G = \frac{12\,(1+\beta)\sqrt{1-\epsilon}}{d^2\,(1-\sqrt{1-\epsilon})^2} + \frac{\rho\, q\, c_d}{\mu\, d} \cdot \frac{\sqrt{1-\epsilon}}{2(1-\sqrt{1-\epsilon})^2}. \tag{2.33}$$

The hydrodynamic permeability for a unidirectional fibre bed is given as:

$$k \equiv \frac{\epsilon}{G_o} = \frac{\epsilon\, d^2\,(1-\sqrt{1-\epsilon})^2}{12\,(1+\beta)\,\sqrt{1-\epsilon}}, \tag{2.34}$$

where β is the velocity ratio. Du Plessis and Diedericks [5], assumed the velocity ratio to be unity, simplifying the equation to:

$$k = \frac{\epsilon\, d^2\,(1-\sqrt{1-\epsilon})^2}{24\sqrt{1-\epsilon}}. \tag{2.35}$$

This equation was considered to be adequate for predicting the hydrodynamic permeability through a two-dimensional case of flow through a porous medium. The dimensionless permeability

$$K = \frac{\epsilon\,(1-\sqrt{1-\epsilon})^2}{24\sqrt{1-\epsilon}}, \tag{2.36}$$

is obtained by dividing the hydrodynamic permeability by the cross-sectional area of the unit cell d^2.

2.2 FD analytical model

Another model for the prediction of Darcy permeabilities in a non-isotropic two-dimensional porous medium is the FD analytical model proposed by Firdaouss and Du Plessis [12]. In this model it is shown that it is necessary to introduce two other parameters, in addition to porosity, for the prediction of Darcy permeabilities. These parameters are concerned with the geometric properties of the solid microstructure in the streamwise direction, namely a particular shape factor and the discrimination between non-staggered and staggered configurations in the streamwise direction.

2.2.1 Rectangular representation of the porous microstructure

As with the RRUC model, the FD analytical model uses rectangular unit cells to represent the porous microstructure. The direction of $\underline{q}$, as defined in equation (2.8), is also referred

to as the *streamwise direction*, denoted by a subscript $||$ and the direction perpendicular to it is denoted by a subscript $\perp$. A unit cell is considered here as a solid rectangle embedded in a rectangular volume of dimensions $d_{||}$ and $d_{\perp}$, as shown in Figure 2.3. The solid particle is represented by a rectangle of length $d_{s||}$ in the streamwise direction and length $d_{s\perp}$ perpendicular to it, also shown in Figure 2.3.

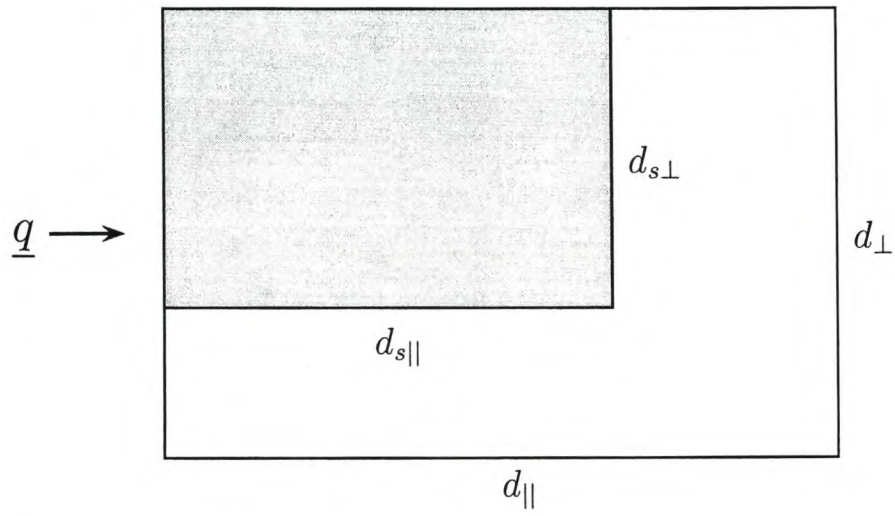

Figure 2.3: Notation for unit cell with respect to streamwise direction.

For a porous structure with a fairly evenly spread of solid particles it seems reasonable that the following assumption, (to which all of the examples that were computed adhere), could be made

$$\frac{d_{\perp}}{d_{||}} = \frac{d_{s\perp}}{d_{s||}} \equiv \lambda. \tag{2.37}$$

Using the geometry, we obtain the following expression for the porosity for the rectangular unit cell

$$\epsilon = \frac{U_f}{U_o} = \frac{d_{||}d_{\perp} - d_{s||}d_{s\perp}}{d_{||}d_{\perp}} \tag{2.38}$$

and using assumption (2.37) it can be rewritten as

$$\epsilon = 1 - \left(\frac{d_{s\perp}}{d_{\perp}}\right)^2. \tag{2.39}$$

This gives the following expression for the ratio of the cross-stream solid width to cell width ratio:

$$\frac{d_{s\perp}}{d_\perp} = \sqrt{1-\epsilon}. \tag{2.40}$$

The hydrodynamic permeability (equation (2.22)) for the streamwise direction, in the notation of the rectangular representation of the solid particles, can be written as

$$k = \frac{\mu q}{\Delta p / d_{||}}, \tag{2.41}$$

where Δp is the streamwise pressure drop per unit cell. The dimensionless permeability, K, is defined as the hydrodynamic permeability divided by the cross-sectional area of a unit cell, and is therefore given as

$$K \equiv \frac{k}{d_{||}\, d_\perp} = \frac{\mu q}{d_\perp \Delta p}. \tag{2.42}$$

2.2.2 FD analytical model for non-staggered configuration

In the non-staggered configuration, solid rectangles are lined up in straight rows in the streamwise direction. The fluid volume U_f is considered as three distinct volumes, as indicated in Figure 2.4, the streamwise volume $U_{||}$, the transfer volume U_t and the fluid volume between the solids in the perpendicular direction, U_g[1].

The FD analytical model assumes that the fluid volume, U_g, is stagnant and that the solid surfaces in this region create no shear stress which could be attributed to the pressure gradient. Sets of parallel plate sections are formed between the solid rectangles in the streamwise direction and between which shear stresses are created during Stokes flow. The cross-stream distance between the plates is $(d_\perp - d_{s\perp})$ so that the magnitude of the average streamwise velocity, $w_{||}$, between the plates of each section is related to the magnitude, q, of the Darcy velocity, by the following:

$$w_{||} = \frac{q\, d_\perp}{d_\perp - d_{s\perp}} = \frac{q}{1-\sqrt{1-\epsilon}}. \tag{2.43}$$

[1]The volume U_g is sometimes referred to as U_s in other work [12].

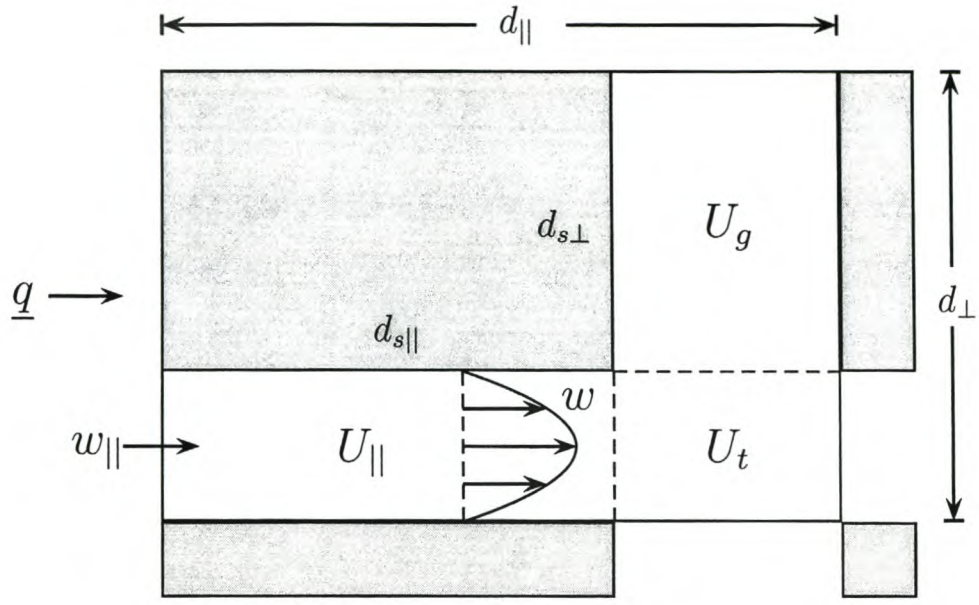

Figure 2.4: Unit cell geometry in case of no streamwise staggering.

Assuming fully developed Stokes flow to be present in $U_{||}$, i.e. between all pairs of streamwise parallel plates, the following streamwise pressure gradient between the parallel plates is obtained:

$$-\nabla_{||}p = \frac{12\,\mu\,w_{||}}{(d_\perp - d_{s\perp})^2} = \frac{12\,\mu\,q\,d_\perp}{(d_\perp - d_{s\perp})^3} = \frac{12\,\mu\,q}{d_\perp^2\,(1-\sqrt{1-\epsilon})^3}. \tag{2.44}$$

The pressure drop in the transfer volume of the unit cell is assumed to be zero, due to the absence of solid induced shear stresses, so that the volume, U_t, simply acts as a transfer volume for the fluid between the two adjacent shear-inducing pairs of parallel plates. The total pressure drop across the cell thus originates only in $U_{||}$ and can be written as

$$\Delta p = \Delta p_{U_{||}} = -\nabla_{||}p\,d_{s||}. \tag{2.45}$$

From equations (2.42), (2.44) and (2.37) the dimensionless hydrodynamic permeability

$$K = \frac{(1-\sqrt{1-\epsilon})^3}{12\sqrt{1-\epsilon}} \cdot \lambda \tag{2.46}$$

for the case of regular arrays in the streamwise direction is obtained.

If streamwise staggering of some cross-stream columns occurs, there will be no net effect on permeability since only the transfer volumes U_t, which have assumed to not contribute

to the pressure gradient, will be influenced. Independent streamwise staggering of rows or single solid parts will also only result in streamwise shifts between members of the parallel pairs (i.e. the parallel plates do not face each other directly). At low porosities this influence would be especially small and its effects could be neglected.

2.2.3 FD analytical model for staggered configuration

For the FD staggered configuration the solid rectangles are staggered cross-stream, forcing the fluid to deviate and actively traverse all void areas. Therefore, unlike the non-staggered model, no stagnant volumes exist. The upper half of a unit cell for such a case is shown in Figure 2.5.

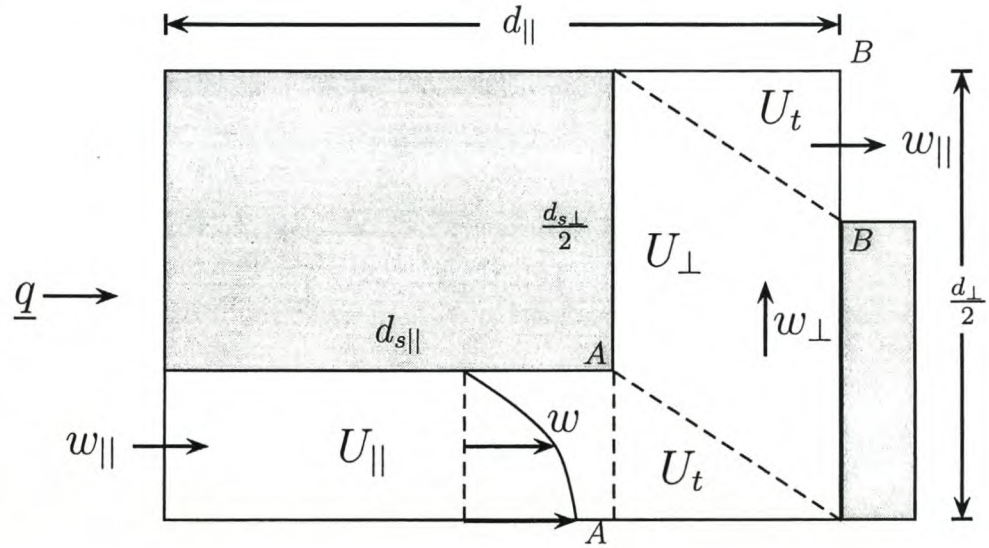

Figure 2.5: Geometry of top half of unit cell in case of streamwise staggering.

Unlike the FD analytical model for the non-staggered configuration, there are also flow and shear stresses between the cross-stream pairs of parallel plates, i.e. those facing streamwise. The streamwise flux is split into two perpendicular sections as shown in Figure 2.5, with the average speed in each cross-stream section $U_\perp$ being denoted by $w_\perp$. Using this fact and equation (2.37), we obtain the following relation:

$$w_\perp = \frac{w_{||}}{2} \cdot \frac{d_\perp - d_{s\perp}}{d_{||} - d_{s||}} = \frac{w_{||}}{2} \cdot \frac{d_{s\perp}}{d_{s||}} = \frac{w_{||}}{2}\lambda. \tag{2.47}$$

The streamwise pressure drop resulting from shear stresses in the perpendicular sections, now also contributes to the total pressure drop over the unit cell, so that

$$\Delta p = \Delta p_{U_{||}} + \Delta p_{U_{\perp}}. \tag{2.48}$$

The transfer volumes are again considered stress free and as already mentioned there are no stagnant volumes. The first term on the RHS of equation (2.48) follows identically to the result of equation (2.45). For the contribution to Δp in the perpendicular sections, it follows from equation (2.47) that the streamwise pressure drop between planes AA and BB in Figure 2.5 is given by

$$\Delta p_{U_{\perp}} = -\nabla_{\perp} p \frac{d_{s\perp}}{2} = \frac{-12\,\mu\, w_{\perp}}{(d_{||} - d_{s||})^2} \cdot \frac{d_{s\perp}}{2} = \frac{-12\,\mu\, w_{||}\lambda}{(d_{\perp} - d_{s\perp})^2} \cdot \frac{d_{s\perp}}{4} \cdot \frac{(d_{\perp} - d_{s\perp})^2}{(d_{||} - d_{s||})^2}. \tag{2.49}$$

Simplifying the above equation leads to

$$\Delta p_{U_{\perp}} = -\nabla_{||} p \frac{d_{s||}}{4} \lambda^4. \tag{2.50}$$

The total pressure drop over the unit cell is therefore given by

$$\Delta p = -\nabla_{||} p\, d_{s||} \left(1 + \frac{\lambda^4}{4}\right). \tag{2.51}$$

The dimensionless permeability, K, for an array of which the solids are staggered in the cross-stream direction is therefore

$$K = \frac{\left(1 - \sqrt{1-\epsilon}\right)^3}{12\sqrt{1-\epsilon}} \cdot \frac{\lambda}{1 + \lambda^4/4}. \tag{2.52}$$

In order to combine equations (2.46) and (2.52) to obtain a single general equation for the prediction of permeability, another coefficient γ [2], where

$$\gamma = \begin{cases} 0 & \text{unstaggered} \\ 1 & \text{cross-stream staggered} \end{cases} \tag{2.53}$$

[2]The coefficient γ is referred to as β in other work [12].

is introduced. The following equation is then sufficient to predict all the Darcy permeabilities for conditions covered in this work and should apply generally to porous media falling into this class:

$$K = \frac{\left(1-\sqrt{1-\epsilon}\right)^3}{12\sqrt{1-\epsilon}} \cdot \frac{\lambda}{1+\gamma\lambda^4/4}. \tag{2.54}$$

Five different geometrical case studies were considered [12], namely: square cells aligned in a square array (SCASA); rectangular cells aligned in a square array (RCASA); rectangular cells staggered in a square array (RCSSA); square cells staggered in a rectangular array (SCSRA) and rectangular cells staggered in a rectangular array (RCSRA). The values of the coefficients used in equation (2.54) for these different geometrical cases are given in Table 2.1.

	SCASA	RCASA		RCSSA		SCSRA		RCSRA	
		x	y	x	y	x	y	x	y
γ	0	0	0	1	0	1	0	0	1
λ	1	1/2	2	2	1/2	1	1	1/4	4
$\frac{\lambda}{1+\gamma\lambda^4/4}$	1	1/2	2	2/5	1/2	4/5	1	1/4	4/65

Table 2.1: Geometric coefficients for the cases studied by Firdaouss and Du Plessis [12].

In this thesis we are only concerned with the geometries with square cells, therefore the three geometries with rectangular cells, presented in Figure 2.6, were not analysed further.

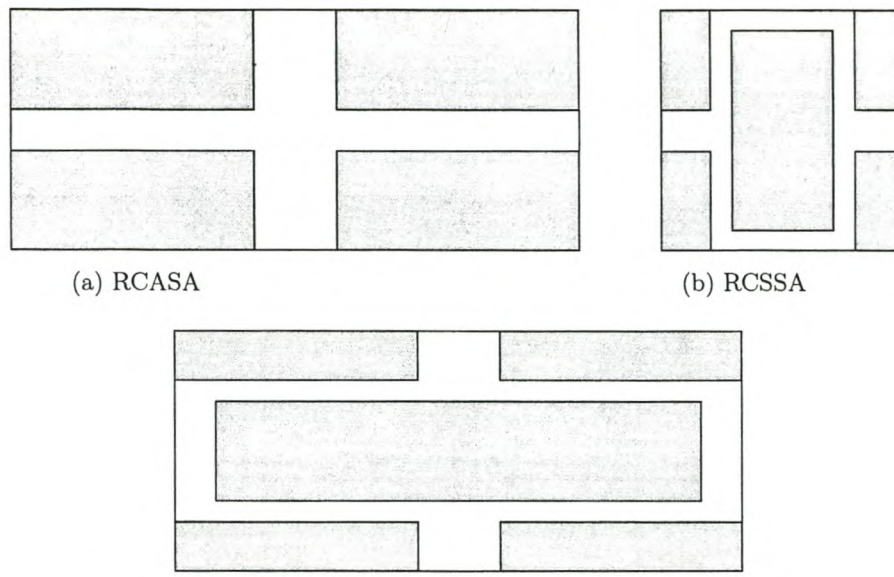

Figure 2.6: Geometry of FD case studies [12]: (a) Rectangles in a square array, (b) Rectangles in a staggered square array, (c) Rectangles in a staggered rectangular array.

The unit cell (dashed line) for the configuration of square cells aligned in a square array (SCASA) is shown in Figure 2.7. For the remainder of this thesis, this configuration will be referred to as the *FD non-staggered configuration.*

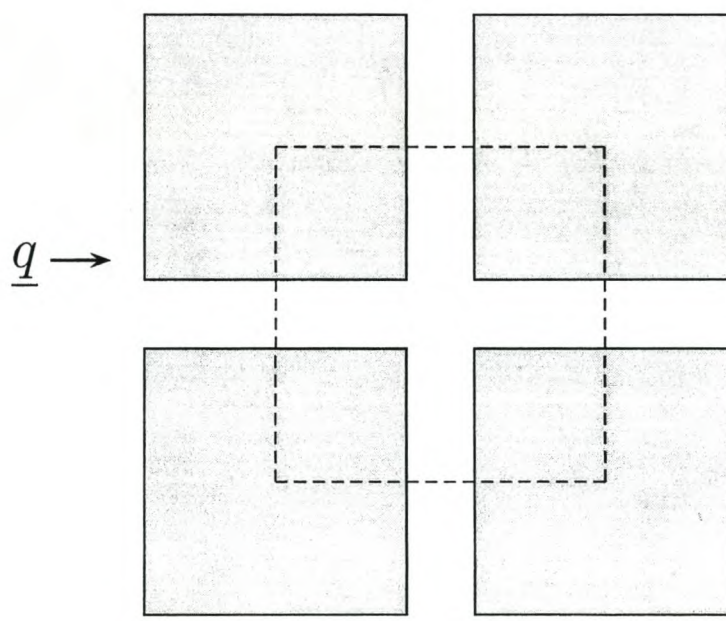

Figure 2.7: A unit cell for the SCASA (square cells aligned in a square array) case.

The unit cell (dashed line) for the configuration of square cells staggered in a rectangular array (SCSRA) is shown in Figure 2.8. This configuration will be referred to as the *FD staggered configuration* for the remainder of this thesis.

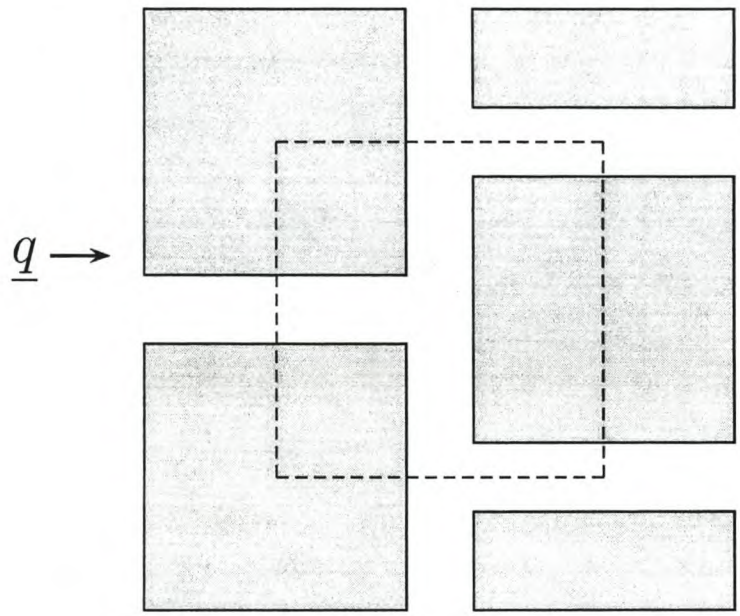

Figure 2.8: A unit cell for the SCSRA (square cells staggered in a rectangular array) case.

2.2.4 FD numerical results

Using a numerical code developed at LIMSI in France [12], based on the finite element technique, numerical results for the dimensionless permeability were obtained for the five different geometrical case studies that were considered. However, as already stated, we are only concerned with two of these, namely: square cells lined in a square array (SCASA) and square cells staggered in a rectangular array (SCRSA). For the remainder of this thesis, these numerical results will be referred to as the FD numerical results (FD_{num}).

Table 2.2 lists the complete set of FD numerical results [12] obtained for the dimensionless hydrodynamic permeability, K, for the non-staggered configuration (SCASA) and the staggered configuration (SCRSA).

In following chapters the FD numerical results, listed in Table 2.2, for a selection of porosities, will be used to validate the results obtained using the commercial CFD code CFX.

ϵ	Dimensionless permeability K	
	SCASA	SCRSA
0.0396	6.73×10^{-7}	
0.0784	5.42×10^{-6}	
0.1164	1.85×10^{-5}	
0.1536	4.41×10^{-5}	
0.1900	8.69×10^{-5}	6.92×10^{-5}
0.2256	1.51×10^{-4}	1.20×10^{-4}
0.2604	2.43×10^{-4}	1.93×10^{-4}
0.2944	3.65×10^{-4}	2.90×10^{-4}
0.3276	5.25×10^{-4}	4.16×10^{-4}
0.3600	7.26×10^{-4}	5.75×10^{-4}
0.4224	1.28×10^{-3}	1.01×10^{-3}
0.5100	2.56×10^{-3}	2.02×10^{-3}
0.5644	3.80×10^{-3}	2.99×10^{-3}
0.6400	6.73×10^{-3}	5.04×10^{-3}
0.7500	1.31×10^{-2}	1.06×10^{-2}
0.8400	2.38×10^{-2}	2.02×10^{-2}
0.9100	4.05×10^{-2}	3.63×10^{-2}
0.9600	6.78×10^{-2}	6.34×10^{-2}
0.9900	1.20×10^{-1}	1.16×10^{-1}

Table 2.2: FD numerical results [12] of dimensionless hydrodynamic permeability, K, for two of the geometric structures.

Chapter 3

Non-staggered configurations

3.1 CFX model

In an attempt to model the non-staggered configuration, a model, as shown in Figure 3.1, was constructed in CFX-5, for a selection of porosities $\epsilon = 0.1164, 0.36, 0.51, 0.75, 0.91$. Since we did not succeed in constructing a repetitive boundary on the inlet (according to which the outlet values would become the new inlet values after each iteration) using the CFX package, more than one unit cell were constructed in line so as to obtain more realistic results. Since the top and bottom halves of the unit cells are the same in a non-staggered case, a symmetry plane was used and only the top halves of the unit cells were constructed. Less grid points were therefore needed and the computational time was decreased considerably.

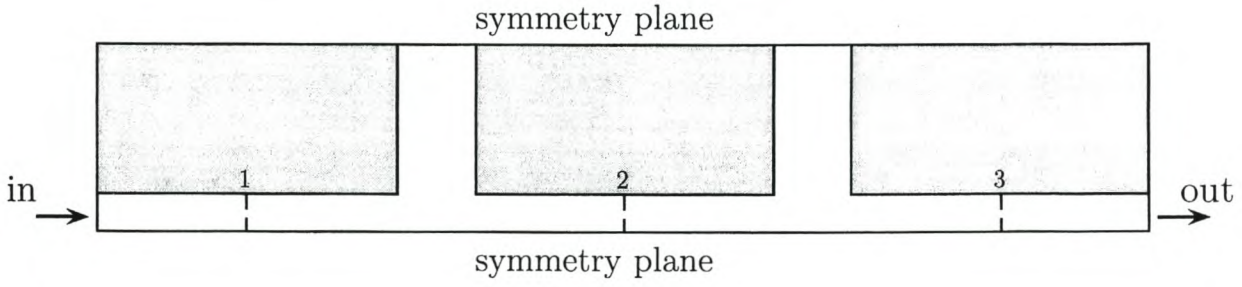

Figure 3.1: Construction used in CFX modelling for no streamwise staggering.

The CFX-5 post processor was used to analyse the model. Planes (for numerical calculations) were created at positions 1, 2 and 3 as indicated in Figure 3.1. Numerical values for the average velocity and pressure on these planes were obtained. These allowed us to calculate the change in pressure through a unit cell. As predicted it was found that the average velocities at the planes were all the same for the respective porosities. The numerical values obtained using the CFX-5 model are listed in Table 3.1 for five cases of different porosities.

ϵ	$\Delta p\ [Pa]$	$d_\perp\ [m]$	$w_{\|\|}\ [m/s]$	$q\ [m/s]$	K
0.1164	0.3374	0.005	5.19×10^{-4}	3.11×10^{-5}	1.85×10^{-5}
0.3600	0.3485	0.005	6.31×10^{-3}	1.26×10^{-3}	7.24×10^{-4}
0.5100	0.03575	0.005	1.53×10^{-3}	4.58×10^{-4}	2.56×10^{-3}
0.7500	0.03820	0.005	4.90×10^{-3}	2.45×10^{-3}	1.28×10^{-2}
0.9100	0.00412	0.005	1.19×10^{-3}	8.30×10^{-4}	4.05×10^{-2}

Table 3.1: Numerical values (SI) obtained using CFX for the case of no staggering.

The velocity $w_{||}$ is the average velocity at the planes and therefore the average velocity in the streamwise channels. The superficial velocity q used in the Darcy equation was calculated as

$$q = \left(1 - \frac{d_{s||}}{d_{||}}\right) w_{||}.$$

The dimensionless hydrodynamic permeability, K, was calculated using equation (2.42), namely

$$K = \frac{k}{d_{||}\, d_\perp} = \frac{\mu\, q}{d_\perp \Delta p}, \tag{3.1}$$

where $\mu = 0.001\ N \cdot s/m^2$ is the dynamic viscosity of the traversing fluid.

For a worked example, equations (B.1) to (B.3) in Appendix B can be referred to, which show the actual calculations used for the model with porosity $\epsilon = 0.51$.

3.2 Comparison of results

The values given by CFX for the dimensionless hydrodynamic permeability K (listed in Table 3.1), closely match those given, for the respective porosity, by the FD set of numerical results (FD_{num}) for a non-staggered configuration (SCASA), given in Table 2.2. However, the FD set of numerical results were obtained using pure Stokes' flow with no inertial influence, explaining the slight differences in the numerical values for some of the porosities. In Table 3.2 the results obtained by the FD analytical model (equation (2.54)) for a non-staggered configuration, i.e. $\lambda = 1$, $\gamma = 0$ and thus

$$K = \frac{(1 - \sqrt{1-\epsilon})^3}{12\sqrt{1-\epsilon}}, \tag{3.2}$$

are compared to those obtained by these two sets of numerical values for varying porosities.

	Dimensionless permeability K		
ϵ	FD_{an} (Equation (3.2))	FD_{num}	CFX
0.1164	1.91×10^{-5}	1.85×10^{-5}	1.85×10^{-5}
0.3600	8.33×10^{-4}	7.26×10^{-4}	7.24×10^{-4}
0.5100	3.21×10^{-3}	2.56×10^{-3}	2.56×10^{-3}
0.7500	2.08×10^{-2}	1.31×10^{-2}	1.28×10^{-2}
0.9100	9.53×10^{-2}	4.05×10^{-2}	4.05×10^{-2}

Table 3.2: Predictions of dimensionless hydrodynamic permeability, K.

These values are shown in Figure 3.2 on a log-lin scale. According to the results presented in Figure 3.2 the analytical model gives higher values than those obtained numerically, but is also evident that the model performs better at low porosities than at higher porosities. The reason for the discrepancies between the numerical results and the predictions of the FD equations at high porosities, were presumed to be due to the different physical character of the flow at high porosities, which is discussed in the following section.

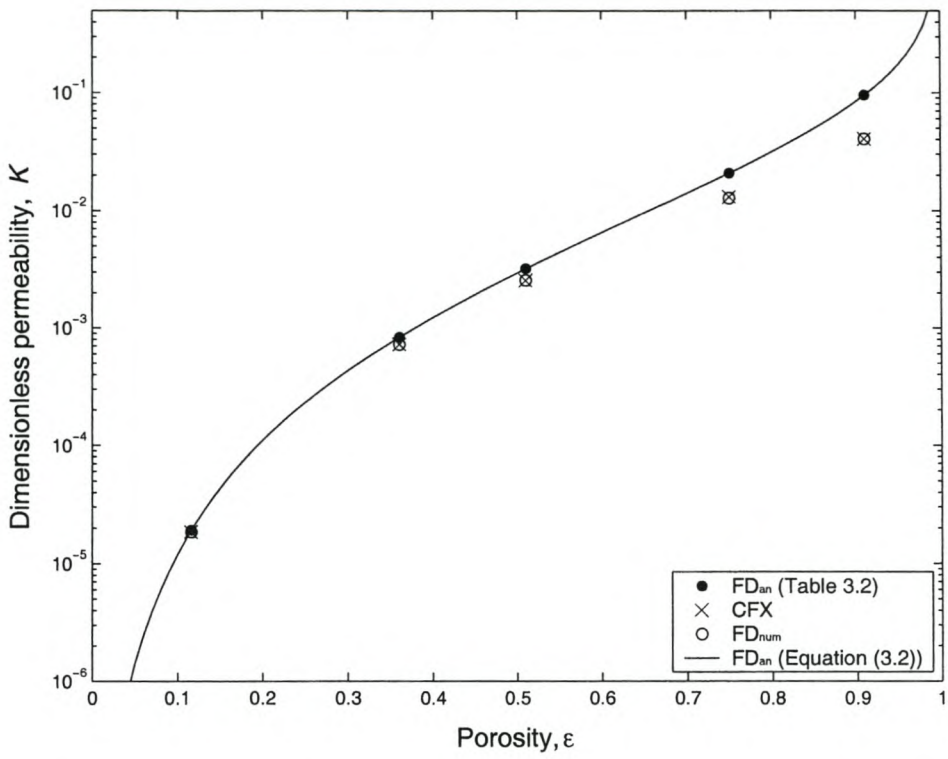

Figure 3.2: Predicted dimensionless permeability, K, for non-staggered configuration.

3.3 Analysing FD analytical model using CFX

In the FD analytical model the fluid volume is treated as three distinct volumes $U_{||}$, U_g and U_t each with their own characteristics. Using the CFX post-processor we consider each fluid volume, as shown in Figure 3.3, and attempt to verify the respective assumptions made on each of them. The model constructed, with porosity $\epsilon = 0.51$, was analysed thoroughly and the results for this specific case can be found from equations (B.4) to (B.7) in Appendix B.

Flow characteristics in streamwise channel

The FD analytical model assumes that plane Poiseuille flow is present in all the streamwise channels $U_{||}$, so that spatially constant wall shear stresses

$$\tau = \frac{6\,\mu\, w_{||}}{(d_{\perp} - d_{s\perp})} \tag{3.3}$$

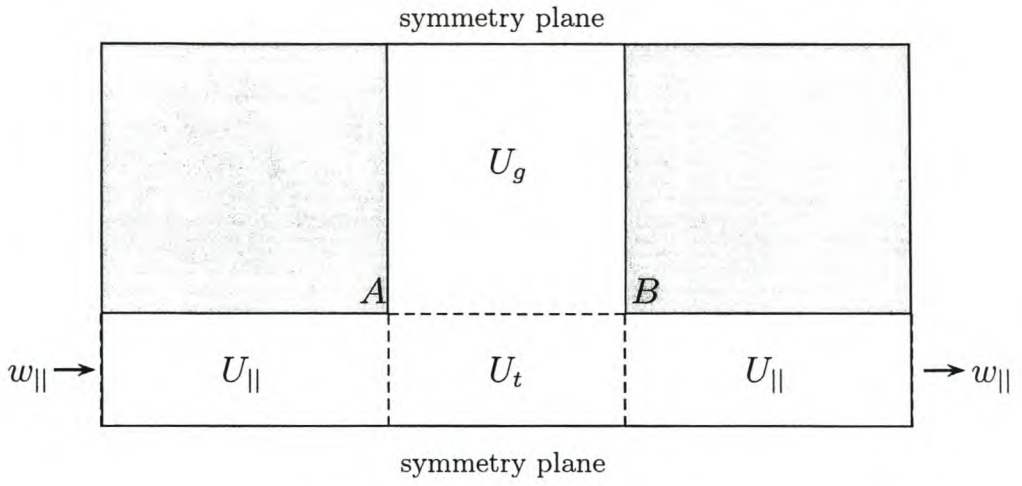

Figure 3.3: Top half of a unit cell constructed in CFX for a non-staggered configuration.

are created. The channel pressure gradient, $-\nabla_{||}p$, is therefore given by the equation

$$-\nabla_{||}p = \frac{12\,\mu\,w_{||}}{(d_\perp - d_{s\perp})^2} = \frac{12\,\mu\,q\,d_\perp}{(d_\perp - d_{s\perp})^3} = \frac{12\,\mu\,q}{d_\perp^2(1-\sqrt{1-\epsilon})^3} \tag{3.4}$$

and is constant for all streamwise channels. This is confirmed by using the numerical results obtained by CFX-5 (given in Table B.1 for the model with $\epsilon = 0.51$). We find that the channel pressure gradients are indeed constant in the all the streamwise volumes and from equations (B.4) and (B.5) we know that this pressure gradient can be calculated by assuming plane Poiseuille flow between the parallel plates as the FD analytical model does.

Flow characteristics in stagnant region

The model considers the volume U_g as a stagnant volume of fluid, where no shear stress, which can be attributed to the pressure gradient, is created by the solid surfaces. This region is assumed therefore not to contribute to the pressure gradient in the streamwise direction. The model assumes that, although streamlines may appear in this stagnant volume, the corresponding velocities will be very small and their lengths should therefore not contribute to the tortuosity of the medium.

The numerical results, however, show that wall shear stresses are created by the walls very close to the streamwise volume and that there exists a low pressure point at A in Figure 3.3 and a high pressure point at B in Figure 3.3 as can be seen in Figure B.3. Therefore

the stagnant volume does contribute to the pressure gradient in the streamwise direction (equation (B.7)), but this is a relatively small contribution and therefore it seems reasonable that it can be ignored, even for models of higher porosity.

Flow characteristics in transit region

The FD analytical model assumes the pressure drop to be zero in the transit region due to the absence of solid induced shear stresses. It is therefore assumed to simply act as a transfer volume for the fluid between the two adjacent shear-inducing pairs of parallel plates.

The CFX numerical results show however that there does in fact exist a pressure gradient across the transit region (equation (B.6)), probably caused by the change in the velocity profile on entering and exiting the parallel plate (streamwise) sections. This contribution was assumed to be negligible by the FD analytical model. However, even though this pressure gradient is smaller than the pressure gradient in the streamwise volume, for higher porosities this contribution to the overall pressure gradient should perhaps be taken into consideration in order to obtain more accurate predicted values.

Obviously for configurations of low porosities the transit region will be very small and will not contribute much to the overall pressure drop.

Chapter 4

Staggered configurations

4.1 Analysing FD analytical model using CFX

4.1.1 CFX modelling of FD analytical model

In an attempt to model the FD staggered configuration with a square array of solid blocks, a model, as shown in Figure 4.1, was constructed in CFX-5, for the porosities $\epsilon = 0.1164$, and 0.51. Once again it was chosen that more than one unit cell be constructed so as to obtain more realistic results and since the top and bottom halves of the unit cells are the same in this case, a symmetry plane was used and only the top halves of the unit cells were constructed.

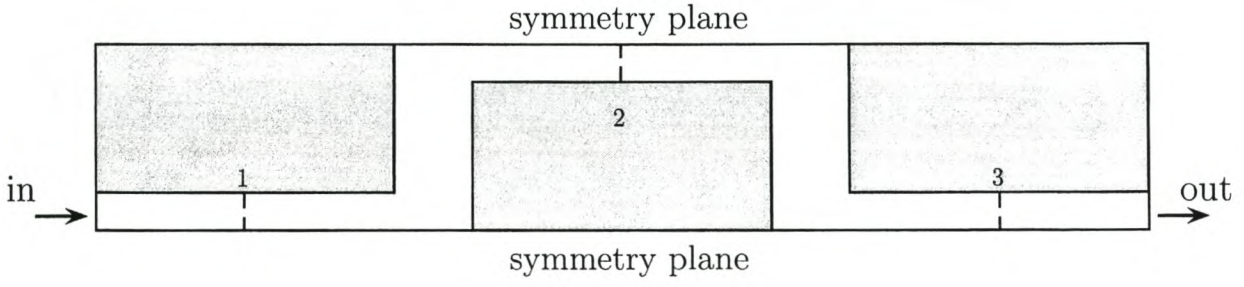

Figure 4.1: Construction used in CFX modelling for streamwise staggering.

Using the CFX-5 post processor, planes were created at positions 1, 2 and 3 as indicated in Figure 4.1. Numerical values for the average velocity and pressure on the planes were obtained, allowing the change in pressure through a unit cell to be calculated. The average velocities $w_{||}$, at the planes were all the same for the respective porosities. The numerical values obtained using the CFX-5 model are given in Table 4.1 for the two models. These values are very similar to the previously attained numerical results and therefore there was no need to construct models for a wider selection of porosities as the results obtained previously, could be used.

ϵ	$\Delta p\ [Pa]$	$d_{\perp}\ [m]$	$w_{\|\|}\ [m/s]$	$q\ [m/s]$	K
0.1164	3.612×10^{-1}	0.01	8.92×10^{-4}	5.35×10^{-5}	1.48×10^{-5}
0.5100	3.802×10^{-3}	0.01	2.57×10^{-4}	7.72×10^{-5}	2.03×10^{-3}

Table 4.1: Numerical values (SI) obtained using CFX for the staggered case.

4.1.2 Comparison of FD and CFX results

In the case of a staggered configuration with a square array of solid blocks (where $\lambda = 1$, and $\gamma = 1$), equation (2.54), reduces to

$$K = \frac{\left(1-\sqrt{1-\epsilon}\right)^3}{15\sqrt{1-\epsilon}}. \tag{4.1}$$

Table 4.2 shows the comparison between the results predicted by this equation and those obtained numerically. As can be seen from the table, the CFX numerical results obtained are very similar to the FD numerical results obtained, therefore there was no need to obtain more numerical results for all selected porosities.

The values given in Table 4.2 are shown on a log-lin scale graph, Figure 4.2.

ϵ	Dimensionless permeability K		
	FD_{an} (Equation (4.1))	FD_{num}	CFX
0.1164	1.53×10^{-5}		1.48×10^{-5}
0.3600	6.67×10^{-4}	5.75×10^{-4}	
0.5100	2.57×10^{-3}	2.02×10^{-3}	2.03×10^{-3}
0.7500	1.67×10^{-2}	1.06×10^{-2}	
0.9100	7.62×10^{-2}	3.63×10^{-2}	

Table 4.2: Numerical predictions of the dimensionless permeability, K.

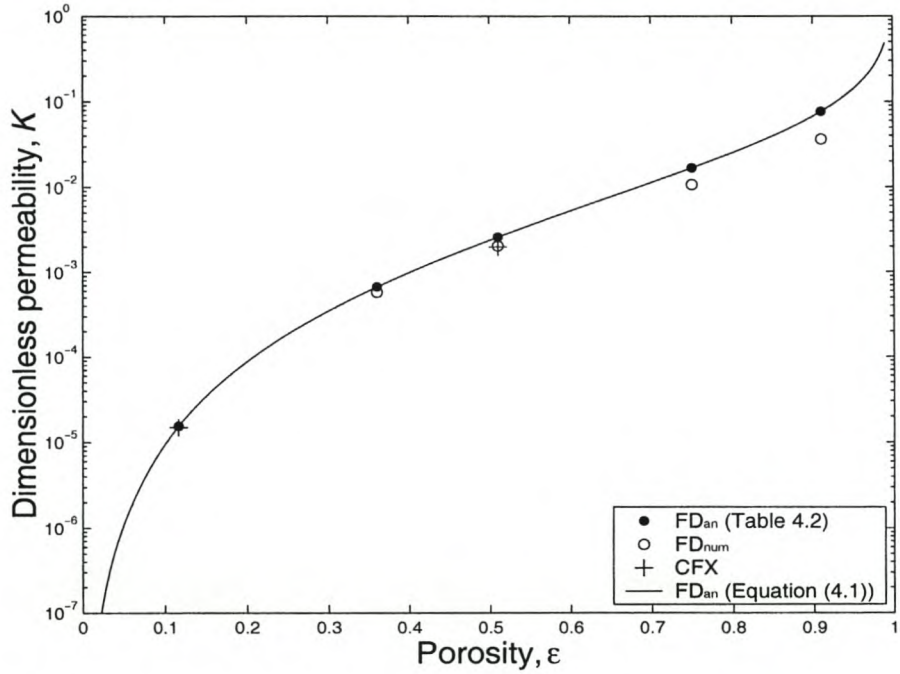

Figure 4.2: Predicted dimensionless permeability, K, for staggered configuration.

Once again, it is evident that the model performs well at low porosities but at high porosities there are discrepancies between the predictions of equation (2.54) and the numerical results. This is assumed to be because of the distinct physical character of the flow at high porosities, which is discussed later in the next section. The physics involved at higher porosities are markedly different from the parallel plate Stokes flow which forms the basis of the present predictive model.

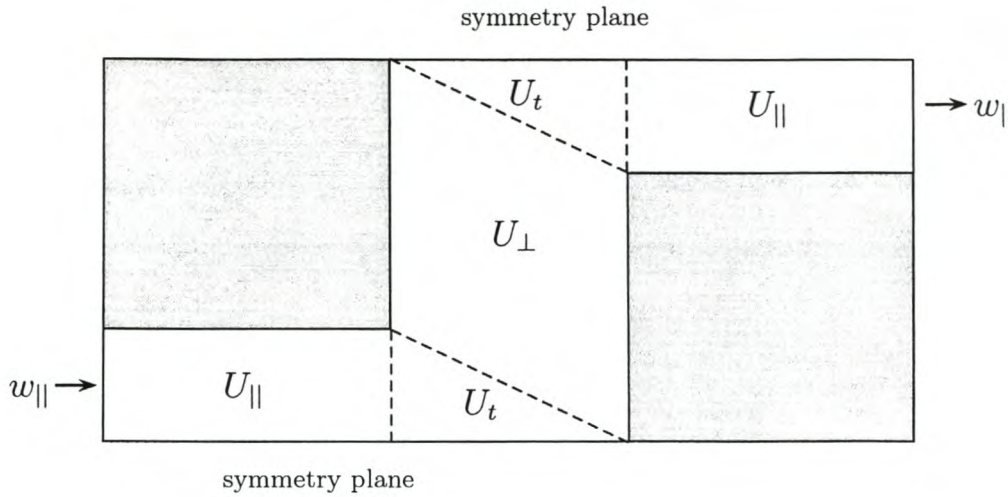

Figure 4.3: Top half of a unit cell constructed in CFX for a model with $\epsilon = 0.51$.

4.1.3 Analysing the fluid volumes using CFX

In the FD staggered model the fluid volume is treated as three distinct volumes $U_{||}$, $U_\perp$ and U_t as shown in Figure 4.3. Using the CFX post-processor we attempt to verify the assumptions made by the model by considering the three volumes separately. The model constructed with porosity $\epsilon = 0.1164$ was analysed more thoroughly and the results for this specific case can be found from equations (C.5) to (C.8) in Appendix C.

Flow characteristics in streamwise channel

In the streamwise channels, between all pairs of parallel plates, the FD analytical model assumes that plane Poiseuille flow is present. Constant wall shear stresses

$$\tau = \frac{6\,\mu\,w_{||}}{(d_\perp - d_{s\perp})} \tag{4.2}$$

are therefore assumed to be created in this region and the channel pressure gradient, $-\nabla_{||}p$, is given by the equation

$$-\nabla_{||}p = \frac{12\,\mu\,w_{||}}{(d_\perp - d_{s\perp})^2} = \frac{12\,\mu\,q\,d_\perp}{(d_\perp - d_{s\perp})^3} = \frac{12\,\mu\,q}{d_\perp^2(1-\sqrt{1-\epsilon})^3} \tag{4.3}$$

and is constant for all streamwise channels.

Using the numerical results obtained by CFX-5 (given in Table C.1 for the model of $\epsilon = 0.1164$), we find that the channel pressure gradients are indeed constant in the all the streamwise volumes. From equations (C.5) and (C.6) we know that this pressure gradient can be calculated by assuming plane Poiseuille flow between the parallel plates as in the case of the FD analytical model.

Flow characteristics in transverse channel

In the transverse channel the model again assumes that plane Poiseuille flow is present between all pairs of parallel plates. Using the numerical values obtained by CFX-5 (equation (C.8) for the model of porosity $\epsilon = 0.1164$), we know that, for configurations of low porosities, parallel plate flow does occur in the transverse region, with the average flow being half the value of the average flow velocity in the streamwise region, as assumed by the model.

However at high porosities these parallel plates will not be opposite to one other, resulting in parallel plate flow not necessarily being present. This probably contributes greatly to the deviation of the predictions of the model from the numerical results at high porosities.

We can conclude therefore, that the physics involved at higher porosities are different from the parallel plate Stokes flow which forms the basis of the FD analytical model and therefore an alternative model should be considered for configurations of high porosity.

4.2 Analysing the RRUC model using CFX

4.2.1 CFX modelling for RRUC model

In an attempt to model the maximally streamwise staggered configuration used in the RRUC model, models similar to the one shown in Figure 4.4 were constructed in CFX-5, for a selection of porosities $\epsilon = 0.1164$, 0.36, 0.51 and 0.75. Since, as already mentioned, we did not succeed in constructing a repetitive boundary on the inlet using the CFX package, it was chosen that a few unit cells be constructed in line so as to obtain more realistic results for

infinitely long arrays of obstacles. Since for the RRUC model we assumed there are parallel plates in the streamwise direction, it was chosen to position the opposite plates as shown in Figure 4.4.

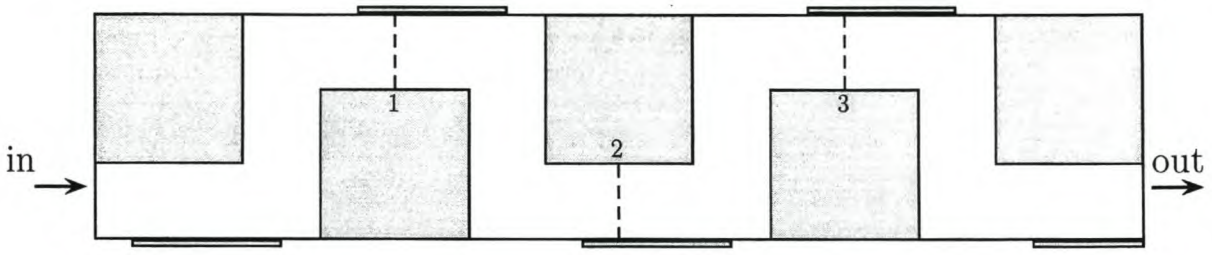

Figure 4.4: Construction used in CFX modelling for maximal streamwise staggering.

As with the analytical model, all walls are assumed to be no-slip walls. The CFX-5 post processor was used to analyse the model. Planes were created at positions 1, 2 and 3 as indicated in Figure 4.4. Numerical values for the average velocity and pressure on the planes were obtained. These allowed us to calculate the change in pressure through a unit cell. As predicted it was found that the average velocities at the planes were all the same for the respective porosities. The numerical values obtained using the CFX-5 model are given in Table 4.3 for models with varying porosities.

ϵ	χ	$\Delta p\ [Pa]$	$d_\perp\ [m]$	$w_{\|\|}\ [m/s]$	$q\ [m/s]$	K
0.1164	1.94	0.2227	0.005	1.81×10^{-4}	1.09×10^{-5}	9.75×10^{-6}
0.3600	1.8	0.2240	0.005	2.33×10^{-3}	4.66×10^{-4}	4.16×10^{-4}
0.5100	1.7	0.0222	0.005	5.93×10^{-4}	1.78×10^{-4}	1.60×10^{-3}
0.7500	1.5	0.0228	0.005	2.20×10^{-3}	1.10×10^{-3}	9.62×10^{-3}

Table 4.3: Numerical values (SI) obtained using CFX for the RRUC staggered configuration.

4.2.2 Comparison of RRUC and CFX Results

In Table 4.4 the predicted values for the dimensionless permeability, K, obtained using the RRUC equation (equation (2.36)) and the numerical values obtained from CFX-5 are

compared. The results given in Table 4.4 are plotted on a lin-log graph, shown in Figure 4.5.

	Dimensionless permeability K	
ϵ	RRUC (Equation (2.36))	CFX
0.1164	1.86×10^{-5}	9.75×10^{-6}
0.3600	7.50×10^{-4}	4.16×10^{-4}
0.5100	2.73×10^{-3}	1.60×10^{-3}
0.7500	1.56×10^{-2}	9.62×10^{-3}
0.9100	6.19×10^{-2}	

Table 4.4: Numerical predictions of the dimensionless permeability, K.

As can be seen from Table 4.4 and Figure 4.5, the RRUC model does not give very accurate predictions for the dimensionless permeability, since the predicted values differ by almost a factor of two to the CFX numerical results. On further analysis it was found that the difference is actually a factor of the respective tortuosity. This is discussed further in the following chapters.

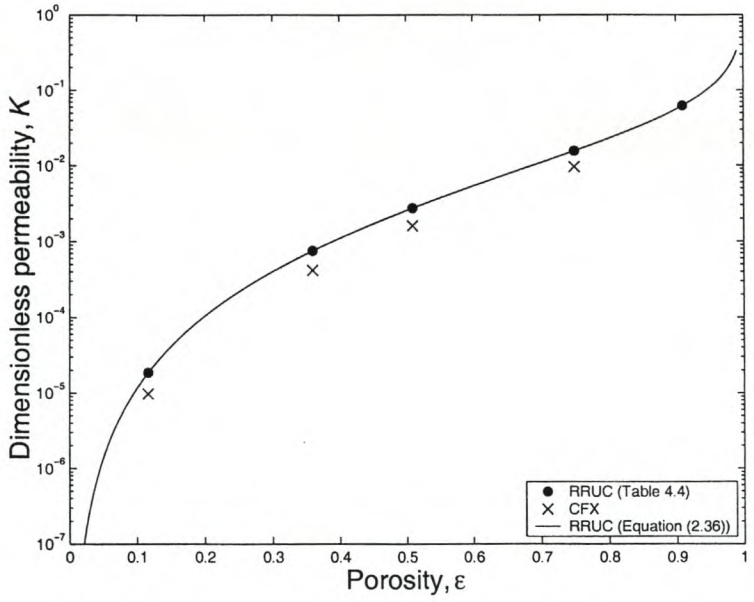

Figure 4.5: Dimensionless predicted permeability, K, for the RRUC staggered configuration.

Chapter 5

Modelling with pore-scale volumes

5.1 Definition of volumes

The RRUC and FD analytical models are defined using different 'volumes' and so, in an attempt to compare these two models, it is necessary to first define volumes that are applicable to both models.

For both the non-staggered and staggered configurations, the volumes can be defined as follows: U_o is the total volume including all fluid U_f and solid U_s volumes, so that

$$U_o = U_f + U_s. \tag{5.1}$$

The fluid volume U_f is comprised of four volumes, namely the streamwise volume $U_{||}$, the fluid volume between the solids where the flow is in the perpendicular direction $U_\perp$, the transfer volume U_t and the stagnant fluid volume U_g, i.e.

$$U_f = U_{||} + U_\perp + U_t + U_g. \tag{5.2}$$

We now consider a two-dimensional situation, where $U_s = d_{s||}\, d_{s\perp}$ is the volume of the solid rectangle embedded in a total volume $U_o = d_{||}\, d_\perp$, for both the non-staggered and staggered configurations.

5.1.1 Non-staggered Configuration

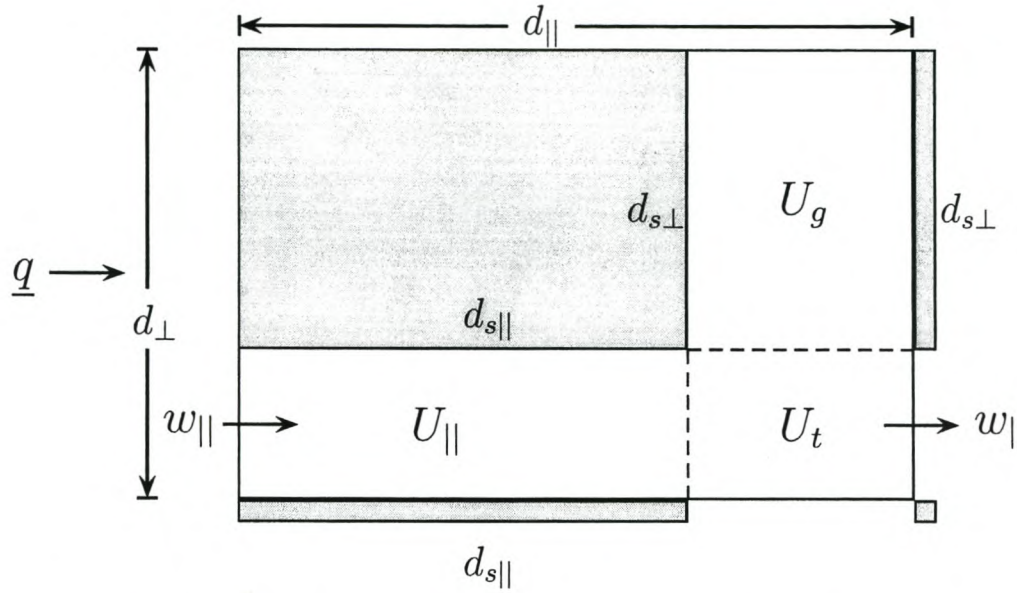

Figure 5.1: Unit cell geometry in case of no streamwise staggering.

We first consider a two-dimensional non-staggered configuration, as shown in Figure 5.1. Since the fluid only moves in the streamwise direction, there are no $U_\perp$ volumes, but there do exist stagnant volumes between the solids in the streamwise direction. In terms of the lengths as shown in Figure 5.1 the volumes for a non-staggered configuration can be expressed as listed in Table 5.1.

U_o	$d_{\|\|}\, d_\perp$
U_s	$d_{s\|\|}\, d_{s\perp}$
U_f	$d_{\|\|}\, d_\perp - d_{s\|\|}\, d_{s\perp}$
$U_{\|\|}$	$d_{s\|\|}\, (d_\perp - d_{s\perp})$
U_t	$(d_\perp - d_{s\perp})\, (d_{\|\|} - d_{s\|\|})$
U_g	$d_{s\perp}\, (d_{\|\|} - d_{s\|\|})$.

Table 5.1: Expressions for volumes in a non-staggered configuration.

5.1.2 Staggered Configuration

We now consider the two-dimensional RRUC staggered configuration, as shown in Figure 5.2, and the two-dimensional FD staggered configuration, as shown in Figure 5.3.

In both the staggered configurations there are no stagnant volumes U_g however the fluid flows perpendicularly between the solids in the streamwise direction and so $U_\perp$ exists. The total of the respective volumes are the same for both configurations and can be expressed in terms of the lengths given in Figure 5.2 and in Figure 5.3, as listed in Table 5.2.

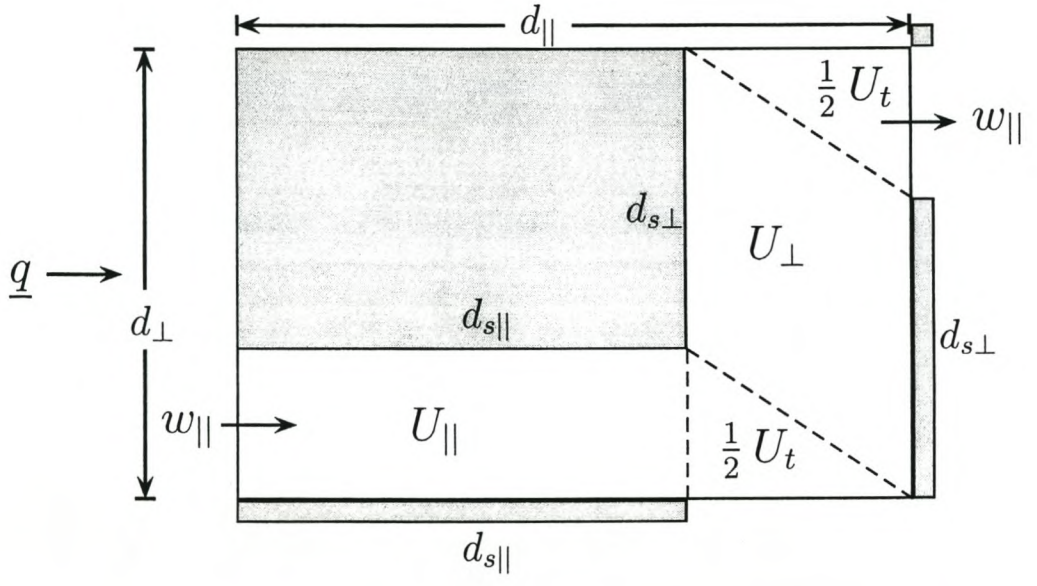

Figure 5.2: Unit cell geometry in case of RRUC streamwise staggering.

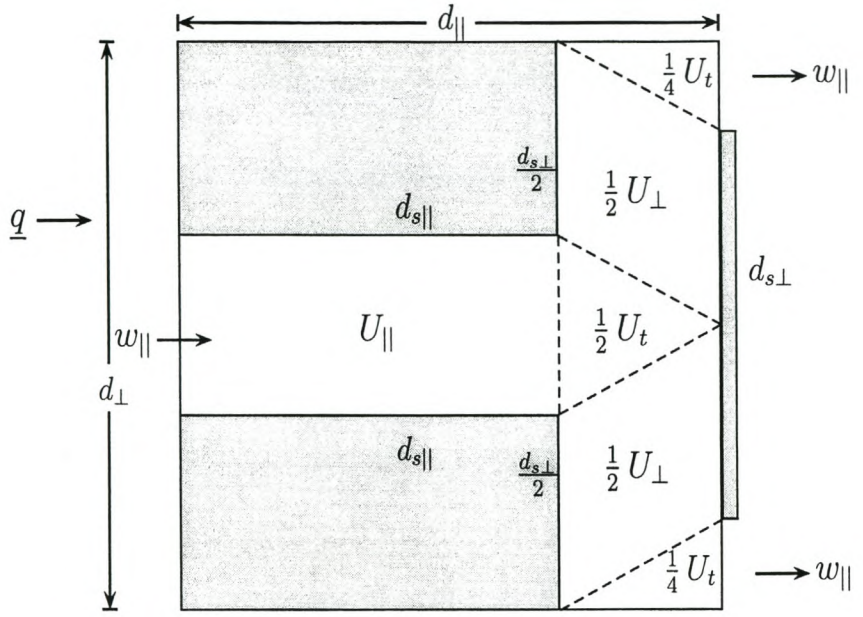

Figure 5.3: Unit cell geometry in case of FD streamwise staggering.

U_o	$d_{\|\|}\, d_\perp$
U_s	$d_{s\|\|}\, d_{s\perp}$
U_f	$d_{\|\|}\, d_\perp - d_{s\|\|}\, d_{s\perp}$
$U_{\|\|}$	$d_{s\|\|}\, (d_\perp - d_{s\perp})$
$U_\perp$	$d_{s\perp}\, (d_{\|\|} - d_{s\|\|})$
U_t	$(d_\perp - d_{s\perp})\, (d_{\|\|} - d_{s\|\|})$

Table 5.2: Expressions for volumes in a staggered configuration.

The volumes that have been defined here are very similar to those defined in the rectangular representation of the FD analytical model, in Section 2.2.1.

5.1.3 Tortuosity

The tortuosity of streamlines in a porous medium can be considered as a measure of the non-straightness of streamlines in the pore space, as stated in Section 2.1.3. Piecewise straight streamlines between and parallel to the plates, as shown in Figure 2.1, are assumed for the staggered configuration and piecewise straight streamlines in the streamwise direction are assumed in the volumes $U_{||}$ and U_t for the non-staggered configurations.

The most basic definition of tortuosity is the path length tortuosity [3], which is defined as the ratio of the average length of the tortuous flow path L_e to the straight line length L in the streamwise direction, namely

$$\chi \equiv \frac{L_e}{L}. \tag{5.3}$$

According to the rectangular geometry and associated assumptions all the streamlines in the staggered configuration are of equal length L_e. For the RRUC model $L_e = d_{||} + d_{s\perp}$ and for the FD analytical model $L_e = d_{||} + \frac{d_{s\perp}}{2}$. The straight line length is $L = d_{||}$ for both configurations. Therefore, in terms of the volumes defined in the previous section, the tortuosity can be given as

$$\chi = \frac{U_f}{U_{||} + U_t} = \frac{U_{||} + U_t + U_\perp}{U_{||} + U_t}, \tag{5.4}$$

for the RRUC staggered configuration and

$$\chi = \frac{U_f - \frac{1}{2}U_\perp}{U_{||} + U_t} = \frac{U_{||} + U_t + \frac{1}{2}U_\perp}{U_{||} + U_t}, \tag{5.5}$$

for the FD staggered configuration.

The tortuosity for the non-staggered configuration is

$$\chi = 1, \tag{5.6}$$

since the streamlines are straight lines in the streamwise direction. Figure 5.4 shows graphically the comparison between the tortuosity of the staggered configurations and non-staggered configuration for the respective porosity.

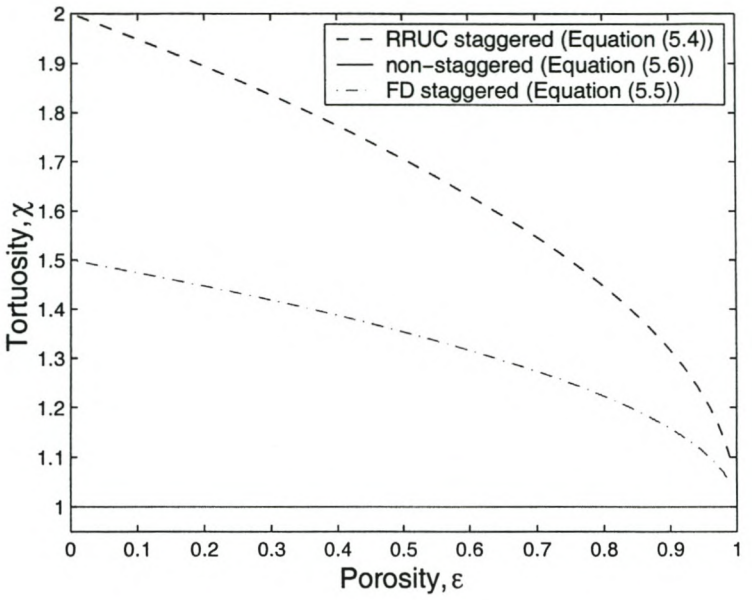

Figure 5.4: The comparison of tortuosity for staggered and non-staggered configurations.

In order to obtain a general equation for the tortuosity, we introduce a velocity ratio β, so that $w_\perp = \beta\, w_{||}$. The following equation can thus be used to calculate the tortuosity of all the configurations mentioned in this work:

$$\chi = \frac{U_{||} + U_t + \beta\, U_\perp}{U_{||} + U_t} = 1 + \frac{\beta\, U_\perp}{U_{||} + U_t}. \tag{5.7}$$

If equation (5.7) is used for the tortuosity, it should be noted that equation (2.16) will not hold, unless $\beta = 1$.

Chapter 6

Analysis of pressure averaging equation

The volume averaging equation [22] applied to the pressure variable is as follows:

$$\langle \nabla p \rangle = \nabla \langle p \rangle + \frac{1}{U_o} \iint_{S_{fs}} \underline{n} p \, dS. \tag{6.1}$$

In this chapter this equation will be closely analysed towards the discrepancy encountered with the predictions of the RRUC model.

6.1 Non-staggered configuration

We now look at each term in equation (6.1) by considering the rectangular representation of a porous medium for a non-staggered configuration shown in Figure 6.1. Each term of this equation can be written in terms of symbols, where Δp is the total change in pressure in the streamwise volume, as indicated in Figure 6.1.

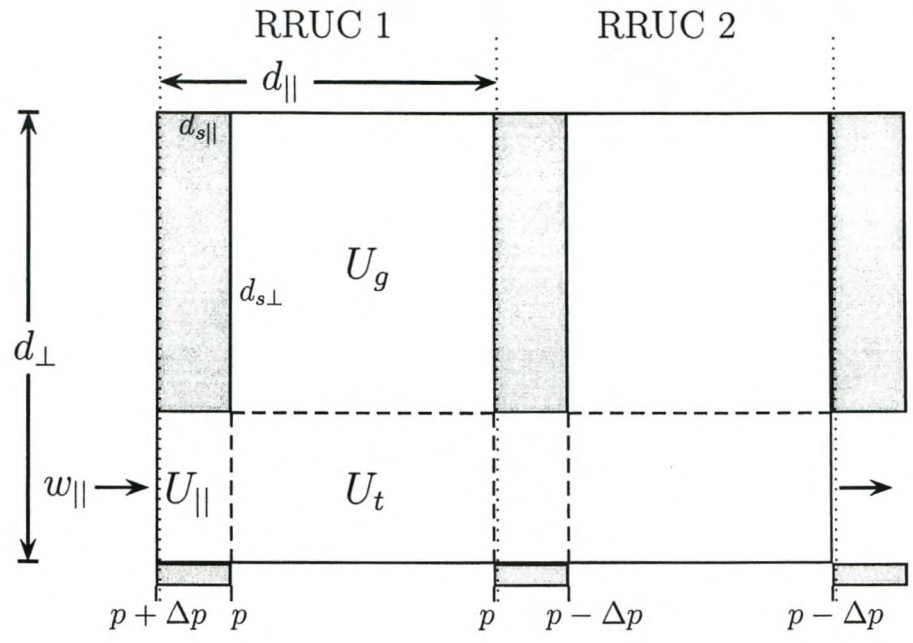

Figure 6.1: Unit cell geometry in case of no streamwise staggering (first case).

First case

We first consider a unit cell, where the boundaries in the perpendicular direction of the unit cell go through the solid region, as indicated by RRUC 1 (RRUC 2 is therefore the neighbouring unit cell in this case) in Figure 6.1. In terms of symbols, the first term in equation (6.1) can be expressed as follows:

$$\begin{aligned} \langle \nabla p \rangle &= \frac{1}{U_o} \iiint_{U_f} \nabla p \, dU \\ &= \frac{1}{U_o} \left(\iiint_{U_{||}} \nabla p \, dU + \iiint_{U_t} \nabla p \, dU + \iiint_{U_g} \nabla p \, dU \right). \end{aligned} \tag{6.2}$$

Since the pressure is constant in both the transfer and the stagnant volumes, the pressure gradient will be zero here. Therefore we have

$$\begin{aligned}\langle \nabla p \rangle &= -\frac{1}{U_o}\left[\frac{\Delta p}{d_{s||}}.U_{||}\right] \\ &= -\frac{U_{||}}{U_o}\left[\frac{\Delta p}{d_{s||}}\right]. \end{aligned} \tag{6.3}$$

The second term in equation (6.1) can be expressed as:

$$\nabla \langle p \rangle = \nabla \frac{1}{U_o} \iiint_{U_f} p \, dU = \frac{1}{U_o} \nabla \iiint_{U_f} p \, dU. \tag{6.4}$$

If we consider two streamwisely adjacent RRUCs, as shown in Figure 6.1, and take the gradient of their two pressure averages we obtain the following

$$\begin{aligned}\nabla \langle p \rangle &= \frac{1}{U_o}\left(\frac{\left[(p-\frac{\Delta p}{2})U_{||} + (p-\Delta p)\,U_t + (p-\Delta p)\,U_g\right]}{d_{||}}\right. \\ &\quad \left. - \frac{\left[(p+\frac{\Delta p}{2})\,U_{||} + p\,U_t + p\,U_g\right]}{d_{||}}\right) \qquad (6.5) \\ &= -\frac{1}{U_o}\left(\frac{\Delta p U_{||} + \Delta p U_t + \Delta p U_g}{d_{||}}\right) \\ &= -\frac{U_f}{U_o}\left[\frac{\Delta p}{d_{||}}\right]. \qquad (6.6)\end{aligned}$$

The surface integral term is zero in this case,

$$\frac{1}{U_o} \iint_{S_{fs}} \underline{n}\, p \, dS = 0, \tag{6.7}$$

since the pressure at the walls will cancel out.

The above results for the three terms will be true for all RRUCs whose boundaries cut through the solid rectangle (i.e. for $d_{s||}/d_{||}$ of the possible RRUCs if shifted in the streamwise direction).

Second case

If we now shift the unit cell in the streamwise direction so that its boundaries do not pass through the solid region (i.e. consider the unit cell to be as shown in Figure 6.2), the surface integral term will not be zero, but the other two terms in the pressure averaging equation will be the same, as shown below. This will be true for all RRUCs whose boundaries do not cut through the solid rectangle (i.e. for $1 - d_{s||}/d_{||}$ of the cases).

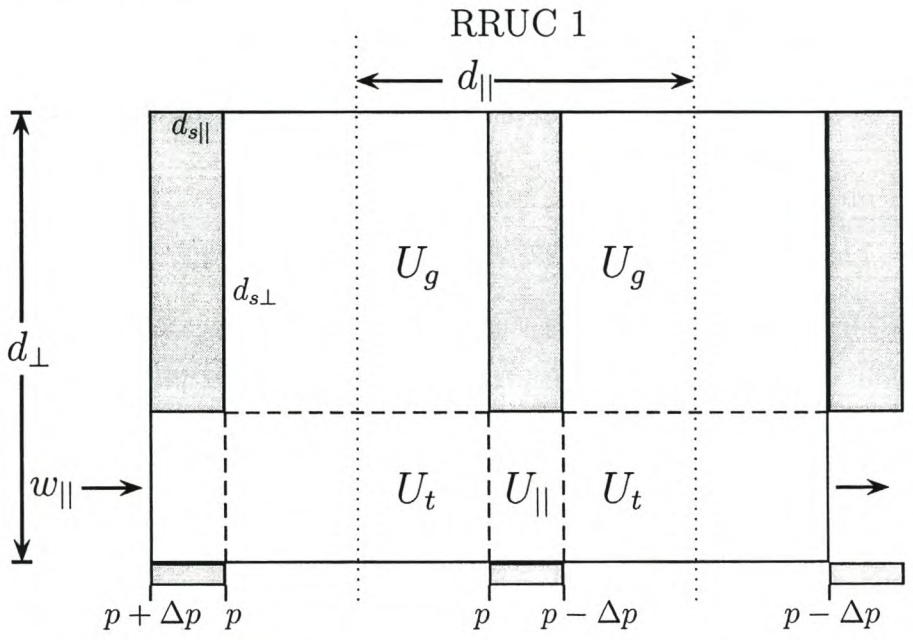

Figure 6.2: Unit cell geometry in case of no streamwise staggering (second case).

In this case the first term of equation (6.1) will be the same as for the first case, as shown below:

$$\begin{aligned}\langle \nabla p \rangle &= \frac{1}{U_o} \iiint_{U_f} \nabla p \, dU \\ &= \frac{1}{U_o} \left(\iiint_{U_{||}} \nabla p \, dU + \iiint_{U_t} \nabla p \, dU + \iiint_{U_g} \nabla p \, dU \right). \end{aligned} \tag{6.8}$$

Since the pressure is constant in both the transfer and the stagnant volumes, the pressure gradient will be zero here. Therefore we have

$$\begin{aligned} \langle \nabla p \rangle &= -\frac{1}{U_o}\left[\frac{\Delta p}{d_{s||}}.U_{||}\right] \\ &= -\frac{U_{||}}{U_o}\left[\frac{\Delta p}{d_{s||}}\right]. \end{aligned} \tag{6.9}$$

The second term of equation (6.1) is given by:

$$\nabla \langle p \rangle = \frac{1}{U_o} \nabla \iiint_{U_f} p \, dU. \tag{6.10}$$

If we consider two streamwisely adjacent RRUCs, similar to the one shown in Figure 6.2, and take the gradient of their two pressure averages we obtain the following

$$\begin{aligned} \nabla \langle p \rangle &= -\frac{1}{U_o}\left(\frac{\Delta p U_{||} + \Delta p U_t + \Delta p U_g}{d_{||}}\right) \\ &= -\frac{U_f}{U_o}\left[\frac{\Delta p}{d_{||}}\right]. \end{aligned} \tag{6.11}$$

This can be shown by considering each component of the volumes separately and realising that they all differ by Δp to the corresponding component in the neighbouring RRUC.

The surface integral term is not zero, yielding

$$\begin{aligned} \frac{1}{U_o} \iint_{S_{fs}} \underline{n} p \, dS &= \frac{1}{U_o}\left(p \, d_{s\perp} - [p - \Delta p] \, d_{s\perp}\right) \\ &= \frac{d_{s\perp}}{U_o}(\Delta p) \end{aligned} \tag{6.12}$$

in this case.

Combination of Cases 1 and 2

Combining cases 1 and 2 we obtain the overall value for each term in equation (6.1) for a non-staggered configuration:

$$\langle \nabla p \rangle = -\frac{U_{||}}{U_o}\left(\frac{\Delta p}{d_{s||}}\right), \tag{6.13}$$

$$\nabla \langle p \rangle = -\frac{U_f}{U_o}\left(\frac{\Delta p}{d_{||}}\right), \tag{6.14}$$

$$\begin{aligned}\frac{1}{U_o}\iint_{S_{fs}} \underline{n}\, p\, dS &= \frac{(d_{||}-d_{s||})}{d_{||}}\left[\frac{d_{s\perp}}{U_o}(\Delta p)\right] + \frac{d_{s||}}{d_{||}}(0) \\ &= \frac{(d_{||}-d_{s||})}{d_{||}}\left[\frac{d_{s\perp}}{U_o}(\Delta p)\right].\end{aligned} \tag{6.15}$$

Checking equation (6.1), with the help of Table 5.1, we obtain the following:

$$\begin{aligned}\langle \nabla p \rangle &= \nabla \langle p \rangle + \frac{1}{U_o}\iint_{S_{fs}} \underline{n}\, p\, dS \\ &= -\frac{U_f}{U_o}\left(\frac{\Delta p}{d_{||}}\right) + \frac{(d_{||}-d_{s||})}{d_{||}}\left(\frac{d_{s\perp}}{U_o}\Delta p\right) \\ &= -\frac{\Delta p}{U_o}\cdot\left(\frac{U_f - U_g}{d_{||}}\right) \\ &= -\frac{\Delta p}{U_o}\cdot\left(\frac{(d_{||}d_{\perp} - d_{s||}d_{s\perp}) - (d_{||}-d_{s||})\,d_{s\perp}}{d_{||}}\right) \\ &= -\frac{\Delta p}{U_o}\cdot\left(\frac{(d_{\perp}-d_{s\perp})\,d_{||}}{d_{||}}\cdot\frac{d_{s||}}{d_{s||}}\right) \\ &= -\frac{U_{||}}{U_o}\cdot\frac{\Delta p}{d_{s||}},\end{aligned} \tag{6.16}$$

which agrees with equation (6.13). Comparing equation (6.13) with equation (6.14) we find that

$$
\begin{aligned}
-\langle \nabla p \rangle &= \frac{U_{||}}{U_o}\left[\frac{\Delta p}{d_{s||}}\right] \\
&= \left(\frac{(d_\perp - d_{s\perp})\, d_{s||}}{d_{||}\, d_\perp}\right).\frac{\Delta p}{d_{s||}} \\
&= \left(\frac{(d_\perp - d_{s\perp})\, d_{||}}{d_{||}\, d_\perp}\right).\frac{\Delta p}{d_{||}} \\
&= \left(\frac{(d_\perp - d_{s\perp})\, d_{s||} + (d_\perp - d_{s\perp})\,(d_{||} - d_{s||})}{d_{||}\, d_\perp}\right).\frac{\Delta p}{d_{||}} \\
&= \left(\frac{U_{||} + U_t}{U_o}\right).\frac{\Delta p}{d_{||}} \qquad (6.17)
\end{aligned}
$$

Therefore from equation (6.14) and equation (6.17) we can conclude that

$$
\boxed{\langle \nabla p \rangle = \left(\frac{U_{||} + U_t}{U_f}\right).\nabla \langle p \rangle .} \qquad (6.18)
$$

This is an important result as it provides us with a connection between the average pressure gradient and the gradient of the pressure average for a non-staggered configuration.

Combining equations (6.1) and (6.18) we have

$$
\nabla \langle p \rangle + \frac{1}{U_o} \iint_{S_{fs}} \underline{n}\, p \, dS = \left(\frac{U_{||} + U_t}{U_f}\right).\nabla \langle p \rangle , \qquad (6.19)
$$

and therefore

$$
\begin{aligned}
\frac{1}{U_o} \iint_{S_{fs}} \underline{n}\, p \, dS &= \left(\frac{U_{||} + U_t}{U_f}\right).\nabla \langle p \rangle - \nabla \langle p \rangle \\
&= \left(\frac{U_{||} + U_t}{U_f} - 1\right).\nabla \langle p \rangle . \qquad (6.20)
\end{aligned}
$$

Equation (6.20) can now be used to express the surface integral, in the pressure averaging equation (equation (6.1)) for a non-staggered configuration, in terms of pore-scale volumes and the gradient of the pressure average.

6.2 Non-staggered RRUC model

It is now proposed to generalise the RRUC model to also fit a configuration where no staggering takes place in the streamwise direction (as in the configuration for the FD non-staggered model), i.e. where the solid rectangles are lined up in straight rows in the streamwise direction, as shown in Figure 6.3.

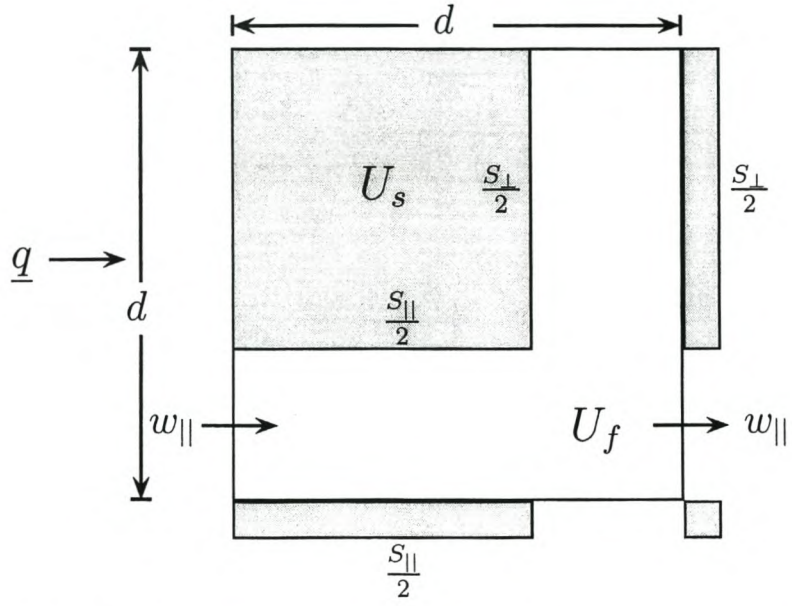

Figure 6.3: Unit cell geometry of an RRUC for a non-staggered configuration.

We start with the simplified volume averaged Navier-Stokes equation (equation (2.13))

$$-\epsilon \nabla p_f = \frac{1}{U_0} \iint_{S_{fs}} \left(\underline{n} \{p\} - \underline{n} \cdot \underline{\underline{\tau}} \right) dS, \tag{6.21}$$

which assumes uniform discharge through a homogeneous isotropic porous medium. From equation (2.6) we have

$$\frac{1}{U_0} \iint_{S_{fs}} \underline{n} \{p\} dS = \frac{1}{U_0} \iint_{S_{fs}} \underline{n} p dS - \frac{1}{U_0} \iint_{S_{fs}} \underline{n} \langle p \rangle_f dS, \tag{6.22}$$

and since $\langle p \rangle_f$ is assumed to be constant over the RRUC, the last term in equation (6.22) is zero and the simplified volume averaged Navier-Stokes equation can be rewritten as

$$-\epsilon \nabla p_f = \frac{1}{U_0} \iint_{S_{fs}} \left(\underline{n} p - \underline{n} \cdot \underline{\underline{\tau}} \right) dS. \tag{6.23}$$

We consider just the Darcy regime of pure viscous drag at low Reynolds number ($Re_p << 1$). No flow is assumed in the transverse pore sections, hence no shear stresses are developed in these sections. The transverse pore sections can thus be considered as stagnant volumes U_g. Therefore equation (6.23) can be written as

$$-\epsilon \nabla p_f = \frac{1}{U_0} \iint_{S_{||}} \left(-\underline{n} \cdot \underline{\underline{\tau}} \right) dS + \frac{1}{U_0} \iint_{S_{fs}} \left(\underline{n} p \right) dS. \tag{6.24}$$

Substituting equation (6.20) into this equation we obtain

$$-\epsilon \nabla p_f = \frac{1}{U_0} \iint_{S_{||}} \left(-\underline{n} \cdot \underline{\underline{\tau}} \right) dS + \left(\frac{U_{||} + U_t}{U_f} - 1 \right) . \nabla \langle p \rangle , \tag{6.25}$$

which can be rewritten as

$$-\left(\frac{U_{||} + U_t}{U_f} \right) \epsilon \nabla p_f = \frac{1}{U_0} \iint_{S_{||}} \left(-\underline{n} \cdot \underline{\underline{\tau}} \right) dS, \tag{6.26}$$

since, for constant ϵ,

$$\begin{aligned} \epsilon \nabla p_f &= \frac{U_f}{U_o} \nabla \frac{1}{U_f} \iiint_{U_f} p \, dU \\ &= \nabla \frac{1}{U_0} \iiint_{U_f} p \, dU \\ &= \nabla \langle p \rangle . \end{aligned} \tag{6.27}$$

If the wall shear stress is assumed to be uniform and equal to a constant, τ_w, over $S_{||}$ equation (6.26) reduces further to

$$\boxed{-\left(\frac{U_{||}+U_t}{U_o}\right)\nabla p_f \;=\; \hat{\underline{n}}\,\frac{1}{U_0}\iint_{S_{||}}\tau_w\,dS.} \tag{6.28}$$

For Newtonian flow between parallel plates a distance d_p apart and, if the average velocity in the streamwise area is $\underline{w}_{||}$, it follows that

$$-\left(\frac{U_{||}+U_t}{U_o}\right)\nabla p_f \;=\; \left(\frac{S_{||}}{U_o}\right).\left(\frac{6\,\mu\,w_{||}}{d_p}\right)\hat{\underline{n}} \;=\; \frac{S_{||}}{U_o}.\frac{6}{d_p}\left(\frac{U_o}{U_{||}+U_t}\right)\mu\,\underline{q}. \tag{6.29}$$

If we then define

$$G_o \;\equiv\; \frac{6}{d_p}\left(\frac{U_o}{U_{||}+U_t}\right)\frac{S_{||}}{U_o} \;=\; \frac{6}{\epsilon\,d_p}\left(\frac{U_f}{U_{||}+U_t}\right)\frac{S_{||}}{U_o} \tag{6.30}$$

the momentum transport equation for uniform average flow for a non-staggered configuration becomes

$$-\left(\frac{U_{||}+U_t}{U_o}\right)\nabla p_f \;=\; G_o\,\mu\,\underline{q} \tag{6.31}$$

in the limit of very slow flow. Comparing this equation with the definition of hydrodynamic permeability (equation (2.22)) yields:

$$k \;=\; \frac{\left(U_{||}+U_t\right)/U_o}{G_o}. \tag{6.32}$$

For a unidirectional fibre bed [5] $S_{||} = 2\,d\,\sqrt{1-\epsilon}$ and $d_p = d\,(1-\sqrt{1-\epsilon})$ so that equation (6.30) becomes

$$\begin{aligned} G_o \;&=\; \frac{2\,d_s}{d^2}\cdot\frac{6}{d\,(1-\sqrt{1-\epsilon})^2} \\ &=\; \frac{12\sqrt{1-\epsilon}}{d^2(1-\sqrt{1-\epsilon})^2}. \end{aligned} \tag{6.33}$$

The hydrodynamic permeability for a unidirectional fibre bed is therefore given as:

$$\begin{aligned} k &\equiv \frac{\left(U_{||} + U_t\right)/U_o}{G_o} \\ &= \frac{(1 - d_s/d)\, d^2\, (1 - \sqrt{1-\epsilon})^2}{12\sqrt{1-\epsilon}} \\ &= \frac{d^2\, (1 - \sqrt{1-\epsilon})^3}{12\sqrt{1-\epsilon}}, \end{aligned} \tag{6.34}$$

since from equation (2.3) we know that $d_s/d = \sqrt{1-\epsilon}$.

The dimensionless hydrodynamic permeability K, is defined as the hydrodynamic permeability divided by the cross-sectional area of a unit cell, so that

$$\boxed{K \equiv \frac{(1 - \sqrt{1-\epsilon})^3}{12\sqrt{1-\epsilon}},} \tag{6.35}$$

which is identical to the equation given by the FD analytical model for the dimensionless permeability of a non-staggered configuration (equation (3.2)). The same assumptions were used here as for the FD non-staggered model, and therefore the analysis and conclusions that were made in Section 3.3, can be repeated here. The model performs well at low porosities, but the different physical character of the flow at high porosities leads to discrepancies in the results for the models of high porosity.

6.3 Staggered configuration

We now address each term in the pressure averaging equation (equation (6.1)) by considering the rectangular representation of a porous medium for a staggered configuration as shown in Figure 6.4. In the figure the relative size of the transverse sections is exaggerated to better illustrate the various volumetric regimes present.

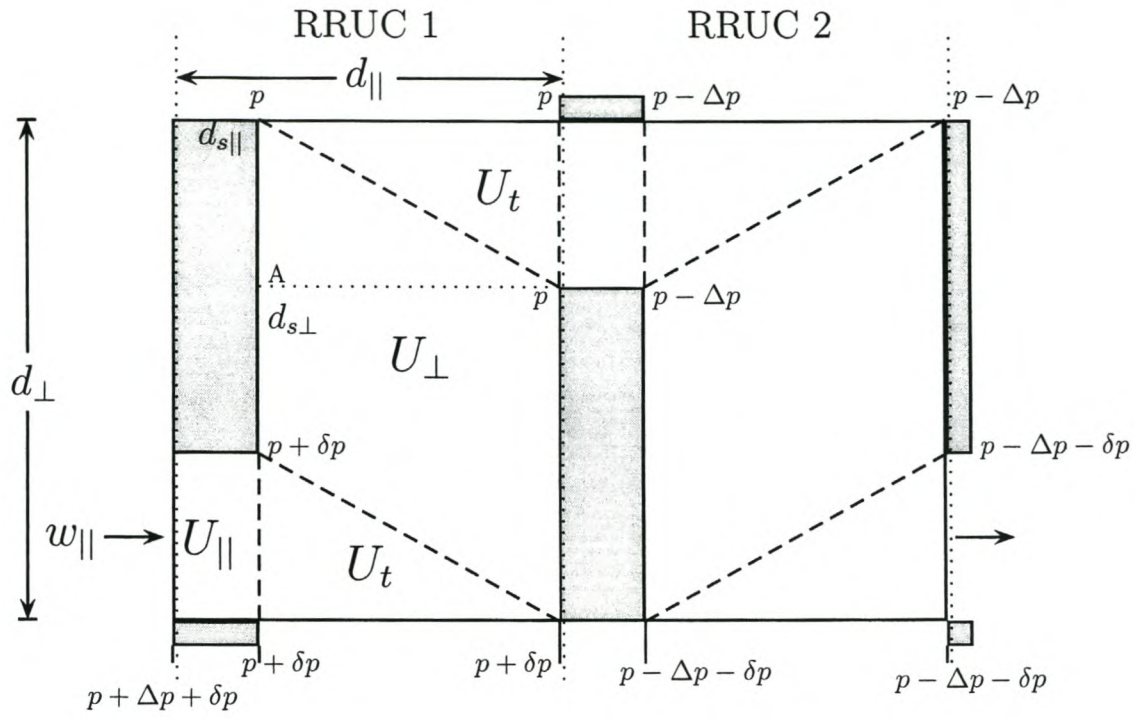

Figure 6.4: Unit cell geometry in case of streamwise staggering (first case).

First case

We first consider a unit cell, where the boundaries in the perpendicular direction of the unit cell go through the solid region, as indicated by RRUC 1 (RRUC 2 is therefore the neighbouring unit cell in this case). In terms of symbols, where Δp is the total change in pressure in the streamwise volume and δp is the total change of pressure in the transverse volume, as indicated in Figure 6.4, the first term in equation (6.1) can be written as

$$\begin{aligned} \langle \nabla p \rangle &= \frac{1}{U_o} \iiint_{U_f} \nabla p \, dU \\ &= \frac{1}{U_o} \left(\iiint_{U_{||}} \nabla p \, dU + \iiint_{U_t} \nabla p \, dU + \iiint_{U_\perp} \nabla p \, dU \right). \end{aligned} \tag{6.36}$$

The pressure is constant in the transfer volumes so the pressure gradient will be zero here. In the transverse volume, however, even though the flow is in the perpendicular direction, we assume that there is a pressure gradient in the streamwise direction. The pressure at A, in Figure 6.4, is given by $p + [(d_\perp - d_{s\perp})/d_{s\perp}]\,\delta p$. Therefore, for the first term we have

$$\begin{aligned}
\langle \nabla p \rangle &= \frac{1}{U_o}\left(-\frac{\Delta p}{d_{s||}}.U_{||} + \frac{-[(d_\perp - d_{s\perp})/d_{s\perp}]\,\delta p}{d_{||} - d_{s||}}.U_\perp\right) \\
&= -\frac{1}{U_o}\left(\frac{\Delta p}{d_{s||}}.U_{||} + \frac{(d_\perp - d_{s\perp})\,\delta p}{U_\perp}.U_\perp\right) \\
&= -\frac{1}{U_o}\left(\frac{\Delta p}{d_{s||}}.U_{||} + \frac{\delta p}{d_{s||}}.U_{||}\right) \\
&= -\frac{U_{||}}{U_o}\left(\frac{\Delta p + \delta p}{d_{s||}}\right). \qquad (6.37)
\end{aligned}$$

The second term in equation (6.1) is

$$\nabla \langle p \rangle = \frac{1}{U_o}\nabla \iiint_{U_f} p\, dU. \qquad (6.38)$$

The average pressure in the total transfer region of the unit cell is equal to the average pressure in the perpendicular region. Therefore if we consider two different RRUCs, as shown in Figure 6.4, and take the gradient of their two pressure averages we obtain the following

$$\begin{aligned}
\nabla \langle p \rangle &= \frac{1}{U_o}\left(\frac{\left[(p + \delta p + \frac{\Delta p}{2})U_{||} + (p + \frac{\delta p}{2})\,U_t + (p + \frac{\delta p}{2})\,U_\perp\right]}{d_{||}}\right. \qquad (6.39) \\
&\quad \left. - \frac{\left[(p - \frac{\Delta p}{2})\,U_{||} + (p - \Delta p - \frac{\delta p}{2})\,U_t + (p - \Delta p - \frac{\delta p}{2})\,U_\perp\right]}{d_{||}}\right) \\
&= -\frac{1}{U_o}\left(\frac{(\Delta p + \delta p)\,U_{||} + (\Delta p + \delta p)\,(U_t + U_\perp)}{d_{||}}\right) \\
&= -\frac{U_f}{U_o}\left(\frac{\Delta p + \delta p}{d_{||}}\right). \qquad (6.40)
\end{aligned}$$

The surface integral term is zero in this case,

$$\frac{1}{U_o} \iint_{S_{fs}} \underline{n}\, p\, dS = 0, \tag{6.41}$$

since it is assumed that the pressure at the walls cancel out. In a more realistic situation, the surface term here would not be zero, since the pressures at the streamwisely up and down facing surfaces would not cancel out. However, for the pressure averaging equation this has been compensated for by including a pressure gradient in the transverse region.

The above results for the three terms will be true for all RRUCs whose boundaries cut through the solid rectangle (i.e. for $d_{s||}/d_{||}$ of the possible RRUCs if shifted in the streamwise direction).

Second case

If we now shift the unit cell in the streamwise direction so that its boundaries do not pass through the solid region (i.e. consider the unit cell to be as shown in Figure 6.5), the surface integral term will not be zero, but the other two terms in the pressure averaging equation will be the same, as shown below. This will be true for all RRUCs whose boundaries do not cut through the solid rectangle (i.e. for a proportion of $1 - d_{s||}/d_{||}$ of the cases).

In terms of symbols, as indicated in Figure 6.4, the first term in equation (6.1) is

$$\begin{aligned} \langle \nabla p \rangle &= \frac{1}{U_o} \iiint_{U_f} \nabla p\, dU \\ &= \frac{1}{U_o} \left(\iiint_{U_{||}} \nabla p\, dU + \iiint_{U_t} \nabla p\, dU + \iiint_{U_\perp} \nabla p\, dU \right). \end{aligned} \tag{6.42}$$

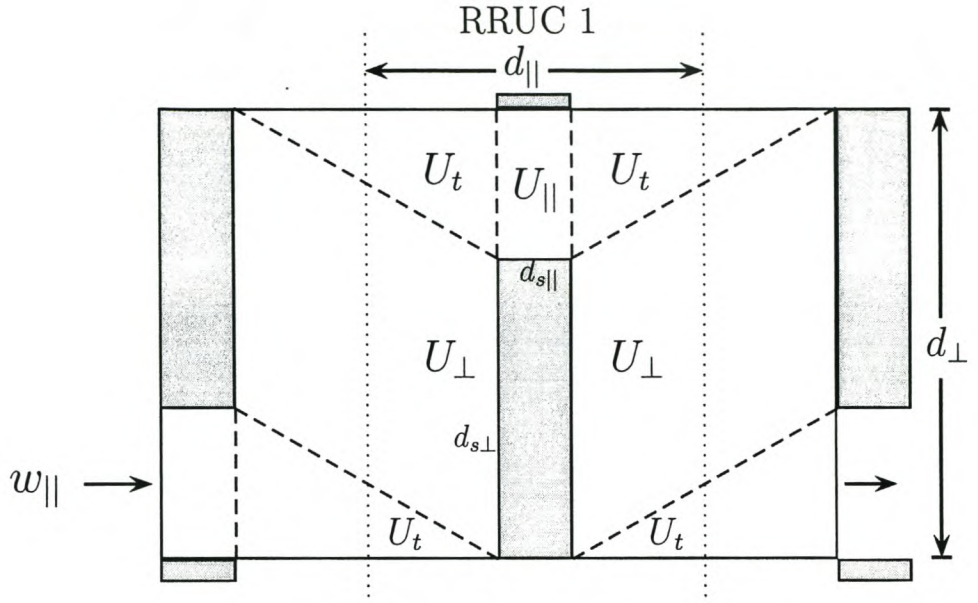

Figure 6.5: Unit cell geometry in case of streamwise staggering (second case).

The pressure is constant in the transfer volumes so the pressure gradient will be zero here, but in the transverse volumes there is a pressure gradient in the streamwise direction. Therefore we have

$$\begin{aligned}
\langle \nabla p \rangle &= \frac{1}{U_o}\left(\frac{-\Delta p}{d_{s||}}.U_{||} + \frac{p - [p + \frac{(d_\perp - d_{s\perp})}{2\,d_{s\perp}}\,\delta p]}{(d_{||} - d_{s||})/2}.\frac{U_\perp}{2}\right. \\
&\quad \left. + \frac{[p + \Delta p] - [p + \Delta p - \frac{(d_\perp - d_{s\perp})}{2\,d_{s\perp}}\,\delta p]}{(d_{||} - d_{s||})/2}.\frac{U_\perp}{2}\right) \qquad (6.43) \\
&= \frac{1}{U_o}\left(-\frac{\Delta p}{d_{s||}}.U_{||} - \frac{(d_\perp - d_{s\perp})\,\delta p}{U_\perp}.U_\perp\right) \\
&= \frac{1}{U_o}\left(-\frac{\Delta p}{d_{s||}}.U_{||} + \frac{\delta p}{d_{s||}}.U_{||}\right) \\
&= -\frac{U_{||}}{U_o}\left(\frac{\Delta p + \delta p}{d_{s||}}\right). \qquad (6.44)
\end{aligned}$$

The second term can be written as

$$\nabla \langle p \rangle = \frac{1}{U_o} \nabla \iiint_{U_f} p \, dU. \qquad (6.45)$$

If we consider two neighbouring RRUCs, similar to the one shown in Figure 6.5, and take the gradient of their two pressure averages we obtain the following

$$\begin{aligned}\nabla \langle p \rangle &= -\frac{1}{U_o}\left(\frac{(\Delta p + \delta p)\, U_{||} + (\Delta p + \delta p)\, U_t + (\Delta p + \delta p)\, U_{\perp}}{d_{||}}\right) \\ &= -\frac{U_f}{U_o}\left(\frac{\Delta p + \delta p}{d_{||}}\right). \end{aligned} \tag{6.46}$$

This can be shown by considering each component of the volumes separately and realising that they all differ by $(\Delta p + \delta p)$ to the corresponding component in the neighbouring RRUC.

The surface integral in this case is not zero and is given by:

$$\begin{aligned}\frac{1}{U_o}\iint_{S_{fs}} \underline{n}\, p\, dS &= \frac{1}{U_o}\left(\frac{[p + (p + \delta p)]}{2}\, d_{s\perp} - \frac{[(p - \Delta p) + (p - \Delta p - \delta p)]}{2}\, d_{s\perp}\right) \\ &= \frac{d_{s\perp}}{U_o}\left(\frac{2p + \delta p}{2} - \frac{2p - 2\Delta p - \delta p}{2}\right) \\ &= \frac{d_{s\perp}}{U_o}\left(\frac{2\Delta p + 2\delta p}{2}\right) \\ &= \frac{d_{s\perp}}{U_o}(\Delta p + \delta p). \end{aligned} \tag{6.47}$$

Combination of Cases 1 and 2

Combining cases 1 and 2 we obtain the overall value for each term in equation (6.1):

$$\langle \nabla p \rangle = -\frac{U_{||}}{U_o}\left[\frac{\Delta p + \delta p}{d_{s||}}\right], \tag{6.48}$$

$$\nabla \langle p \rangle = -\frac{U_f}{U_o}\left[\frac{\Delta p + \delta p}{d_{||}}\right], \tag{6.49}$$

$$\begin{aligned}\frac{1}{U_o}\iint_{S_{fs}} \underline{n}\, p\, dS &= \frac{(d_{||} - d_{s||})}{d_{||}}\left[\frac{d_{s\perp}}{U_o}(\Delta p + \delta p)\right] + \frac{d_{s||}}{d_{||}}(0) \\ &= \frac{(d_{||} - d_{s||})}{d_{||}}\left[\frac{d_{s\perp}}{U_o}(\Delta p + \delta p)\right]. \end{aligned} \tag{6.50}$$

Checking equation (6.1), with the help of Table 5.2, we obtain the following:

$$\begin{aligned}
\langle \nabla p \rangle &= \nabla \langle p \rangle + \frac{1}{U_o} \iint_{S_{fs}} \underline{n}\, p \, dS \\
&= -\frac{U_f}{U_o} . \left(\frac{\Delta p + \delta p}{d_{||}} \right) + \frac{(d_{||} - d_{s||})}{d_{||}} . \left(\frac{d_{s\perp}}{U_o} (\Delta p + \delta p) \right) \\
&= -\frac{\Delta p + \delta p}{U_o} . \left(\frac{U_f - U_\perp}{d_{||}} \right) \\
&= -\frac{\Delta p + \delta p}{U_o} . \left(\frac{U_{||} + U_t}{d_{||}} \right) \qquad (6.51) \\
&= -\frac{\Delta p + \delta p}{U_o} . \left(\frac{(d_\perp - d_{s\perp})\, d_{s||} + (d_{||} - d_{s||})\, (d_\perp - d_{s\perp})}{d_{||}} \right) \\
&= -\frac{\Delta p + \delta p}{U_o} . \left(\frac{(d_\perp - d_{s\perp})\, d_{||}}{d_{||}} . \frac{d_{s||}}{d_{s||}} \right) \\
&= -\frac{U_\perp}{U_o} . \frac{\Delta p + \delta p}{d_{s||}}, \qquad (6.52)
\end{aligned}$$

which agrees with equation (6.48). From equation (6.1) and (6.51) we can write the surface term as follows

$$\begin{aligned}
\frac{1}{U_o} \iint_{S_{fs}} \underline{n}\, p \, dS &= \langle \nabla p \rangle - \nabla \langle p \rangle \\
&= \left(\frac{U_{||} + U_t}{U_o} \right) . \frac{\Delta p + \delta p}{d_{||}} - \nabla \langle p \rangle \\
&= \left(\frac{U_{||} + U_t}{U_f} \right) . \nabla \langle p \rangle - \nabla \langle p \rangle \\
&= \left(\frac{U_{||} + U_t}{U_f} - 1 \right) . \nabla \langle p \rangle . \qquad (6.53)
\end{aligned}$$

Since, from equation (5.4), the tortuosity is defined as $\chi = U_f/(U_{||} + U_t)$ for the RRUC staggered configuration, equation (6.53) can be written as:

$$\frac{1}{U_o} \iint_{S_{fs}} \underline{n}\, p \, dS = \left(\frac{1}{\chi} - 1 \right) . \nabla \langle p \rangle . \qquad (6.54)$$

Equation (6.54) provides us with an expression for the surface integral, in the pressure averaging equation (equation (6.1)) for a staggered configuration, in terms of pore-scale volumes and the gradient of the pressure average.

6.4 The Revised RRUC model for a staggered configuration

The results obtained from using the RRUC model proposed by Du Plessis and Masliyah [8], given in Table 4.4, clearly show that something is awry with the model. Analysing the RRUC model it was noticed that the model only considers the first case (section before) of the RRUC, and not the second case where the RRUC is shifted so that its perpendicular boundaries do not pass through the solid.

The model is now adjusted slightly so as to include the entire pressure part of the integral.

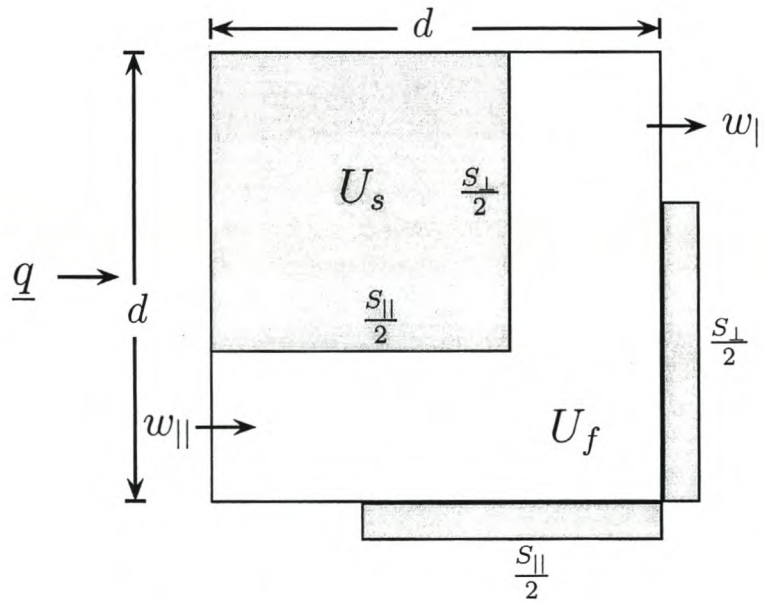

Figure 6.6: Unit cell geometry of a RRUC.

We will consider only the Darcy Regime of pure viscous drag at low Reynolds number ($Re_p << 1$). Assuming uniform discharge through a homogeneous isotropic porous medium,

we start with equation (6.23),

$$-\epsilon \nabla p_f = \frac{1}{U_0} \iint_{S_{fs}} \underline{n}\, p\, dS - \frac{1}{U_0} \iint_{S_{fs}} \left(\underline{n} \cdot \underline{\underline{\tau}}\right) dS. \tag{6.55}$$

In the transverse pores, the shear stresses have no streamwise components. Although, due to the randomness of the medium the transverse shear stresses will cancel vectorially, they will still create interstitial transverse pressure drops. These pressure drops should however contribute to the integral through the pressure part, when evaluated at the streamwisely up- and down- facing surfaces, $S_\perp$.

The pressure integral term can be rewritten in terms of equation (6.54), but as mentioned earlier it does not include the pressure drop in the transverse section, created by the transverse shear stresses, and this must be taken into account separately. It was assumed that this contribution of the pressure integral term may be incorporated by integrating for the wall shear stress over the total solid-fluid interface S_{fs} instead of only over the streamwise part $S_{||}$. Therefore, in the low Reynolds number limit, equation (6.55) yields:

$$-\epsilon \nabla p_f = \frac{1}{U_0} \iint_{S_{||}} (-\underline{n} \cdot \underline{\underline{\tau}})\, dS + \hat{\underline{n}} \frac{1}{U_0} \iint_{S_\perp} \left|\underline{n} \cdot \underline{\underline{\tau}}\right| dS + \left(\frac{1}{\chi} - 1\right) \nabla \langle p \rangle . \tag{6.56}$$

This can be rewritten as

$$-\frac{\epsilon}{\chi} \nabla p_f = \frac{1}{U_0} \iint_{S_{||}} (-\underline{n} \cdot \underline{\underline{\tau}})\, dS + \hat{\underline{n}} \frac{1}{U_0} \iint_{S_\perp} \left|\underline{n} \cdot \underline{\underline{\tau}}\right| dS. \tag{6.57}$$

If the wall shear stress is assumed to be uniform and equal to a constant, τ_w, over S_{fs} in all channel sections, for the low Reynolds number limit, we can reduce equation (6.57) to

$$\boxed{-\frac{\epsilon}{\chi} \nabla p_f = \hat{\underline{n}} \frac{1}{U_0} \iint_{S_{fs}} \tau_w\, dS.} \tag{6.58}$$

Equation (6.58) can be considered as the modified version of equation (2.18). The remainder of this section now follows exactly that of Section 2.1.3. For Newtonian flow between two parallel plates a distance d_p apart and if the average transverse velocity is $\beta w_{||}$ it follows that

$$-\frac{\epsilon}{\chi}\nabla p_f = \left(\frac{S_{||}+\beta S_{\perp}}{U_o}\right).\left(\frac{6\,\mu\, w_{||}}{d_p}\right)\hat{\underline{n}} = \frac{S_{||}+\beta S_{\perp}}{U_o}.\frac{6}{d_p}\left(\frac{\chi}{\epsilon}\right)\mu\,\underline{q}. \tag{6.59}$$

If we define

$$G_o \equiv \frac{6\,\chi}{\epsilon\, d_p}.\frac{S_{||}+\beta S_{\perp}}{U_o}, \tag{6.60}$$

the momentum transport equation for uniform average flow becomes

$$-\frac{\epsilon}{\chi}\nabla p_f = G_o\,\mu\,\underline{q} \tag{6.61}$$

in the limit of very slow flow. Comparing this equation with the definition of hydrodynamic permeability (equation (2.22)) yields:

$$\boxed{k = \frac{\epsilon}{\chi\, G_o}.} \tag{6.62}$$

This is the prime result of this work and presents a crucial correction to the original RRUC model to allow better quantitative predictions for fluid transport in two-dimensional porous structures.

Unidirectional fibre bed

An appropriate RRUC for a unidirectional bundle of uniform fibres was introduced by Du Plessis [6]. Crossflow through this bundle of fibres presents a two-dimensional case of flow through a porous medium.

For a unidirectional fibre bed $S_{||} = S_{\perp} = 2\,d\sqrt{1-\epsilon}$ and $d_p = d\,(1-\sqrt{1-\epsilon})$, so that we have

$$G_o = \frac{12(1+\beta)\sqrt{1-\epsilon}}{d^2(1-\sqrt{1-\epsilon})^2}. \tag{6.63}$$

The tortuosity χ, defined as

$$\chi = \frac{U_f}{U_{||} + U_t}, \tag{6.64}$$

for the RRUC model, can now be written in terms of the porosity as follows

$$\chi = \frac{\epsilon}{1 - \sqrt{1-\epsilon}}. \tag{6.65}$$

The hydrodynamic permeability for a unidirectional fibre bed is given as:

$$k \equiv \frac{\epsilon}{G_o \chi} = \frac{d^2(1-\sqrt{1-\epsilon})^3}{12(1+\beta)\sqrt{1-\epsilon}}, \tag{6.66}$$

where β is the velocity ratio. Du Plessis and Diedericks [5], assumed the velocity ratio to be unity, simplifying the equation to:

$$\boxed{k = \frac{d^2(1-\sqrt{1-\epsilon})^3}{24\sqrt{1-\epsilon}}.} \tag{6.67}$$

This equation is a modification of the RRUC equation (2.35) and should be adequate for predicting the hydrodynamic permeability for flow perpendicularly through a two-dimensional prismatic porous medium. The dimensionless hydrodynamic permeability

$$K = \frac{(1-\sqrt{1-\epsilon})^3}{24\sqrt{1-\epsilon}}, \tag{6.68}$$

is obtained by dividing the hydrodynamic permeability (equation (6.67)) by the cross-sectional area of the unit cell d^2, as was done to get equation (2.36).

6.4.1 Comparison of revised RRUC and CFX results

Table 6.1 shows us the comparison between the predicted values for the hydrodynamic permeability obtained using the RRUC equation (equation (2.36)) and the revised RRUC equation (equation (6.68)) in comparison to the numerical values obtained from CFX-5.

ϵ	Dimensionless permeability K		
	RRUC (Equation (2.36))	RRUC (Equation (6.68))	CFX
0.1164	1.86×10^{-5}	9.57×10^{-6}	9.75×10^{-6}
0.3600	7.50×10^{-3}	4.17×10^{-4}	4.16×10^{-4}
0.5100	2.73×10^{-3}	1.61×10^{-3}	1.60×10^{-3}
0.7500	1.56×10^{-2}	1.04×10^{-2}	9.62×10^{-3}

Table 6.1: Numerical predictions of the dimensionless permeability, K.

The graph in Figure 6.7 clearly shows that the values obtained from the revised RRUC model can be used as a good prediction for the dimensionless permeability, K, for a porous medium with a staggered configuration, since they almost match exactly the numerical results obtained by CFX.

For the remainder of this thesis, the 'RRUC model' will refer to the revised RRUC model.

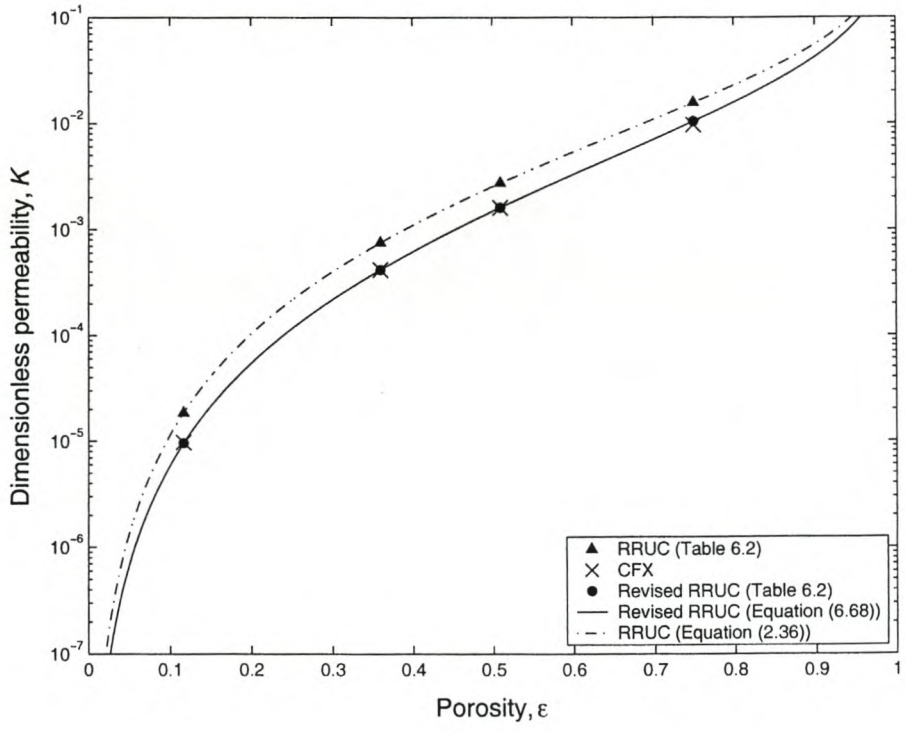

Figure 6.7: Predicted dimensionless permeabilities, K, for the RRUC staggered configuration.

6.5 The RRUC model for the FD staggered configuration

For staggered configurations the FD and RRUC models use different staggering configurations. In a practical situation, the FD configuration is actually maximally staggered and the configuration of the RRUC is not realistic. We now apply the 'RRUC model technique' to the FD staggered configuration, shown in Figure 6.8.

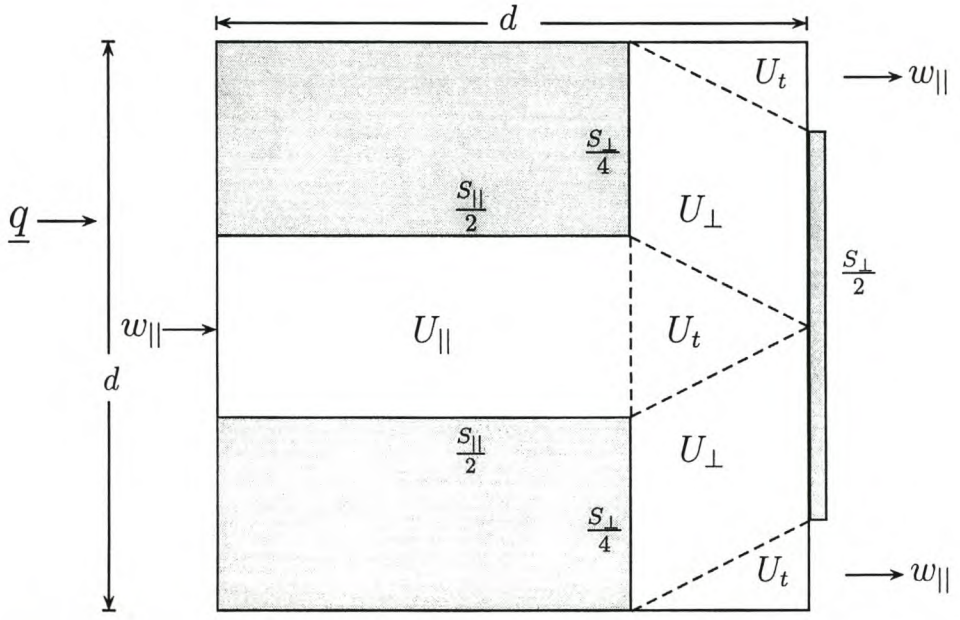

Figure 6.8: Unit cell geometry in case of FD streamwise staggering.

We will consider only the Darcy Regime of pure viscous drag at low Reynolds number ($Re_p << 1$). Assuming uniform discharge through a homogeneous isotropic porous medium, we start with equation (6.23),

$$-\epsilon \nabla p_f = \frac{1}{U_0} \iint_{S_{fs}} \underline{n}\, p\, dS - \frac{1}{U_0} \iint_{S_{fs}} \left(\underline{n} \cdot \underline{\underline{\tau}}\right) dS. \tag{6.69}$$

In the transverse pores, the shear stresses have no streamwise components. Although, due to the randomness of the medium the transverse shear stresses will cancel vectorially, they

will still create interstitial transverse pressure drops. These pressure drops should however contribute to the integral through the pressure part, when evaluated at the streamwisely up- and down- facing surfaces, $S_\perp$.

The pressure integral term can be rewritten in terms of equation (6.53) (refer to Appendix D), but as mentioned earlier it does not include the pressure drop in the transverse section, created by the transverse shear stresses, and this must be taken into account separately. It was assumed that this contribution of the pressure integral term may be incorporated by integrating for the wall shear stress over the total solid-fluid interface S_{fs} instead of only over the streamwise part $S_{||}$. *However in the transverse region the flow splits in two and therefore we only need to include half the transverse part* $S_\perp$. Therefore, in the low Reynolds number limit equation (6.69) is given by

$$-\epsilon\nabla p_f = \frac{1}{U_0}\underset{S_{||}}{\iint}(-\underline{n}\cdot\underline{\underline{\tau}})\,dS + \frac{\hat{\underline{n}}}{2\,U_0}\underset{S_\perp}{\iint}\left|\underline{n}\cdot\underline{\underline{\tau}}\right|dS + \left(\frac{U_{||}+U_t}{U_f}-1\right)\nabla\langle p\rangle\,, \quad (6.70)$$

which can be rewritten as

$$-\frac{\epsilon}{(1+\sqrt{1-\epsilon})}\nabla p_f = \frac{1}{U_0}\underset{S_{||}}{\iint}(-\underline{n}\cdot\underline{\underline{\tau}})\,dS + \frac{\hat{\underline{n}}}{2\,U_0}\underset{S_\perp}{\iint}\left|\underline{n}\cdot\underline{\underline{\tau}}\right|dS. \quad (6.71)$$

If the wall shear stress is assumed to be uniform and equal to a constant, τ_w, over S_{fs} in all channel sections, for the low Reynolds number limit, we reduce equation (6.71) to

$$-\frac{\epsilon}{(1+\sqrt{1-\epsilon})}\nabla p_f = \frac{\hat{\underline{n}}}{U_0}\underset{S_{||}}{\iint}\tau_w\,dS + \frac{\hat{\underline{n}}}{2\,U_0}\underset{S_\perp}{\iint}\tau_w\,dS. \quad (6.72)$$

For Newtonian flow between two parallel plates a distance d_p apart and if the average transverse velocity is $\beta w_{||}$, where β is the velocity ratio, it follows that

$$\begin{aligned}-\frac{\epsilon}{(1+\sqrt{1-\epsilon})}\nabla p_f &= \left(\frac{S_{||}+\frac{\beta}{2}S_\perp}{U_o}\right)\cdot\left(\frac{6\,\mu\,w_{||}}{d_p}\right)\hat{\underline{n}} \\ &= \frac{S_{||}+\frac{\beta}{2}S_\perp}{U_o}\cdot\left(\frac{6}{d_p\,(1-\sqrt{1-\epsilon})}\right)\mu\,\underline{q}, \end{aligned} \quad (6.73)$$

since

$$\underline{w}_{||} \equiv \frac{U_o}{U_{||} + U_t}\underline{q} \equiv \frac{1}{1-\sqrt{1-\epsilon}}\underline{q}. \tag{6.74}$$

If we define

$$G_o \equiv \frac{S_{||} + \frac{\beta}{2}S_{\perp}}{d_p U_o} \cdot \left(\frac{6}{1-\sqrt{1-\epsilon}}\right), \tag{6.75}$$

the momentum transport equation for uniform average flow becomes

$$-\frac{\epsilon}{(1+\sqrt{1-\epsilon})}\nabla p_f = G_o \mu \underline{q} \tag{6.76}$$

in the limit of very slow flow. Comparing this equation with the definition of hydrodynamic permeability (equation (2.22)) yields:

$$k \equiv \frac{\epsilon}{(1+\sqrt{1-\epsilon})\,G_o} = \frac{(1-\sqrt{1-\epsilon})}{G_o}. \tag{6.77}$$

Unidirectional fibre bed

An appropriate RRUC for a unidirectional bundle of uniform fibres was introduced by Du Plessis [6]. Crossflow through this bundle of fibres presents a two-dimensional case of flow through a porous medium.

For a unidirectional fibre bed $S_{||} = S_{\perp} = 2\,d\sqrt{1-\epsilon}$ and $d_p = d\,(1-\sqrt{1-\epsilon})$, so that we have

$$G_o = \frac{12\,(1+\beta/2)\sqrt{1-\epsilon}}{d^2(1-\sqrt{1-\epsilon})^2}. \tag{6.78}$$

The hydrodynamic permeability for a unidirectional fibre bed is given as:

$$k \equiv \frac{d^2(1-\sqrt{1-\epsilon})^3}{12(1+\beta/2)\sqrt{1-\epsilon}}, \tag{6.79}$$

where β is the velocity ratio. *For the FD staggered configuration* $w_{\perp} = \frac{1}{2}w_{||}$, *so the velocity ratio is 1/2.* Therefore

$$k = \frac{d^2(1-\sqrt{1-\epsilon})^3}{15\sqrt{1-\epsilon}}. \tag{6.80}$$

The dimensionless hydrodynamic permeability

$$\boxed{K = \frac{(1-\sqrt{1-\epsilon})^3}{15\sqrt{1-\epsilon}},} \tag{6.81}$$

is obtained by dividing the hydrodynamic permeability (equation (6.80)) by the cross-sectional area of the unit cell d^2. Equation (6.81) is identical to the FD equation for the prediction of the dimensionless permeability for a staggered configuration (equation (4.1)). This shows that the RRUC model and the FD analytical model obtain the same equations for the prediction of the hydrodynamic permeability for configurations of similar staggering.

6.5.1 Simplified expression for permeability

Equation (6.81) may be rewritten as follows:

$$\begin{aligned} K &= \frac{(1-\sqrt{1-\epsilon})^3}{15\sqrt{1-\epsilon}} \\ &= \frac{1-3\sqrt{1-\epsilon}+3(1-\epsilon)-(\sqrt{1-\epsilon})^3}{15\sqrt{1-\epsilon}} \\ &= \frac{1}{15}\left(\frac{1}{\sqrt{1-\epsilon}}-3+3\sqrt{1-\epsilon}-(1-\epsilon)\right) \\ &= \frac{1}{15}\left(\epsilon-4+(4-3\,\epsilon)(1-\epsilon)^{-1/2}\right). \end{aligned}$$

The factor $(1-\epsilon)^{-1/2}$ may now be approximated by a binomial series expansion [10], yielding

$$K = \frac{1}{120}\epsilon^3+\frac{5}{480}\epsilon^4+O(\epsilon^5) \tag{6.82}$$

$$= \frac{\epsilon^3}{120}\left[1+\frac{5}{4}\epsilon+O(\epsilon^2)\right]. \tag{6.83}$$

If this series is truncated to a linear expression, we obtain

$$K = \frac{\epsilon^3}{120}\left[1+\frac{5}{4}\epsilon\right] = 0.00833\,\epsilon^3+0.0104\,\epsilon^4, \tag{6.84}$$

and further truncating to a constant expression yields

$$K = \frac{\epsilon^3}{120} = 0.00833\,\epsilon^3. \tag{6.85}$$

It is evident that the truncation will have less effect as $\epsilon \to 0$. The higher the porosity the less accurate the truncated expression for K will be.

The error introduced by truncation of the binomial series expansion at non-zero ϵ, as shown above, can be lessened at any porosity by introducing a throwback method [10], [11]. In this method the coefficient of the highest retained power of ϵ is changed to incorporate the neglected higher-order terms of the series. This is accomplished through the difference between the original equation and the approximation, at the particular porosity.

ϵ	Linear (Equation (6.84))	Constant (Equation (6.85))
0.1	$\frac{\epsilon^3}{120}\left[1+\frac{5.583}{4}\epsilon\right] = 0.00833\,\epsilon^3 + 0.0116\,\epsilon^4$	$\frac{1.140\,\epsilon^3}{120} = 0.00950\,\epsilon^3$
0.2	$\frac{\epsilon^3}{120}\left[1+\frac{6.311}{4}\epsilon\right] = 0.00833\,\epsilon^3 + 0.0131\,\epsilon^4$	$\frac{1.316\,\epsilon^3}{120} = 0.0110\,\epsilon^3$
0.3	$\frac{\epsilon^3}{120}\left[1+\frac{7.244}{4}\epsilon\right] = 0.00833\,\epsilon^3 + 0.0151\,\epsilon^4$	$\frac{1.543\,\epsilon^3}{120} = 0.0129\,\epsilon^3$
0.4	$\frac{\epsilon^3}{120}\left[1+\frac{8.481}{4}\epsilon\right] = 0.00833\,\epsilon^3 + 0.0177\,\epsilon^4$	$\frac{1.848\,\epsilon^3}{120} = 0.0154\,\epsilon^3$
0.5	$\frac{\epsilon^3}{120}\left[1+\frac{10.19}{4}\epsilon\right] = 0.00833\,\epsilon^3 + 0.0212\,\epsilon^4$	$\frac{2.274\,\epsilon^3}{120} = 0.0190\,\epsilon^3$
0.6	$\frac{\epsilon^3}{120}\left[1+\frac{12.72}{4}\epsilon\right] = 0.00833\,\epsilon^3 + 0.0265\,\epsilon^4$	$\frac{2.908\,\epsilon^3}{120} = 0.0242\,\epsilon^3$
0.7	$\frac{\epsilon^3}{120}\left[1+\frac{16.80}{4}\epsilon\right] = 0.00833\,\epsilon^3 + 0.0350\,\epsilon^4$	$\frac{3.940\,\epsilon^3}{120} = 0.0328\,\epsilon^3$
0.8	$\frac{\epsilon^3}{120}\left[1+\frac{24.51}{4}\epsilon\right] = 0.00833\,\epsilon^3 + 0.0511\,\epsilon^4$	$\frac{5.902\,\epsilon^3}{120} = 0.0492\,\epsilon^3$
0.9	$\frac{\epsilon^3}{120}\left[1+\frac{44.86}{4}\epsilon\right] = 0.00833\,\epsilon^3 + 0.0935\,\epsilon^4$	$\frac{11.09\,\epsilon^3}{120} = 0.0925\,\epsilon^3$

Table 6.2: Resulting equations for, K, after the throwback method has been applied at the particular porosity.

Table 6.2 shows the resulting equations if the throwback method is applied to equations (6.84) and (6.85) for the respective porosities. For models with very low porosity truncation without any throwback, as shown in equations (6.84) and (6.85), seems appropriate since applying the throwback method does not alter the equations much.

In figure 6.9 the result of throwback at $\epsilon = 0.4$ as given in Table 6.2 compared to the RRUC equation for the FD staggered configuration (equation (6.81)) is shown graphically. The

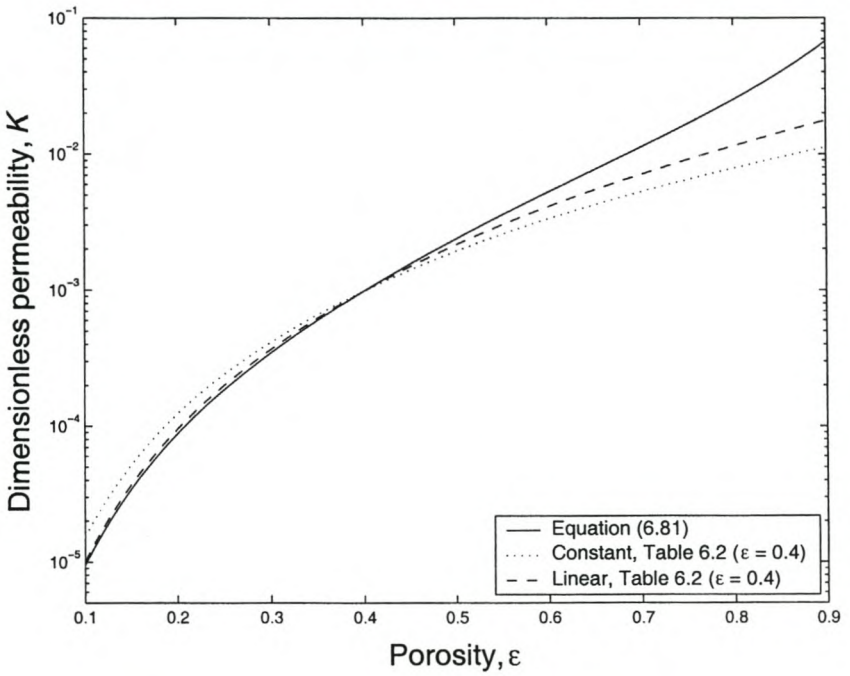

Figure 6.9: Dimensionless permeability, K, with throwback at $\epsilon = 0.4$.

truncated expression, supplemented by throwback, thus yields an accurate value of K at the particular porosity and is also reasonably accurate in a small range of porosities around the particular porosity.

Chapter 7

Summary and comparisons

In this chapter we give a summary of the models presented in this thesis and consider their percentage errors in comparison to the FD and CFX numerical results. The results given by the analytical models discussed in this thesis are also compared to other results found in the literature for two-dimensional prismatic porous medium.

7.1 Non-staggered configurations

For a non-staggered configuration of square cells, we have shown that both the FD analytical model (equation (3.2)) and the RRUC non-staggered model (equation (6.35)) obtain the same equation for the prediction of the dimensionless permeability

$$K \equiv \frac{(1-\sqrt{1-\epsilon})^3}{12\sqrt{1-\epsilon}}. \tag{7.1}$$

As discussed in previous chapters, this equation performs well at low porosities, but at 'high' porosities the predictions for the dimensionless hydrodynamic permeability differ considerably from the numerical values obtained.

7.1.1 Percentage errors of the non-staggered analytical model

In Table 7.1 we compare the predictions of the dimensionless permeabilities (equation (7.1)), to the complete set of FD numerical results, listed in Table 2.2, for the non-staggered case (SCASA). As shown in Table 3.2, the results given by CFX for the dimensionless permeability for a non-staggered configuration were almost the same as the FD numerical results and are therefore not shown in Table 7.1. The percentage error is calculated as the percentage of the difference between the two results over the numerically obtained value, i.e.

$$Percentage\ error\ =\ \frac{100(K_{RRUC} - K_{FD_{num}})}{K_{FD_{num}}}, \tag{7.2}$$

and is also given in Table 7.1. The percentage error given in Table 7.1 is plotted against the porosity on a graph, shown in Figure 7.1.

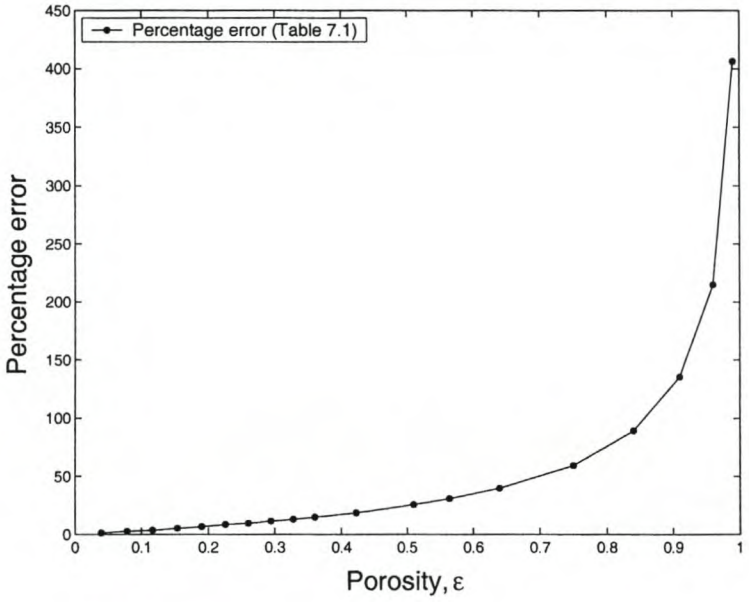

Figure 7.1: Percentage error of RRUC equation (7.1) versus the FD numerical results.

From Figure 7.1 it can be seen that at low porosities the percentage error is very small, but extremely large at very high porosities. As discussed in Chapter 3 this is assumed to be due to the different physical character of the flow at high porosities. For any model with a porosity higher than $\epsilon = 0.75$ one can expect more than a 50% error. It is therefore suggested that an alternative model be used for configurations of $\epsilon > 0.75$ in order to obtain

more accurate predictions.

ϵ	FD_{num}	RRUC (Equation (7.1))	RRUC - FD_{num}	Percentage Error
0.0396	6.73×10^{-7}	6.80×10^{-7}	7.27×10^{-9}	1.08
0.0784	5.42×10^{-6}	5.56×10^{-6}	1.36×10^{-7}	2.50
0.1164	1.85×10^{-5}	1.91×10^{-5}	6.49×10^{-7}	3.51
0.1536	4.41×10^{-5}	4.64×10^{-5}	2.28×10^{-6}	5.16
0.1900	8.69×10^{-5}	9.26×10^{-5}	5.69×10^{-6}	6.55
0.2256	1.51×10^{-4}	1.64×10^{-4}	1.26×10^{-5}	8.37
0.2604	2.43×10^{-4}	2.66×10^{-4}	2.29×10^{-5}	9.42
0.2944	3.65×10^{-4}	4.06×10^{-4}	4.13×10^{-5}	11.3
0.3276	5.25×10^{-4}	5.93×10^{-4}	6.77×10^{-5}	12.9
0.3600	7.26×10^{-4}	8.33×10^{-4}	1.07×10^{-4}	14.8
0.4224	1.28×10^{-3}	1.52×10^{-3}	2.36×10^{-4}	18.4
0.5100	2.56×10^{-3}	3.21×10^{-3}	6.54×10^{-4}	25.6
0.5644	3.80×10^{-3}	4.96×10^{-3}	1.16×10^{-3}	30.6
0.6400	6.73×10^{-3}	8.89×10^{-3}	2.52×10^{-3}	39.5
0.7500	1.31×10^{-2}	2.08×10^{-2}	7.73×10^{-3}	59.0
0.8400	2.38×10^{-2}	4.50×10^{-2}	2.12×10^{-2}	89.1
0.9100	4.05×10^{-2}	9.53×10^{-2}	5.48×10^{-2}	135
0.9600	6.78×10^{-2}	2.13×10^{-1}	1.46×10^{-1}	214
0.9900	1.20×10^{-1}	6.08×10^{-1}	4.87×10^{-1}	406

Table 7.1: Percentage error (equation (7.2)) of the RRUC model predictions of the dimensionless hydrodynamic permeability, K, compared to the FD numerical results.

7.1.2 Comparison with other literature

As mentioned in Section 1.1, Sangani and Acrivos [18] determined solutions for flow past a square array of cylinders by using a somewhat non-conventional numerical method. They obtained numerical results for the dimensionless drag $\frac{F}{\mu q}$, where F is the force per unit length on a cylinder. Their results were shown to be in excellent agreement with two analytical expressions, the one, which applies to dilute arrays, being derived by extending the earlier analysis of Hasimoto [14].

The results Sangani and Acrivos [18] obtained for the dimensionless drag are now compared to the predictions for the dimensionless drag $1/K$, where K is the dimensionless permeability obtained using equation (7.1), for a selection of porosities. Both the results are plotted on a graph, shown in Figure 7.2.

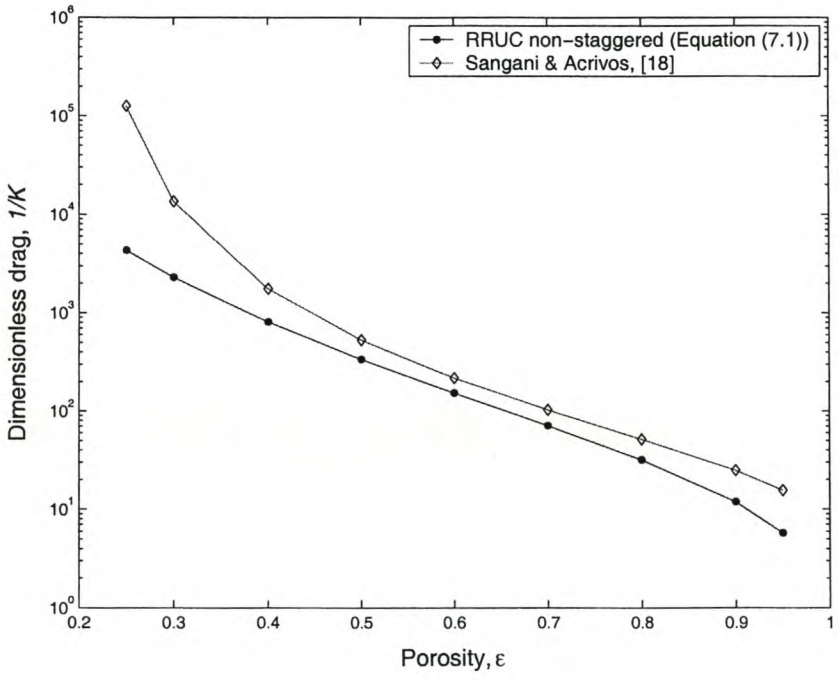

Figure 7.2: Predictions for the dimensionless drag of flow past a square array of cylinders [18] and the corresponding drag on a square array of rectangular fibres predicted by equation (7.1).

From Figure 7.2 it is clear that the predicted drag on the cylinders is higher than the predicted

drag on the rectangular fibres for all porosities. This is most likely due to the absence of a shape factor to account for the difference in drag-inducing geometries. Equation (7.1) has already been shown to not give accurate results for higher porosities, which is probably the reason for the increased difference between the sets of results at higher porosities. At low porosities there exists a minimum porosity for when the cylinders are touching each other and this would be the cause of the sudden high dimensionless drag at low porosities for the Sangani results.

7.2 Staggered configurations

For the staggered configurations we have two different models for the prediction of the dimensionless hydrodynamic permeability, K, the FD analytical model (equation (4.1)) and the RRUC staggered model (equation (6.68)). Even though it has been shown that the RRUC model predicts the same equation as the FD analytical model for the 'FD staggering,' for clarity this equation will be referred to as the FD staggered equation in this chapter.

7.2.1 Staggered FD analytical model

For a staggered configuration of square cells (SCSRA) the FD analytical model is given by equation (4.1)

$$K = \frac{\left(1-\sqrt{1-\epsilon}\right)^3}{15\sqrt{1-\epsilon}}, \tag{7.3}$$

for the predictions of the dimensionless hydrodynamic permeability. In Table 7.2 the percentage errors of the FD analytical model predictions for the dimensionless permeability for the staggered case compared to the complete set of FD numerical results, listed in Table 2.2, for the staggered case (SCSRA). The percentage errors are again calculated as the percentage of the difference between the two results over the numerically obtained value. The percentage error given in Table 7.2 is plotted against the porosity on a graph shown in Figure 7.3. As with the FD non-staggered model, the percentage error is small for the cases

ϵ	FD_{num}	FD_{an} (Equation (7.3))	FD_{an} - FD_{num}	Percentage Error
0.1900	6.92×10^{-5}	7.41×10^{-5}	4.87×10^{-6}	7.04
0.2256	1.20×10^{-4}	1.31×10^{-4}	1.09×10^{-5}	9.09
0.2604	1.93×10^{-4}	2.13×10^{-4}	1.97×10^{-5}	10.2
0.2944	2.90×10^{-4}	3.25×10^{-4}	3.51×10^{-5}	12.1
0.3276	4.16×10^{-4}	4.74×10^{-4}	5.82×10^{-5}	14.0
0.3600	5.75×10^{-4}	6.67×10^{-4}	9.17×10^{-4}	15.9
0.4224	1.01×10^{-3}	1.21×10^{-3}	2.03×10^{-4}	20.1
0.5100	2.02×10^{-3}	2.57×10^{-3}	5.51×10^{-4}	27.3
0.5644	2.99×10^{-3}	3.97×10^{-3}	9.80×10^{-4}	32.8
0.6400	5.04×10^{-3}	7.11×10^{-3}	2.07×10^{-3}	41.1
0.7500	1.06×10^{-2}	1.67×10^{-2}	6.07×10^{-3}	57.2
0.8400	2.02×10^{-2}	3.60×10^{-2}	1.58×10^{-2}	78.2
0.9100	3.63×10^{-2}	7.62×10^{-2}	3.99×10^{-2}	110
0.9600	6.34×10^{-2}	1.71×10^{-1}	1.07×10^{-1}	169
0.9900	1.16×10^{-1}	4.86×10^{-1}	3.70×10^{-1}	319

Table 7.2: Percentage error of the FD staggered model predictions of the dimensionless hydrodynamic permeability compared to the FD numerical results.

of low porosities, but very high for the high porosity cases. This is assumed to be due to the different physical character of the flow at high porosities, as discussed in Chapter 4.

From Figure 7.3 it can be seen that more than a 50% error can be expected for any model with a porosity higher than $\epsilon = 0.75$. An alternative model should therefore be used when considering models of high porosities in order to obtain more accurate results.

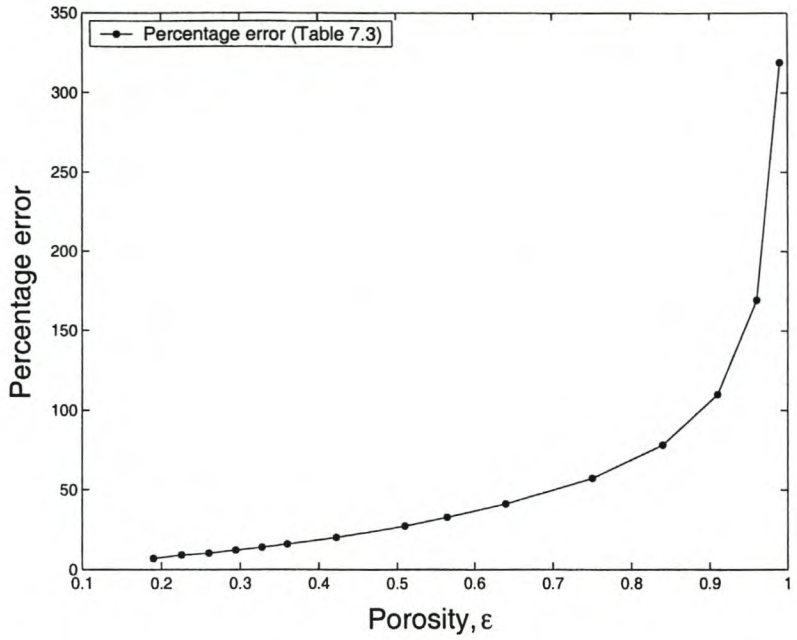

Figure 7.3: Percentage error of FD analytical versus the FD numerical results.

7.2.2 Comparison with other literature

Sangani and Acrivos [18] determined solutions for flow past a hexagonal array of cylinders, as well as for a square array of cylinders. They obtained numerical results for the dimensionless drag $\frac{F}{\mu q}$, where F is the force per unit length on a cylinder.

The RRUC analytical model for a staggered configuration, for the prediction of the dimensionless permeability K, is given by equation (6.68)

$$K = \frac{\left(1-\sqrt{1-\epsilon}\right)^3}{24\sqrt{1-\epsilon}}. \tag{7.4}$$

As shown in Section 6.4.1 these predicted values match very closely to the numerical results obtained from CFX. The results obtained by Sangani and Acrivos [18] for flow past a hexagonal array of cylinders are now compared to the predictions for the dimensionless drag $1/K$, where K is the dimensionless permeability obtained by first using the FD staggered model (equation (7.3)) and then using the RRUC staggered model (equation (7.4)), for a selection of porosities. The results are plotted on a graph, shown in Figure 7.4.

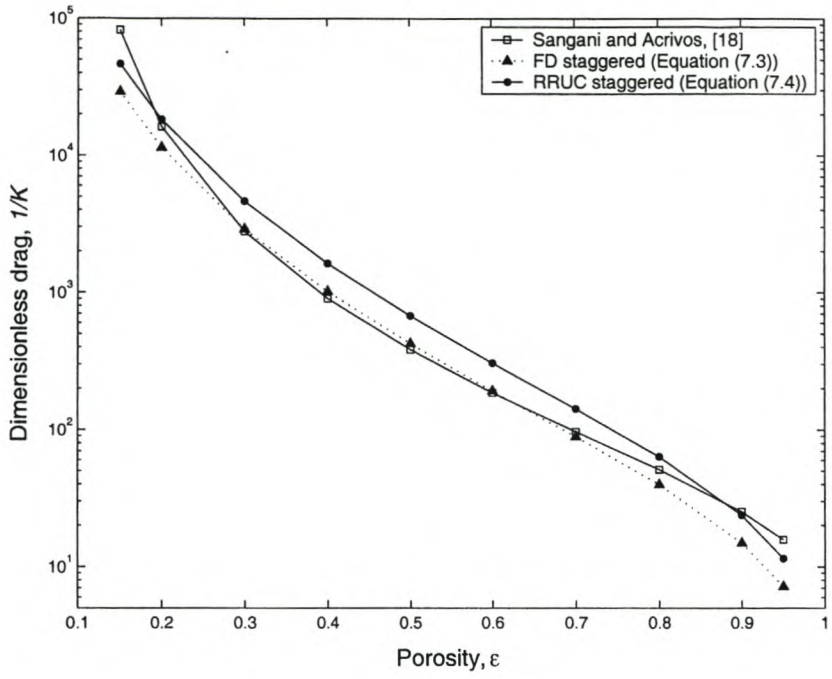

Figure 7.4: Predictions for the dimensionless drag of flow past a hexagonal array of cylinders [18], and FD (equation (7.3)) and RRUC (equation (7.4)) staggered models.

From Figure 7.4 it can be seen that the calculated drag on the cylinders for an hexagonal array as defined by Sangani and Acrivos [18], matches very closely to the predicted drag on the FD staggered configuration of rectangular fibres. The predicted drag is highest for the RRUC staggered configuration, which is understandable, since the RRUC staggered configuration is considered as being 'over staggered'. Equation (7.3) has already been shown not to give accurate results for higher porosities, which is probably the reason for the increased difference between the sets of results at higher porosities. At low porosities there exists a minimum porosity for when the cylinders are touching each other and this would be the cause of the high dimensionless drag at low porosities for the Sangani and Acrivos results.

7.3 Comparison of models

The RRUC (equation (7.4)) and FD (equation (7.3)) staggered models and the non-staggered model (equation (7.1)) given by both the FD and the RRUC models, as well as the FD numerical results are plotted on a graph, shown in figure 7.5.

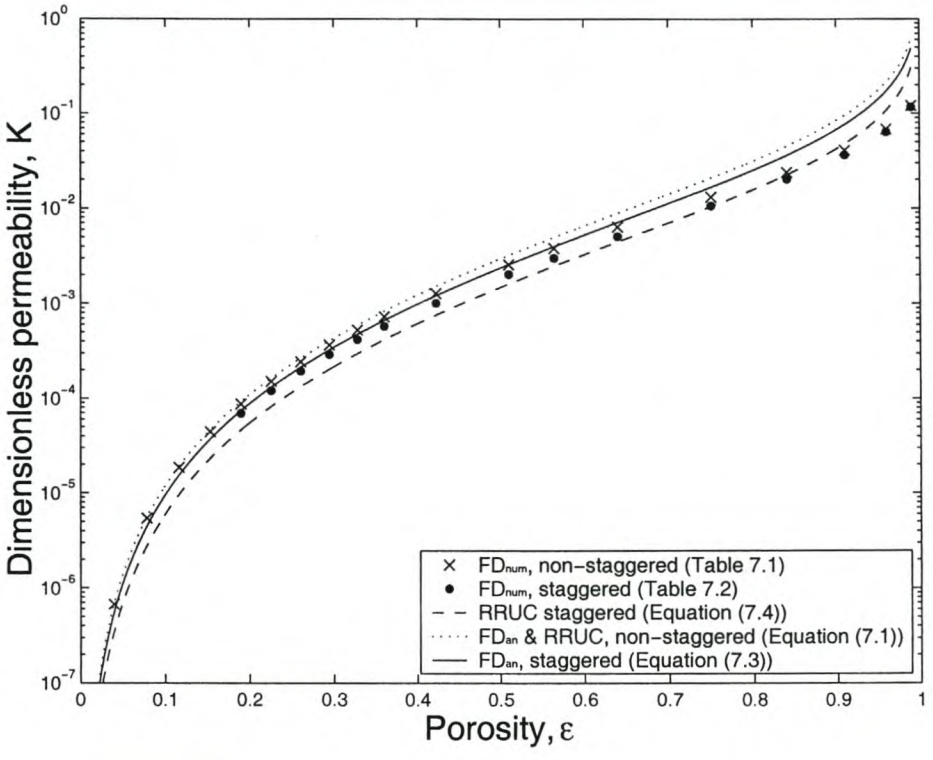

Figure 7.5: Predictions for the dimensionless permeability of the RRUC and FD non-staggered model, the RRUC staggered model, the FD staggered model and the FD numerical results.

From the graph it can be seen that the permeability is higher for the non-staggered model than for both the staggered models. The permeability is however higher for the FD staggered model than for the RRUC staggered model, which makes sense since, as mentioned already, the RRUC staggered configuration is considered as 'over staggered' because while flowing around the block the fluid is forced to flow perpendicular to the entire upstream face of the block, where as the FD staggered model only forces the fluid to flow perpendicular to half the upstream face of the block.

Chapter 8

Conclusions and Recommendations

This study was directed at the numerical verification, by the commercial code CFX, of two geometric models used for the prediction of flow through two-dimensional porous media. Both models utilize a rectangular geometric representation of the two-dimensional porous matrix coupled with simplistic assumptions regarding the flow conditions, namely the assumption of laminar plane Poiseuille flow between solid parts and the remaining void sections acting only as passive transfer sections. In this respect the fluid volume is compartementalized into sub-volumes pertaining to each of the predominant flow conditions, namely the streamwise motion between parallel plates, transverse flow between parallel plates and passive streamwise transfer.

The FD analytical model is a direct method, capturing the relation between the pressure drop over and the resulting discharge through a rectangular unit cell of the porous matrix. In the RRUC model the porous medium transport equations are volumetrically averaged and closure is obtained by a secondary pore-scale modelling of flow through a rectangular representative unit cell orientated streamwise. Although philosophically different, the two methods appear to have a lot in common and one purpose of this thesis was to investigate closely the similarities and differences between the two approaches.

Numerically it was established that the FD analytical model is indeed substantiated especially in the lower porosity range. A need for better modelling in the higher porosity range, however, is evident from present results.

In the case of the RRUC model the discrepancy between its results and that of the FD analytical model for non-staggered porous arrays was shown to originate in an incorrect treatment on the closure for the pressure deviation term. The correction resulted in a new formulation for the RRUC model which yields the same correct predictions as the FD analytical model, for similar staggering.

The concept of maximum staggering proposed in the original RRUC model tends to 'over stagger' the solid particles and thus yielded a different tortuosity and subsequently different results than the FD analytical model. If this staggering is adjusted to the same level as that of the staggering in the FD case, the two sets of results were shown to be identical. It was shown that the tortuosity can be defined generically in terms of the different volumes weighted according to the average fluid velocities in the respective volumes.

For future work it is thus not necessary to discriminate between the RRUC and FD pore-scale models as they both obtain the same equation

$$K = \frac{\left(1-\sqrt{1-\epsilon}\right)^3}{12\sqrt{1-\epsilon}} \cdot \frac{1}{1+\gamma/4}, \tag{8.1}$$

for the prediction of the dimensionless permeability for flow through a regular array of square obstacles. As was done previously in the FD case [12], the work may also be adapted to include rectangles.

In addition to the high porosity case, this study could be complemented by a similar analysis for the Forchheimer regime. This may then lead to a more general predictive tool of which the results shown here will be the limit of low porosity and low Reynolds number.

Appendix A

Technical notes on CFX package

The CFX-5 package

CFX-5 is a general purpose CFD code, comprising of four software modules, CFX-Build (pre-processor), CFX-Solver Manager, CFX-Solver (solver) and CFX-Post (post-processor). These are linked by the flow of information required to perform a CFD analysis.

CFX-Build is where you 'build' your model and create the input for the solver. This is done by specifying the geometry, flow physics, boundary conditions, mesh parameters, initial values and solver parameters of the model.

The CFX-Solver is the component which solves the CFD problem, specified in CFX-Build, for all the solution variables in the particular simulation. The solution method which CFX-5 uses is based on the finite volume technique. The CFX-Solver Manager provides a graphical user interface to the CFX-Solver, in order to give information about the emerging solution and to provide an easy way to control the CFX-Solver. The CFX-Solver produces a file of results which is then passed to the post-processor.

CFX-Post provides interactive post-processing graphics tools with which to analyse and present the results obtained from the CFX-5 simulations.

Problems experienced with the CFX-5 package

Two-dimensional models, which were needed for this work, could not easily be constructed in CFX-5. CFX-4 build was therefore used to construct and 'mesh' the models, since here a single grid space in z-direction could be defined, so the models could be considered as two-dimensional. These models were then imported into CFX-5 build where the boundary conditions, initial values etc. were defined.

We did not succeed in creating a repetitive boundary (where after each iteration the outlet values could be set to become the new inlet values) using CFX-5. As already mentioned, this was compensated for by constructing a few unit cells instead of just one, so that more accurate results could be obtained.

Appendix B

CFX non-staggered configuration for $\epsilon = 0.51$

In CFX-build we constructed models with non-staggered configurations for a selection of porosities, as mentioned in Chapter 3, similar to the model shown in Figure B.1. In this appendix we examine closely the CFX non-staggered model of porosity $\epsilon = 0.51$.

First we calculate the value given by CFX for the dimensionless hydrodynamic permeability K, which can be compared to the FD numerical value and to the predicted value of the FD analytical model. Then we consider the fluid volume as three different fluid volumes $U_{||}$, U_g and U_t, to attempt to verify the assumptions made for each of these volumes by the FD analytical model.

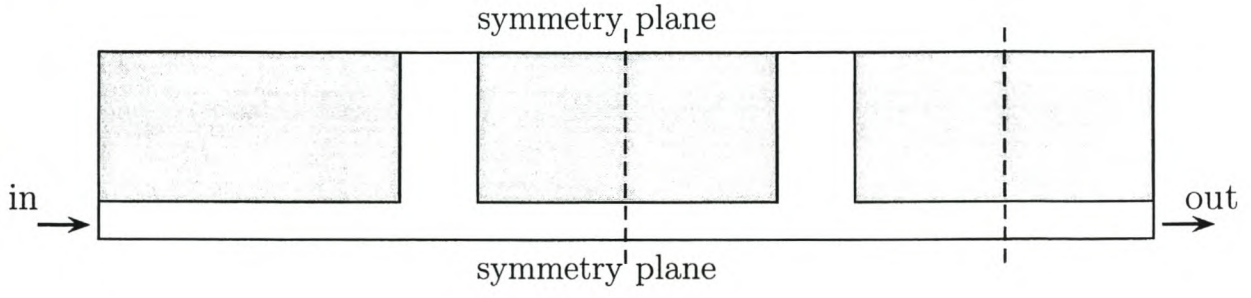

Figure B.1: Construction used in CFX modelling for no streamwise staggering.

We consider the top half of the second unit cell (area bordered by dashed lines in Figure B.1) constructed in CFX-build as shown in Figure B.2. The pressure was set as 0.1 Pa at the inlet and 0 Pa at the outlet, to assure very slow flow in the Darcy regime. The fluid was chosen to be water, with density $\rho = 1000\ kg/m^3$ and dynamic viscosity $\mu = 0.001\ N \cdot s/m^2$. For simplification the unit cells were chosen to be square with $d = d_{||} = d_{\perp} = 0.005\,m$, so that $U_o = 2.5 \times 10^{-5}\,m^2$. Therefore for a porosity of 0.51, we must have $d_s = d_{s||} = d_{s\perp} = 0.0035\,m$, as shown in Figure B.2.

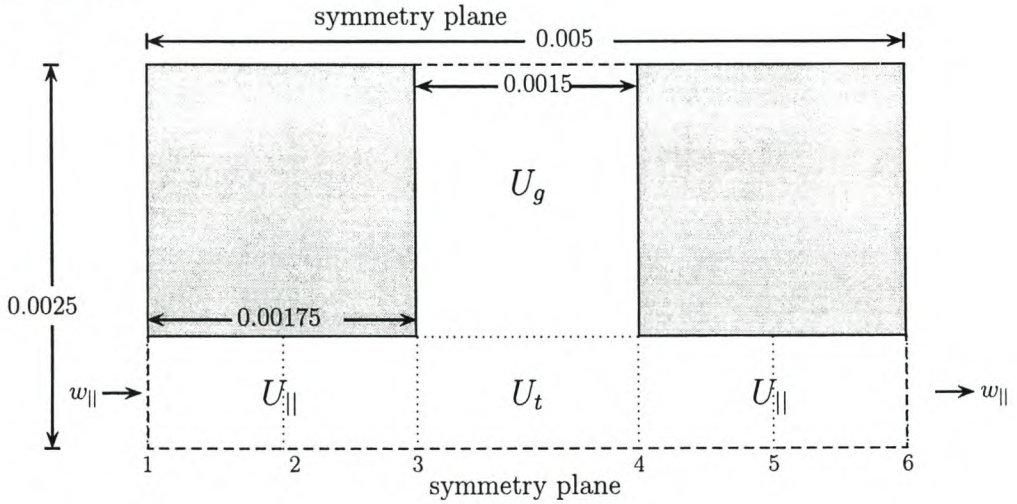

Figure B.2: Top half of a unit cell constructed in CFX for a non-staggered model with $\epsilon = 0.51$ (All measurements in meters).

In the CFX post-processor, planes were created at positions 1 to 6, as indicated in Figure B.2. The numerical values for the average velocity and the average pressure given at these planes are given in Table B.1.

Dimensionless Permeability K

The change in pressure across the entire unit cell is given by

$$\Delta p \;=\; p_1 - p_6 \;=\; 0.03575\ Pa, \tag{B.1}$$

where p_1 and p_6 indicate the average pressure at planes 1 and 6 respectively.

Plane	Average pressure $[Pa]$	Average velocity $[m/s]$
1	0.05000	1.5262×10^{-3}
2	0.04288	1.5262×10^{-3}
3	0.03514	1.5249×10^{-3}
4	0.02950	1.5247×10^{-3}
5	0.02137	1.5262×10^{-3}
6	0.01425	1.5262×10^{-3}

Table B.1: Numerical values obtained using CFX for the case of no staggering.

The superficial velocity q was calculated as

$$q = \left(1 - \frac{d_s}{d}\right) w_{||} = \left(1 - \frac{3.5}{5}\right) 1.5262 \times 10^{-3} = 4.5787 \times 10^{-4}\, m/s, \tag{B.2}$$

where $w_{||}$ is the average velocity at planes in the streamwise channel (planes 1, 2, 5 and 6).

The dimensionless hydrodynamic permeability K, could then be calculated using the Darcy equation (equation (2.42))

$$K = \frac{\mu q}{d_\perp \Delta p} = \frac{0.001\,(4.5787 \times 10^{-4})}{0.005\,(0.03575)} = 2.5613 \times 10^{-3}. \tag{B.3}$$

The numerical value obtained by FD is $K = 2.56 \times 10^{-3}$ which is almost the same as the result given here by CFX. However the predicted value given by the FD analytical model (equation (3.2)) is $K = 3.2143 \times 10^{-3}$ which is higher than both the numerical results.

Assumptions

Figure B.3 shows contours of constant pressure across the unit cell shown in Figure B.2. The 24th contour represents a pressure of 0.049 Pa ($kg\,m^{-1}\,s^{-2}$) and the 2nd contour represents the pressure of 0.014 Pa ($kg\,m^{-1}\,s^{-2}$). The adjacent contours differ by a value of 0.0015 Pa.

From Figure B.3 it is obvious that there are constant pressure gradients in the streamwise channels, but there also exist pressure gradients in the other volumes.

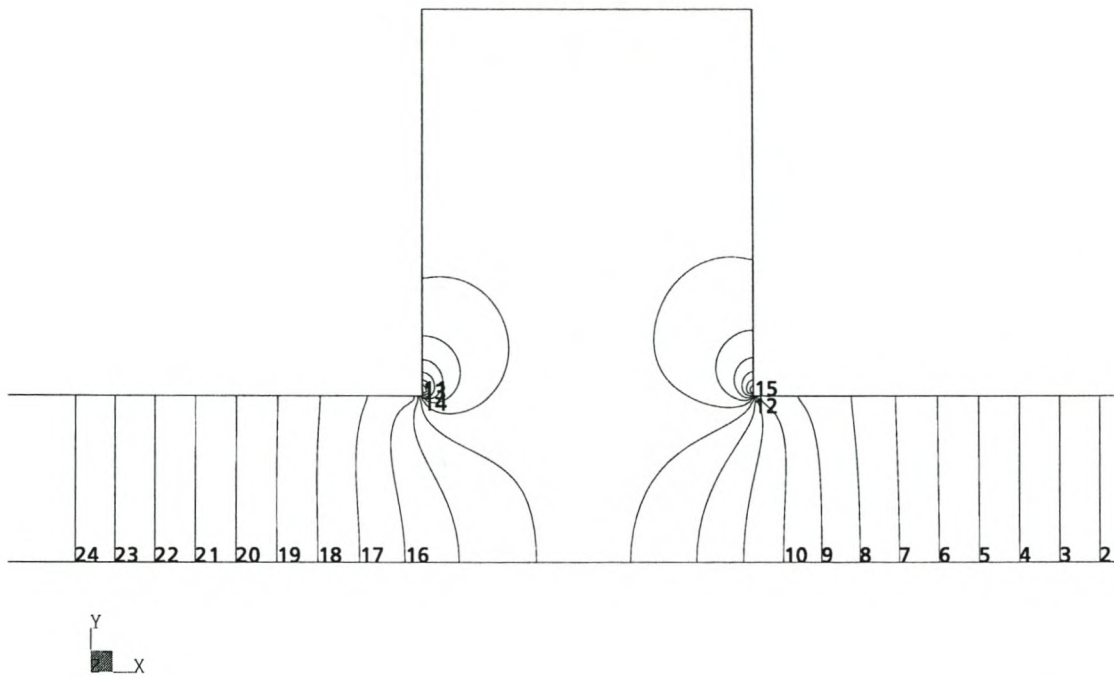

Figure B.3: Isobars for the non-staggered CFX model of $\epsilon = 0.51$, with flow in the positive x-direction.

We now consider the three different fluid volumes $U_{||}$, U_g and U_t, shown in Figure B.2, separately. The pressure gradient in the streamwise volume $U_{||}$ according to the model (equation (2.44)) is

$$-\nabla_{||}p = \frac{12\,\mu\,q}{d_\perp^2(1-\sqrt{1-\epsilon})^3} = 8.13995\ Pa, \tag{B.4}$$

which is almost exactly the same as the pressure gradient given by CFX for the streamwise channel

$$-\nabla_{||}p = \frac{p_1 - p_2}{d_s/4} = \frac{p_5 - p_6}{d_s/4} = \frac{0.0712}{0.000875} = 8.1371\ Pa, \tag{B.5}$$

as expected.

The pressure gradient in the transfer volumes U_t is zero according to the model, however the pressure gradient given by CFX for this volume is

$$-\nabla_t p = \frac{p_3 - p_4}{d - d_s} = \frac{0.0351382 - 0.0295041}{0.0015} = 3.75607\ Pa. \tag{B.6}$$

The assumption in the model that the pressure gradient is zero in the transfer volume U_t, may therefore contribute greatly to the reason why the numerical and predicted values for K differ.

To calculate the pressure gradient in the stagnant volume, average pressure values of the opposing walls in this region were also calculated. The pressure gradient in this region is zero according to the assumptions of the model, however the result of the pressure gradient given across the stagnant volume according to CFX is as follows:

$$-\nabla_g p = \frac{0.03408 - 0.031878}{0.0015} = 1.468\ Pa. \tag{B.7}$$

We assume that the pressure gradient in the transfer and stagnant volumes are caused by the change in the velocity profile on entering and exiting the streamwise (parallel plates) sections. This contribution was assumed to be negligible by the FD analytical model. Obviously at low porosities these volumes are going to be very small and may be neglected, but for higher porosities their contribution should perhaps be considered, to obtain more accurate predictions.

Appendix C

CFX staggered configuration for $\epsilon = 0.1164$

In CFX-build models with staggered configurations, similar to the model shown in Figure C.1, for porosities 0.1164 and 0.51 were constructed as mentioned in Section 4.1. In this appendix we examine closely the CFX staggered model of porosity $\epsilon = 0.1164$, in an attempt to verify the assumptions made in the analytical model.

First we calculate the value given by CFX for the dimensionless hydrodynamic permeability K, which can be compared to the predicted value of the FD analytical model.

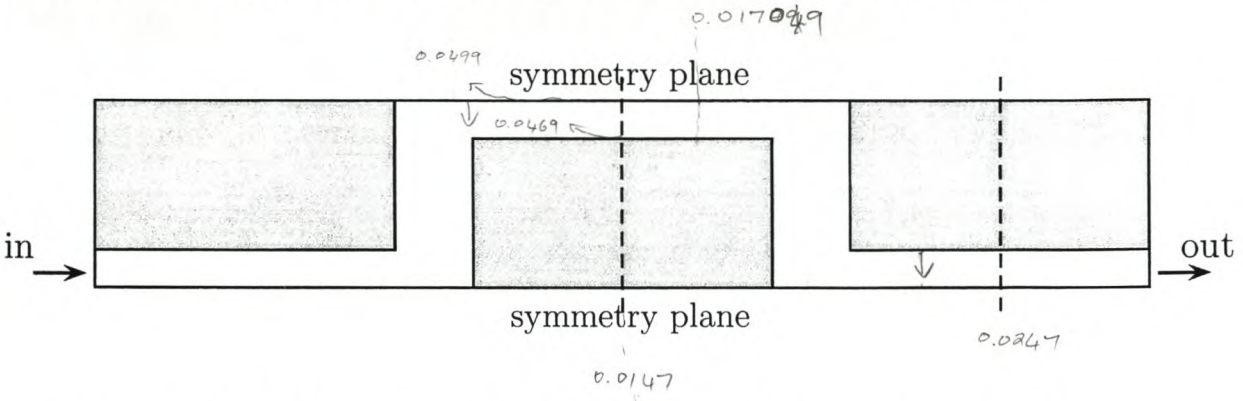

Figure C.1: Construction used in CFX modelling for streamwise staggering.

We consider the top half of the second unit cell (area bordered by dashed lines in Figure C.1) constructed in CFX-build, as shown in Figure C.2. The pressure was set as 0.1 Pa at

the inlet and 0 Pa at the outlet, to assure slow flow in the Darcy regime. As with the models for the non-staggered case, the fluid was chosen to be water, with density $\rho = 1000\ kg/m^3$ and dynamic viscosity $\mu = 0.001\ N \cdot s/m^2$. For simplification the unit cells were chosen to be square with $d = d_{||} = d_{\perp} = 0.01\,m$, so that $U_o = 1 \times 10^{-4}\,m^2$. Therefore, for a porosity of $\epsilon = 0.1164$, we must have $d_s = d_{s||} = d_{s\perp} = 0.0094\,m$ as shown in Figure C.2.

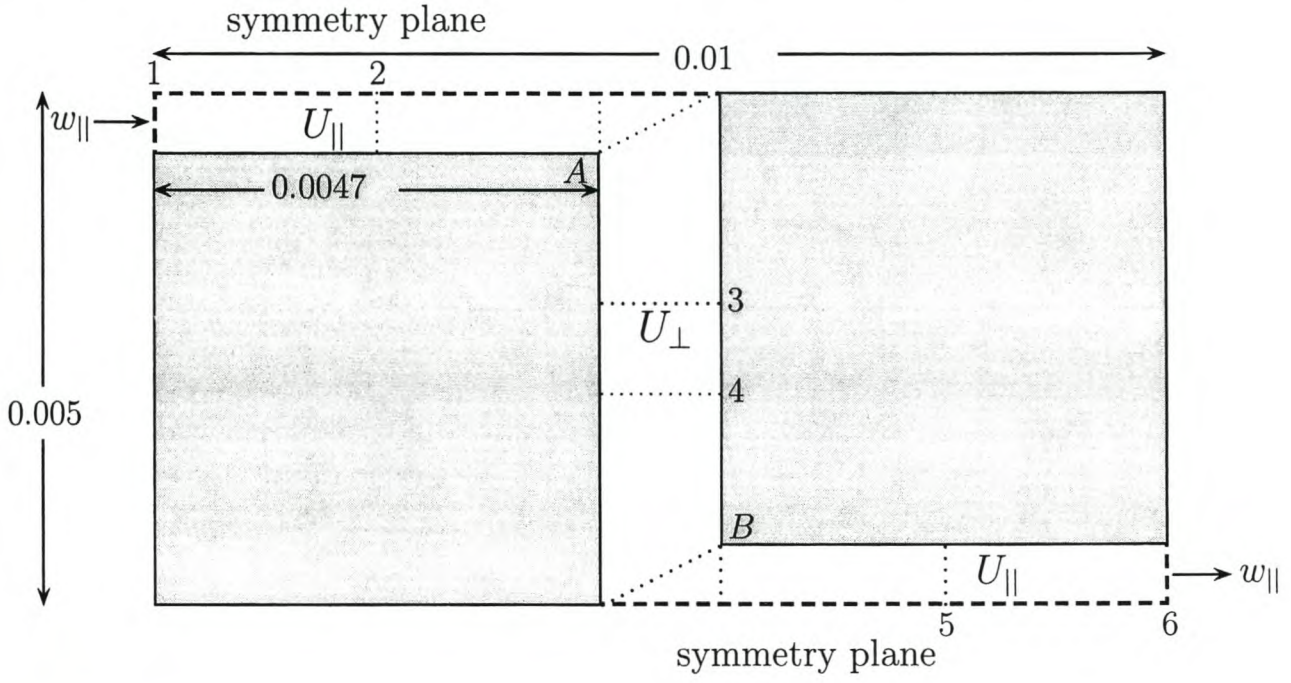

Figure C.2: Top half of a unit cell constructed in CFX for a model with $\epsilon = 0.1164$ (All measurements in meters).

In the CFX post-processor, planes were created at positions 1 to 6, as indicated in Figure C.2. The numerical values for the average velocity and the average pressure given at these planes are given in Table C.1.

Dimensionless Permeability K

The change in pressure across the entire unit cell is given by

$$\Delta p = p_1 - p_6 = 0.0361\ Pa, \tag{C.1}$$

Plane	Average pressure $[Pa]$	Average velocity $[m/s]$
1	0.05000	8.918×10^{-5} $\parallel$
2	0.04305	8.918×10^{-5} $\parallel$
3	0.03269	4.459×10^{-5} $\perp$
4	0.03121	4.459×10^{-5} $\perp$
5	0.02084	8.918×10^{-5} $\parallel$
6	0.01390	8.918×10^{-5} $\parallel$

Table C.1: Numerical values obtained using CFX for the case of streamwise staggering.

where p_1 and p_6 indicate the average pressure at planes 1 and 6 respectively.

The superficial velocity q was calculated as

$$q = \left(1 - \frac{d_s}{d}\right) w_{\parallel} = \left(1 - \frac{0.0094}{0.01}\right) 8.918 \times 10^{-5} = 5.3508 \times 10^{-6}\ m/s, \tag{C.2}$$

where $w_{\parallel}$ is the average velocity at planes in the streamwise channel (planes 1, 2, 3 and 4).

The dimensionless hydrodynamic permeability K, could then be calculated using the Darcy equation (equation (2.42))

$$K = \frac{\mu q}{d_{\perp} \Delta p} = \frac{0.001\,(5.3508 \times 10^{-6})}{0.01\,(0.361)} = 1.4822 \times 10^{-5}. \tag{C.3}$$

The value predicted by the model (equation (2.54)) for the dimensionless permeability of a model of porosity $\epsilon = 0.1164$ is

$$K = \frac{(1 - \sqrt{1-\epsilon})^3}{12\sqrt{1-\epsilon}} = 1.531915 \times 10^{-5}. \tag{C.4}$$

This predicted value is very similar to the value obtained numerically by CFX (equation (C.3)).

Assumptions in the Fluid Volumes

Figure C.3 shows contours of constant pressure across the unit cell shown in Figure C.2, for a model of porosity $\epsilon = 0.1164$. The 36th contour represents a pressure of 0.046 Pa

($kg\,m^{-1}\,s^{-2}$) and the 8th contour represents the pressure of 0.02 Pa ($kg\,m^{-1}\,s^{-2}$). The adjacent contours differ by a value of 0.001 Pa. From Figure C.3 it can be seen that constant

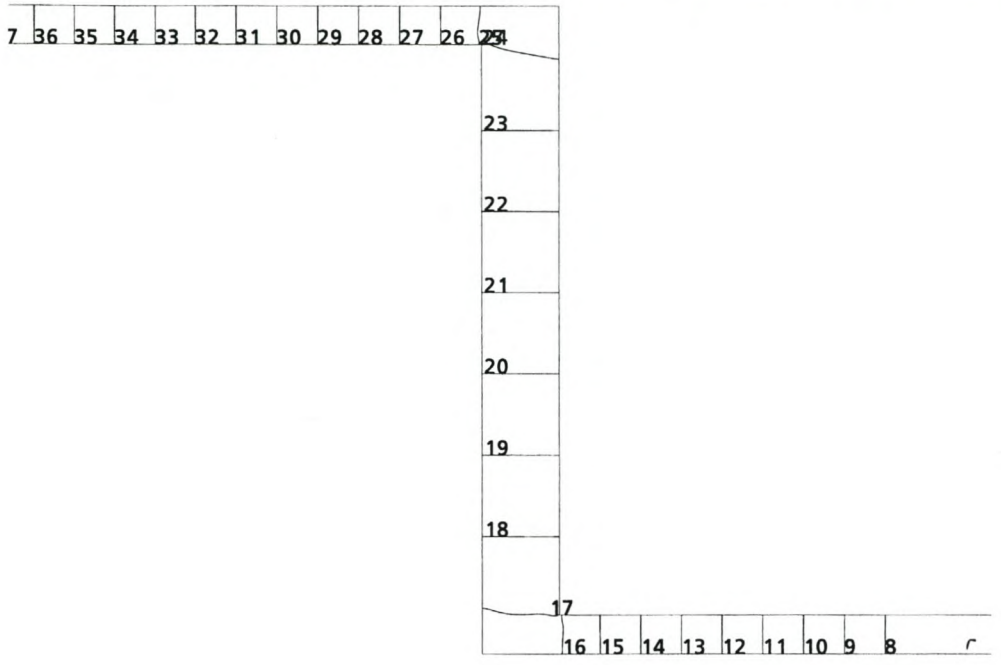

Figure C.3: Isobars for the staggered CFX model of $\epsilon = 0.1164$, with flow in the positive x-direction.

pressure gradients are found in both the streamwise and transverse regions, but the pressure gradient in the transverse region is half the pressure gradient in the streamwise region, as assumed by the model.

The pressure gradient in the streamwise volume $U_{||}$, according to the model (equation (2.44)) is

$$-\nabla_{||}p = \frac{12\,\mu\,q}{d_{\perp}^2(1-\sqrt{1-\epsilon})^3} = 2.972\ Pa, \tag{C.5}$$

which is almost the same as the pressure gradient given by CFX for the streamwise channel

$$-\nabla_{||}p = \frac{p_1 - p_2}{d_s/4} = \frac{p_5 - p_6}{d_s/4} = \frac{6.946 \times 10^{-3}}{2.35 \times 10^{-3}} = 2.956\ Pa, \tag{C.6}$$

as expected. The pressure gradient in the transverse volume $U_\perp$ according to the model (equation (2.49)) is

$$-\nabla_\perp p = \frac{-\nabla_{||} p}{2} = 1.486\ Pa, \tag{C.7}$$

which is almost the same as the pressure gradient given by CFX for the transverse channel

$$-\nabla_\perp p = \frac{p_3 - p_4}{0.001} = 1.478\ Pa. \tag{C.8}$$

However both these results (equation (C.6) and (C.8)) are found in the middle regions of their respective volumes. At the 'edges' of the volumes the results are not quite the same. Around the corners of the solid rectangles, shown by A and B in Figure C.2, the flow is more complex, but the approximation made by the model by assuming a transfer volume, where the pressure remains constant, seems reasonable. For low porosities these transfer volumes are going to be very small and will not have much effect on the model.

Figure C.4 shows contours of constant pressure across the unit cell shown in Figure C.2, for a model of porosity $\epsilon = 0.51$. The 29th contour represents a pressure of $4.462 \times 10^{-3}\ Pa$ $(kg\, m^{-1}\, s^{-2})$ and the 7th contour represents the pressure of $1.577 \times 10^{-3}\ Pa$ $(kg\, m^{-1}\, s^{-2})$. The adjacent contours differ by a value of $1.5 \times 10^{-4}\ Pa$. From the model it can be seen that constant pressure gradients are found in the streamwise regions, however in the transverse regions the flow cannot necessarily be considered as parallel plate flow. This is most likely because at high porosities only a small section (if any) of the parallel plates in the transverse regions are opposite each other.

We can conclude therefore that the physics involved at higher porosities are different from the parallel plate Stokes flow which forms the basis of the FD analytical model and therefore, for configurations of very high porosity this model will not give accurate results and an alternative model should be considered for these configurations.

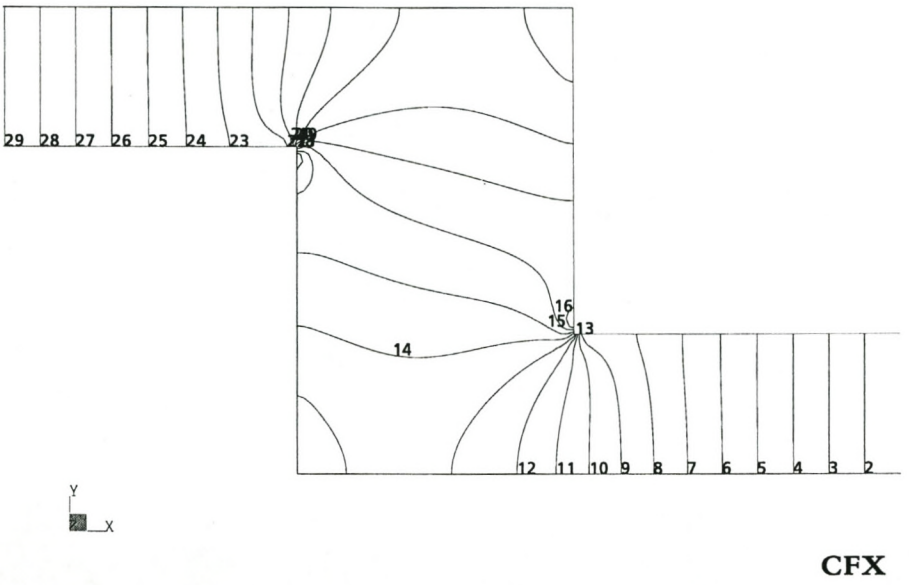

Figure C.4: Isobars for the staggered CFX model of $\epsilon = 0.51$, with flow in the positive x-direction.

Appendix D

Pressure averaging equation for FD staggering

In this appendix we address each term in the pressure averaging equation (equation (6.1))

$$\langle \nabla p \rangle = \nabla \langle p \rangle + \frac{1}{U_o} \iint_{S_{fs}} \underline{n}\, p \, dS. \tag{D.1}$$

by considering the rectangular representation of a porous medium for the FD staggered configuration as shown in Figure D.1.

We first consider a unit cell, where the boundaries in the perpendicular direction of the unit cell go through the solid region, as indicated by RRUC 1 (RRUC 2 is therefore the neighbouring unit cell in this case). In terms of symbols, where Δp is the total change in pressure in the streamwise volume and δp is the change of pressure in the transverse volume, as indicated in Figure D.1, the first term in equation (D.1) can be written as

$$\langle \nabla p \rangle = \frac{1}{U_o} \iiint_{U_f} \nabla p \, dU = \frac{1}{U_o} \left(\iiint_{U_{||}} \nabla p \, dU + \iiint_{U_t} \nabla p \, dU + \iiint_{U_\perp} \nabla p \, dU \right). \tag{D.2}$$

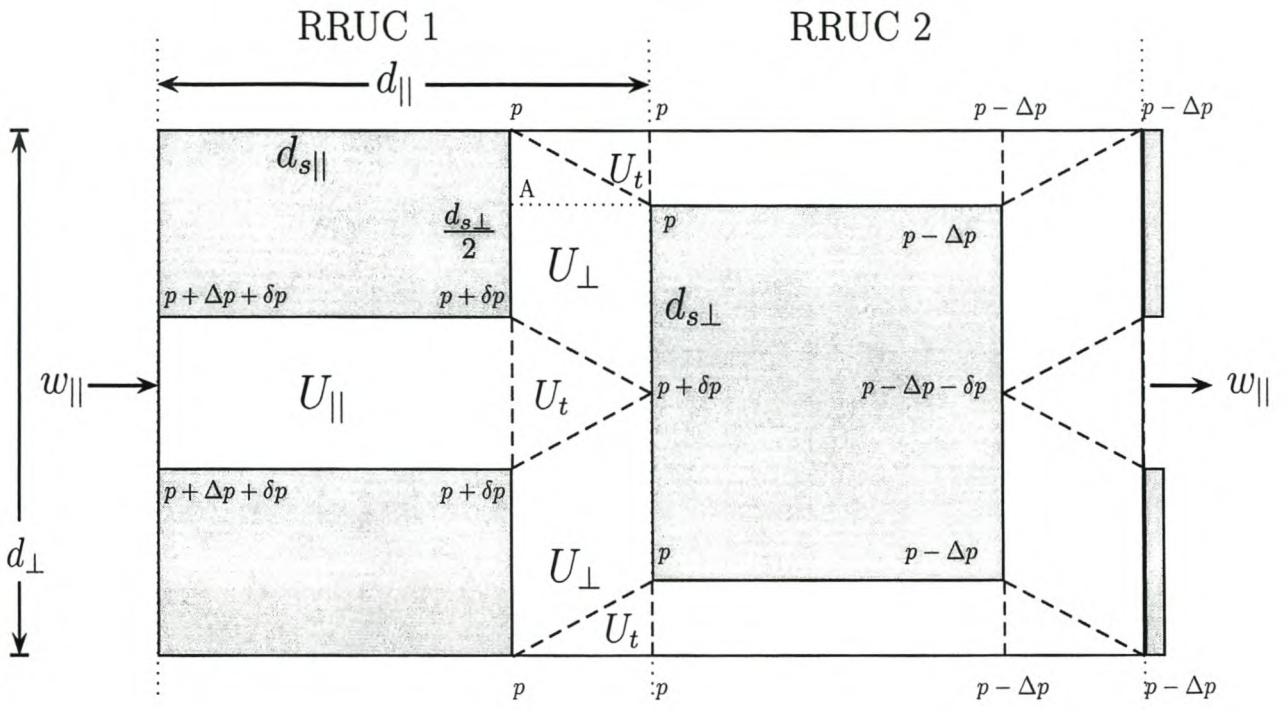

Figure D.1: Unit cell geometry in case of FD streamwise staggering (first case).

The pressure is constant in the transfer volumes so the pressure gradient will be zero here. However, even though the flow is in the perpendicular direction, we assume that there is a pressure gradient in the streamwise direction. The pressure at A, in Figure D.1, is given by $p + [\frac{1}{2}(d_\perp - d_{s\perp})/(\frac{1}{2}d_{s\perp})]\,\delta p$. Therefore, for the first term we have

$$\begin{aligned}
\langle \nabla p \rangle &= \frac{1}{U_o}\left(-\frac{\Delta p}{d_{s||}}.U_{||} + \frac{-[(d_\perp - d_{s\perp})/d_{s\perp}]\,\delta p}{d_{||} - d_{s||}}.U_\perp\right) \\
&= -\frac{1}{U_o}\left(\frac{\Delta p}{d_{s||}}.U_{||} + \frac{(d_\perp - d_{s\perp})\,\delta p}{U_\perp}.U_\perp\right) \\
&= -\frac{1}{U_o}\left(\frac{\Delta p}{d_{s||}}.U_{||} + \frac{\delta p}{d_{s||}}.U_{||}\right) \\
&= -\frac{U_{||}}{U_o}\left(\frac{\Delta p + \delta p}{d_{s||}}\right). \qquad \text{(D.3)}
\end{aligned}$$

The second term in equation (D.1) is

$$\nabla \langle p \rangle = \frac{1}{U_o}\nabla \iiint_{U_f} p\, dU. \qquad \text{(D.4)}$$

The average pressure in the total transfer region of the unit cell is equal to the average pressure in the perpendicular region. Therefore if we consider two different RRUCs, as shown in Figure D.1, and take the gradient of their two averages we obtain the following

$$\begin{aligned}\nabla \langle p \rangle &= \frac{1}{U_o}\left(\frac{\left[(p+\delta p+\frac{\Delta p}{2})U_{||}+(p+\frac{\Delta p}{2})\,U_t+(p+\frac{\Delta p}{2})\,U_\perp\right]}{d_{||}}\right. \qquad \text{(D.5)}\\ &\quad \left.-\frac{\left[(p-\frac{\Delta p}{2})\,U_{||}+(p-\Delta p-\frac{\delta p}{2})\,U_t+(p-\Delta p-\frac{\delta p}{2})\,U_\perp\right]}{d_{||}}\right)\\ &= -\frac{1}{U_o}\left(\frac{(\Delta p+\delta p)\,U_{||}+(\Delta p+\delta p)\,(U_t+U_\perp)}{d_{||}}\right)\\ &= -\frac{U_f}{U_o}\left(\frac{\Delta p+\delta p}{d_{||}}\right). \qquad \text{(D.6)}\end{aligned}$$

This can be shown by considering each component of the volumes separately and realising that they all differ by $(\Delta p+\delta p)$ to the corresponding component in the neighbouring RRUC.

The surface integral term is zero in this case,

$$\frac{1}{U_o}\iint_{S_{fs}} \underline{n}\,p\,dS = 0, \qquad \text{(D.7)}$$

since the pressure at the walls is assumed to cancel out. In a more realistic situation, the surface term here would not be zero, since the pressures at the streamwisely up and down facing surfaces would not cancel out. However, for the pressure averaging equation this has been compensated for by including a pressure gradient in the transverse region.

The above results for the three terms will be true for all RRUCs whose boundaries cut through the solid rectangle (i.e. for $d_{s||}/d_{||}$ of the possible RRUCs if shifted in the streamwise direction).

Second case

If we now shift the unit cell in the streamwise direction so that its boundaries do not pass through the solid region (i.e. consider the unit cell to be as shown in Figure D.2), the surface integral term will not be zero, but the other two terms in the pressure averaging equation will be the same, as shown below. This will be true for all RRUCs whose boundaries do not cut through the solid rectangle (i.e. for $1 - d_{s||}/d_{||}$ of the cases).

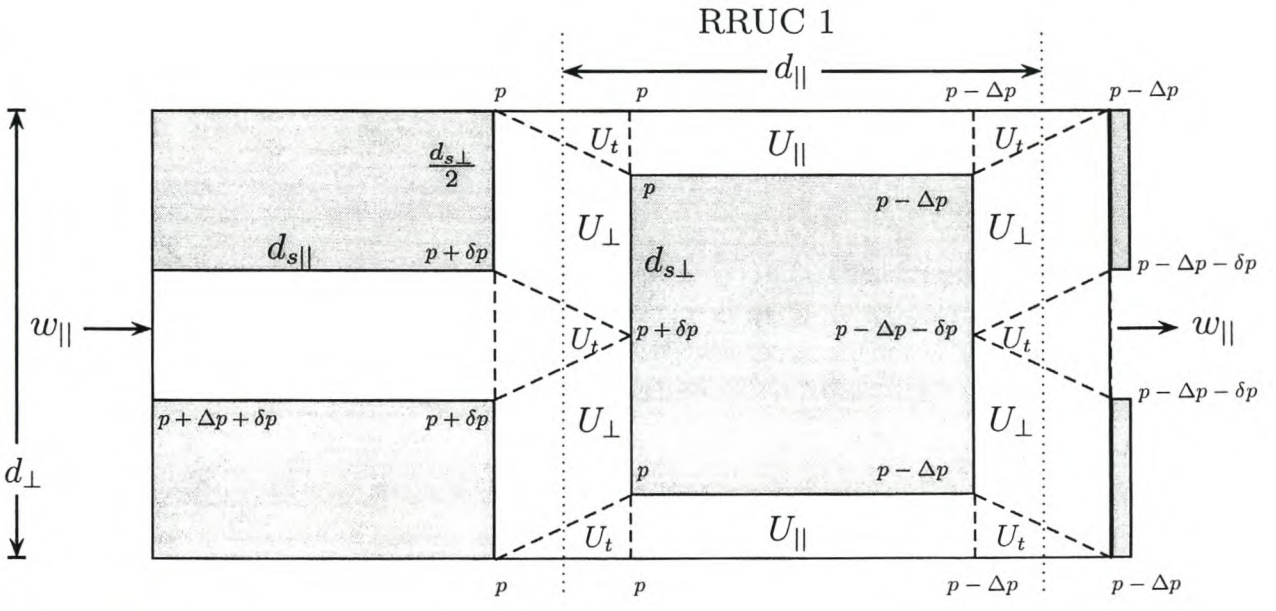

Figure D.2: Unit cell geometry in case of FD streamwise staggering (second case).

In terms of symbols, as indicated in Figure D.2, the first term in equation (D.1) is

$$\langle \nabla p \rangle = \frac{1}{U_o} \iiint_{U_f} \nabla p \, dU = \frac{1}{U_o} \left(\iiint_{U_{||}} \nabla p \, dU + \iiint_{U_t} \nabla p \, dU + \iiint_{U_\perp} \nabla p \, dU \right). \quad \text{(D.8)}$$

The pressure is constant in the transfer volumes so the pressure gradient will be zero here, but in the transverse volumes there is a pressure gradient in the streamwise direction. Therefore

we have

$$\begin{aligned}\langle \nabla p \rangle &= \frac{1}{U_o}\left(\frac{-\Delta p}{d_{s||}}.U_{||} + \frac{p - [p + \frac{(d_\perp - d_{s\perp})}{2\,d_{s\perp}}\,\delta p]}{(d_{||} - d_{s||})/2}.\frac{U_\perp}{2}\right. \\ &\quad \left. + \frac{[p + \Delta p] - [p + \Delta p - \frac{(d_\perp - d_{s\perp})}{2\,d_{s\perp}}\,\delta p]}{(d_{||} - d_{s||})/2}.\frac{U_\perp}{2}\right) \qquad \text{(D.9)} \\ &= \frac{1}{U_o}\left(-\frac{\Delta p}{d_{s||}}.U_{||} - \frac{(d_\perp - d_{s\perp})\,\delta p}{U_\perp}.U_\perp\right) \\ &= \frac{1}{U_o}\left(-\frac{\Delta p}{d_{s||}}.U_{||} + \frac{\delta p}{d_{s||}}.U_{||}\right) \\ &= -\frac{U_{||}}{U_o}\left(\frac{\Delta p + \delta p}{d_{s||}}\right). \qquad \text{(D.10)}\end{aligned}$$

The second term can be written as

$$\nabla \langle p \rangle = \frac{1}{U_o} \nabla \iiint_{U_f} p \, dU. \qquad \text{(D.11)}$$

If we consider two neighbouring RRUCs, similar to the one shown in Figure D.2, and take the gradient of their two averages we obtain the following

$$\begin{aligned}\nabla \langle p \rangle &= -\frac{1}{U_o}\left(\frac{(\Delta p + \delta p)\,U_{||} + (\Delta p + \delta p)\,U_t + (\Delta p + \delta p)\,U_\perp}{d_{||}}\right) \\ &= -\frac{U_f}{U_o}\left(\frac{\Delta p + \delta p}{d_{||}}\right). \qquad \text{(D.12)}\end{aligned}$$

This can be shown by considering each component of the volumes separately and realising that they all differ by $(\Delta p + \delta p)$ to the corresponding component in the neighbouring RRUC.

The surface integral in this case is not zero and is given by:

$$\begin{aligned}\frac{1}{U_o} \iint_{S_{fs}} \underline{n}\, p \, dS &= \frac{1}{U_o}\left(\frac{[p + (p - \delta p)]}{2}\, d_{s\perp} - \frac{[(p - \Delta p) + (p - \Delta p - \delta p)]}{2}\, d_{s\perp}\right) \\ &= \frac{d_{s\perp}}{U_o}\left(\frac{2p + \delta p}{2} - \frac{2p - 2\,\Delta p - \delta p}{2}\right) \\ &= \frac{d_{s\perp}}{U_o}(\Delta p + \delta p). \qquad \text{(D.13)}\end{aligned}$$

Combination of Cases 1 and 2

Combining cases 1 and 2 we obtain the overall value for each term in equation (D.1):

$$\langle \nabla p \rangle = -\frac{U_{||}}{U_o}\left[\frac{\Delta p + \delta p}{d_{s||}}\right], \tag{D.14}$$

$$\nabla \langle p \rangle = -\frac{U_f}{U_o}\left[\frac{\Delta p + \delta p}{d_{||}}\right], \tag{D.15}$$

$$\begin{aligned}\frac{1}{U_o}\iint_{S_{fs}} \underline{n}\, p\, dS &= \frac{(d_{||} - d_{s||})}{d_{||}}\left[\frac{d_{s\perp}}{U_o}(\Delta p + \delta p)\right] + \frac{d_{s||}}{d_{||}}(0) \\ &= \frac{(d_{||} - d_{s||})}{d_{||}}\left[\frac{d_{s\perp}}{U_o}(\Delta p + \delta p)\right].\end{aligned} \tag{D.16}$$

Checking equation (D.1), with the help of Table 5.2, we obtain the following:

$$\begin{aligned}\langle \nabla p \rangle &= \nabla \langle p \rangle + \frac{1}{U_o}\iint_{S_{fs}} \underline{n}\, p\, dS \\ &= -\frac{U_f}{U_o}\cdot\left(\frac{\Delta p + \delta p}{d_{||}}\right) + \frac{(d_{||} - d_{s||})}{d_{||}}\cdot\left(\frac{d_{s\perp}}{U_o}(\Delta p + \delta p)\right) \\ &= -\frac{\Delta p + \delta p}{U_o}\cdot\left(\frac{U_f}{d_{||}} - \frac{(d_{||} - d_{s||})\, d_{s\perp}}{d_{||}}\right) \\ &= -\frac{\Delta p + \delta p}{U_o}\cdot\left(\frac{U_{||} + U_t}{d_{||}}\right) \qquad \text{(D.17)} \\ &= -\frac{\Delta p + \delta p}{U_o}\cdot\left(\frac{(d_\perp - d_{s\perp})\, d_{s||} + (d_{||} - d_{s||})\,(d_\perp - d_{s\perp})}{d_{||}}\right) \\ &= -\frac{\Delta p + \delta p}{U_o}\cdot\left(\frac{(d_\perp - d_{s\perp})\, d_{||}}{d_{||}}\cdot\frac{d_{s||}}{d_{s||}}\right) \\ &= -\frac{U_\perp}{U_o}\cdot\frac{\Delta p + \delta p}{d_{s||}}, \qquad \text{(D.18)}\end{aligned}$$

which agrees with equation (D.14). From equation (D.1) and equation (D.17) we can write the surface term as follow

$$\begin{aligned}\frac{1}{U_o}\iint_{S_{fs}} \underline{n}\, p\, dS &= \left(\frac{U_{||}+U_t}{U_o}\right).\frac{\Delta p+\delta p}{d_{||}} - \nabla\langle p\rangle \\ &= \left(\frac{U_{||}+U_t}{U_f}\right).\nabla\langle p\rangle - \nabla\langle p\rangle \\ &= \left(\frac{U_{||}+U_t}{U_f} - 1\right).\nabla\langle p\rangle\,. \end{aligned} \tag{D.19}$$

This equation is identical to the equation obtained when considering the rectangular representation of a porous medium for the RRUC staggered configuration, equation (6.53).

Bibliography

[1] Carman, P.C., 1937, Fluid Flow through Granular Beds, *Transactions of the Institution of Chemical Engineers*, Vol. 15, pp. 150-166.

[2] Churchill, S.W. and Usagi, R., 1972, A General Expression for the Correlation of Rates of Transfer and Other Phenomena, *American Institue of Chemical Engineering Journal*, Vol. 18, pp. 1121-1128.

[3] Clennel, M.B., 1997, Tortuosity: A guide through the maze, *Developments in Petrophysics*, eds. Lovell, M.A. and Harvey, P.K., Geological Society Special Publication No. 122, pp. 299-344.

[4] Diedericks, G.P.J., 1999, *Pore Scale Modelling of Transport Phenomena in Homogeneous Porous Media*, PhD Thesis, University of Stellenbosch, South Africa.

[5] Du Plessis, J.P., 1997, Fluid Transport in Porous Media, *Advances in Fluid Mechanics*, Vol. 13, pp. 61-104.

[6] Du Plessis, J.P., 1991, Saturated crossflow through a two-dimensional porous medium, *Advances in Water Resources*, Vol. 14(3), pp. 131-137.

[7] Du Plessis, J.P., 2002, personal communication.

[8] Du Plessis, J.P. and Masliyah, J.H., 1988, Mathematical Modelling of Flow Through Consolidated Porous Media, *Transport in Porous Media*, Vol. 3, pp. 145-161.

[9] Du Plessis, J.P. and Van Der Westhuizen, J., 1993, Laminar crossflow through prismatic porous domains, *R&D Journal of the South African Institute of Mechanical Engineers*, Vol. 9(2), pp. 18-24.

[10] Du Plessis, J.P. and Roos, L.I., 1993, Improvement on prediction for water seepage through low porosity granular media, *Water SA*, Vol. 19(2), pp. 147-152.

[11] Du Plessis, J.P. and Roos, L.I., 1994, Improvement on prediction for water seepage through low porosity granular media, *Water SA*, Vol. 20(2), pp. 175-178.

[12] Firdaouss, M. and Du Plessis, J.P., 2003, A new model for the prediction of Darcy permeabilities in non-istropic periodic two-dimensional porous media, *Journal of Porous Media*, to be published.

[13] Gebart, B.R., 1992, Permeability of Unidirectional Reinforcements for RTM, *Journal of Composite Materials*, Vol. 26, pp. 1100-1133.

[14] Hasimoto, H., 1958, On the periodic fundamental solutions of the Stokes equations and their application to viscous flow past a cubic array of spheres, *Journal of Fluid Mechanics*, Vol. 5, pp. 317-328.

[15] Howells, I.D., 1998, Drag on Fixed Beds of Fibres in Slow Flow, *Journal of Fluid Mechanics*, Vol. 355, pp. 163-192.

[16] Jackson, G.W. and James, D.F., 1986, The Permeability of Fibrous Porous Media, *Canadian Journal of Chemical Engineering*, Vol. 64, pp. 364-374.

[17] Kolodziej, J.A., 1986, Filtration Resistance of a System of Parallel Cylinders at a Transverse Creeping Flow, *Mechanika Teoretyczna i Stosowana*, Vol. 24(4), pp. 537-549.

[18] Sangani, A.S. and Acrivos, A., 1982, Slow flow past periodic arrays of cylinders with application to heat transfer, *Int. Journal of Multiphase Flow*, Vol. 8(3), pp. 193-206.

[19] Sangani, A.S. and Yao, C., 1988, Transport processes in random arrays of cylinders. 1. Thermol conduction *Phys. Fluids*, Vol. 31(9), pp. 2426-2434.

[20] Sangani, A.S. and Yao, C., 1988, Transport processes in random arrays of cylinders. 2. Viscous Flow, *Phys. Fluids*, Vol. 31(9), pp. 2435-2444.

[21] Van Brakel, J. and Heertjes, P.M., 1974, Analysis of diffusion in macroporous media in terms of a porosity, a tortuosity and a constrictivity factor, *Int. Journal of Heat Mass Transfer*, Vol. 17, pp. 1093-1103.

[22] Whitaker, S., 1999, The Method of Volume Averaging, *Theory and Applications of Transport in Porous Media*, Vol. 13, Kluwer Academic Publishers.